Science of the Total Environment xxx (xxxx) xxx

Contents lists available at ScienceDirect

Science of the Total Environment

journal homepage: www.elsevier.com/locate/scitotenv

Review

Proximal hyperspectral sensing of abiotic stresses in plants

Alireza Sanaeifar [a], Ce Yang [b], Miguel de la Guardia [c], Wenkai Zhang [a], Xiaoli Li [a,*], Yong He [a]

[a] College of Biosystems Engineering and Food Science, Zhejiang University, 866 Yuhangtang Road, Hangzhou 310058, China
[b] Department of Bioproducts and Biosystems Engineering, University of Minnesota, Saint Paul, MN 55108, United States
[c] Department of Analytical Chemistry, University of Valencia, Dr. Moliner 50, 46100 Burjassot, Valencia, Spain

HIGHLIGHTS

- Advances in proximal hyperspectral sensing of abiotic plant stress are discussed.
- A total of 182 articles published from 2019 to 2022 are reviewed in detail.
- Stressors at leaf and canopy scales are classified into seven categories.
- Combining proximal and airborne sensing has potential as a future research area.

GRAPHICAL ABSTRACT

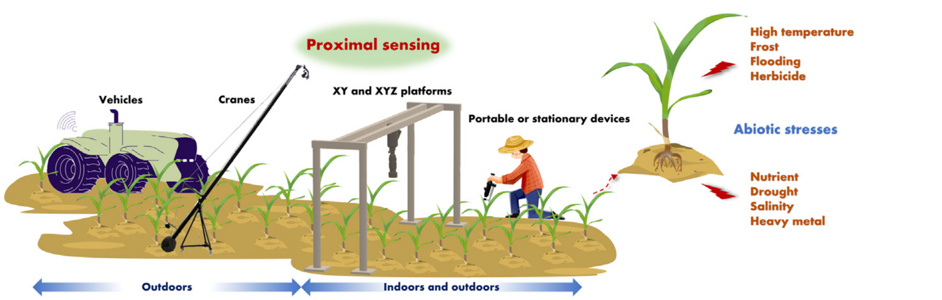

ARTICLE INFO

Editor: Charlotte Poschenrieder

Keywords:
Proximal sensing
Hyperspectral sensing
Abiotic plant stressors
Remote sensing

ABSTRACT

Recent attempts, advances and challenges, as well as future perspectives regarding the application of proximal hyperspectral sensing (where sensors are placed within 10 m above plants, either on land-based platforms or in controlled environments) to assess plant abiotic stresses have been critically reviewed. Abiotic stresses, caused by either physical or chemical reasons such as nutrient deficiency, drought, salinity, heavy metals, herbicides, extreme temperatures, and so on, may be more damaging than biotic stresses (affected by infectious agents such as bacteria, fungi, insects, etc.) on crop yields. The proximal hyperspectral sensing provides images at a sub-millimeter spatial resolution for doing an in-depth study of plant physiology and thus offers a global view of the plant's status and allows for monitoring spatio-temporal variations from large geographical areas reliably and economically. The literature update has been based on 362 research papers in this field, published from 2010, most of which are from four years ago and, in our knowledge, it is the first paper that provides a comprehensive review of the applications of the technique for the detection of various types of abiotic stresses in plants.

Contents

* Corresponding author.
E-mail addresses: asanaei@zju.edu.cn (A. Sanaeifar), ceyang@umn.edu (C. Yang), Miguel.Delaguardia@uv.es (M. de la Guardia), zwkdaai@zju.edu.cn (W. Zhang), xiaolili@zju.edu.cn (X. Li), yhe@zju.edu.cn (Y. He).

http://dx.doi.org/10.1016/j.scitotenv.2022.160652
Received 27 October 2022; Received in revised form 27 November 2022; Accepted 29 November 2022
Available online xxxx

Nomenclature

DWMD	Discrete wavelet multi-scale decomposition
PCA	Principal component analysis
SPA	Successive projections algorithm
IRIV	Iteratively retaining informative variables
ELM	Extreme learning machine
GA	Genetic algorithm
HCA	Hierarchical cluster analysis
KNN	K-nearest neighbors
DT	Decision tree
RF	Random forest
MLP	Multilayer perceptron
RBF	Radial basis function network
CFS	Correlation-based feature selection
PCR	Principal component regression
iPLS	Interval partial least squares
SA-iPLS	Simulated annealing-interval partial least squares
ANN-PSO	Ann-particle swarm optimization
CNN	Unidimensional deep learning convolutional neural networks
ANN-SA	Ann-simulated annealing
SiPLS	Synergy ipls
ANN-ABC	Ann- artificial bee colony
ANN-ICA	Ann- imperialist competitive algorithm
FDA	Finite difference approximation
CR	Continuum-removed
SNV	Standard normal variate
DT	De-trending
SGB	Stochastic gradient boosting
KELM	Kernel-based extreme learning machine
gnls	Generalized nonlinear least squares regression
GDboost	Gradient boost
Adaboost	Adaptive boosting
VIP	Variable importance of projection
ELNET	Elastic net
SVM	Support vector machine
GPR	Gaussian process regression
MARS	Multivariate adaptive regression spline
XGB	Extreme gradient boosting
GAM	Generalized additive model
SRIs	Spectral reflectance indices
DFT	Fourier transform
DWT	Discrete wavelet transform
CWT	Continuous wavelet transform
CR	Continuum removed spectrum
FOD	First-order differential spectrum
VMD	Variational mode decomposition
VCPA	Variable combination cluster analysis
1st Der	First Derivative
2nd Der	Second derivative
3rd Der	Third derivative
4th Der	Fourth derivative
DBN	Deep brief network
WT	Wavelet transform
SG	Savitzky-Golay smoothing
SG-SNVD	SG-SNV coupled with detrending algorithm
CARS	Competitive adaptive weighted sampling
Bw	PLS weighting regression coefficient
WPCA	Wavelet principal component analysis
SAE	Stacked auto-encoders
SCAE	Stack convolution auto encoder
MC	Monte carlo
PSO	Particle swarm optimization
VISSA	Variable iterative space shrinkage approach
GOA	Grasshopper optimization algorithm
CS	Cuckoo search
RDA	Ratio difference of autocorrelation function first derivative
NB	Naive Bayes
MRF	Modified random frog
HHO	Harris hawks optimizer
MSC	Multiplicative scatter correction

LDA	Linear discriminant analysis
MCR	Multivariate curve resolution
Nor	Normalization
Sta	Standardization
PLS-DA	Partial least squares discriminant analysis
UVE	Uninformative variable elimination
KLD	Kullback-leibler divergence
SMLR	Stepwise multiple linear regression
SO-PLS	Sequential orthogonalized-partial least squares
BT	Bagging trees
GPR	Gaussian process regression
VH-GPR	Variational heteroscedastic gaussian process regression
QDA	Quadratic discriminant analysis
LASSO	Least absolute shrinkage and selection operator
RR	Ridge regression
SMA	Spectral mixture analysis
RLR	L2-regularized logistic regression
SAE	Stacked autoencoder
LMT	Logistic model tree

1. Introduction

Abiotic plant stress and the use of hyperspectral technologies to evaluate the reactions in plants have been reviewed, paying special attention to the advantages of early detection of plant problems without damaging crops.

1.1. Stress-induced reactions in plants and their characterization using hyperspectral techniques

Plant growth is typically influenced by adverse environmental conditions, which means that plants are frequently faced with a series of challenges related to temperature, nutrition, water, chemicals, salinity, and other factors. The physiological changes caused by these conditions have a significant impact on plant growth, which has a detrimental effect on agricultural production (Li et al., 2021c). Abiotic stresses, such as nutrient deficiencies and water stress, can have a more serious impact on crop productivity than diseases caused by biotic agents, some of which can reduce crop yields by as much as 70 % (Payne and Kurouski, 2021). Furthermore, plant damage may also adversely affect human health, such as through heavy metal toxicity (Wang et al., 2018). There are various physiological defense mechanisms that are developed in plants in response to adverse abiotic conditions. Early detection of these mechanisms and the implementation of protective measures in conjunction with them could aid in reducing adverse effects (Sanaeifar et al., 2022a). Furthermore, a key component of precision agriculture is the ability to monitor plant health under extreme environmental conditions in order to ensure healthy plant development. As a result, comprehensive monitoring of the state of agricultural crops will contribute to the early and accurate estimation of yield losses and the development of disaster prevention strategies.

Other aspects of precision agriculture that require advanced techniques to achieve success include the development of new varieties of plants as well as selecting the best ones for certain conditions, such as drought or soil salinity tolerance (Das et al., 2020; El-Hendawy et al., 2021a). Hence, the development of phenotyping techniques that are quick, accurate, and non-invasive is necessary for evaluating plant stress and breeding programs.

Advances in imaging technologies have gained significant attention in recent years for the assessment of the effects of abiotic stress on plant characteristics. The use of non-destructive imaging allows measurements to be made over time, which may help in monitoring the resilience of crops to stress (Mohd Asaari et al., 2018). Recently, hyperspectral sensing has emerged as one of the most promising technologies for the assessment of plant physiology, as well as their reactions to stress by combining spatial and spectral information (Mertens et al., 2021). The two main types of hyperspectral sensors are imaging sensors and non-imaging sensors (Cheshkova, 2022; Traversari et al., 2021). In non-imaging sensors, average reflectance is measured in an area without a spatial field of view. The size of the sampling area is also determined by several factors, including the field of view and the distance to the target. There are currently a variety of spectrometers available on the market. For instance, the ASD FieldSpec (Analytical Spectral Devices Inc., USA) is widely used in research studies to provide detailed hyperspectral scans comparable to benchtop instruments in terms of spectral range and resolution (Thomson et al., 2022). The majority of these sensors are lightweight and portable, and do not require a great deal of training to operate. As early signs of plant stress often appear in plant tissue below 1 mm, non-imaging sensors lack the ability to identify early signs of plant stress due to tissue spectrum averaging (Zhang et al., 2020a). Hyperspectral imaging (HSI) sensors combine spatial and spectral information by creating an individual spectrum profile for each pixel. Hence, a three-dimensional array of data is created with two spatial dimensions and one spectral dimension. In addition to imaging whole plants, HSI can image individual leaves from the plants for the purposes of performing quantitative or qualitative analyses. Using this approach, leaf and canopy spectral signatures may be able to indicate changes in vegetation health resulting from abiotic stress (Burnett et al., 2021). Detailed information is contained in each plant pixel, including the chemical composition and physiological conditions of the plant (Mishra et al., 2017). Under greenhouse or field conditions, the plant reflectance spectrum can be used to identify, quantify, and spatially present the effects of stress on plant growth (Fallon et al., 2020). However, the development of methods allowing the accurate monitoring of plant stress is not straightforward, as a number of obstacles must be overcome before this technique can be successfully applied. To address these challenges, it is crucial to understand the requirements for phenotyping, data collection, and analysis, which may vary depending on the conditions, the crop species, measured characteristics, and stage of growth (Liu et al., 2020a). A thorough understanding of plant light interactions, sensors, imaging platforms, and processing algorithms must be acquired to ensure that plant phenotyping meets the required criteria.

The reflectance and absorption of light are strongly influenced by the physiological and chemical characteristics of plants, which can change under stress and cause changes in the reflectance spectrum. During the measurement of plant growth, the near-infrared and visible spectral ranges play an important role. Non-imaging hyperspectral sensors have a wide electromagnetic spectrum range (350–2500 nm), whereas imaging sensors typically cover a limited range, mainly focusing on VIS-NIR (400–1000 nm) and sometimes containing short-wave infrared (1000–2500 nm). The use of these wavelengths enables hyperspectral technologies to observe changes in leaf pigment (400–700 nm), cellular composition (700-1300 nm), and water content (1300-2500 nm) in plants (Lowe et al., 2017; Zhang et al., 2020a). Fig. 1 provides a scheme of the main relationship between light reflectance and plant stress, paying special attention to the plant components which can affect the interactions with light. Considering that chlorophyll plays a role in photosynthesis and acts as a light absorber, fluctuations in chlorophyll levels due to stress may lead to changes in the interaction way between plants and light. As a result of stressful conditions, chlorophyll may be depleted, which can be detected in a broad spectrum as low reflection at 530-630 nm, and increased reflection at 700 nm. In addition to chlorophyll, plant pigments, such as carotenes and xanthophylls, also contribute to the plant's ability to reflect light (Zubler and Yoon, 2020). Also, carotenoids and anthocyanin help plants in defending themselves from a variety of environmental factors (Mishra et al., 2017). Furthermore, physical characteristics of leaves such as tissue morphology, cell wall characteristics, and epidermal thickness may change under stress, influencing the leaf's spectral characteristics. It has been observed that the reflectance around 960 nm is affected by cell elasticity, which decreases when the plant is subjected to drought (Zubler and Yoon, 2020). Moreover, leaf stomata can adversely impact leaf properties under stressful conditions, which are essential for the maintenance of leaf moisture and the regulation of gas exchange. As a result of stomatal closure, leaf temperature can rise, and it can be seen in the

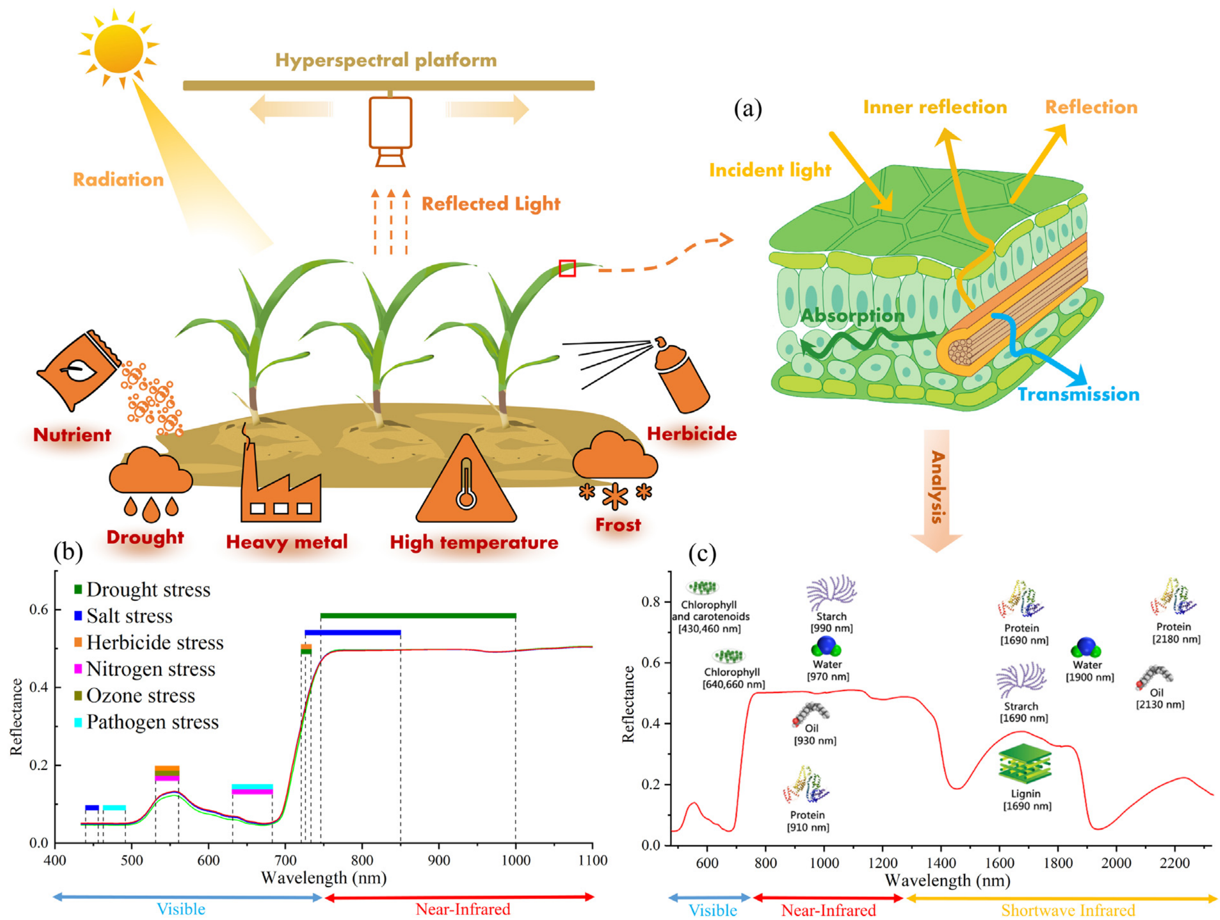

Fig. 1. Plant tissue interacts with incoming radiation for hyperspectral sensing of abiotic stresses. (a) cross-sectional view of a typical leaf and interaction between light and leaf, (b) a brief overview of plant spectral-sensitive regions in response to various stresses (Zhu et al., 2021), (c) characteristic spectral reflectance curve of leaf.

infrared wavelengths (Sawinski et al., 2013). Different cell wall components, proteins and carbohydrates of leaves can also change under various stress conditions and significantly impact their reflectance characteristics. For example, salt stress may adversely impact photosynthetic processes directly through the closing and limiting of mesophyll stomata, or indirectly through changes in cellular metabolism (Sytar et al., 2017). In addition to damaging plant cells, salt stress also causes ion toxicity. Therefore, the blue and red regions were also chosen as indicators of salt stress (Fig. 1b). These wavelengths are useful in characterizations of chlorophyll content, photosynthetic activity, and cellular architecture (Zhu et al., 2021). Moreover, since the light at infrared wavelengths is absorbed by water molecules, leaf water content can also affect the spectral response, and severe drought can change the structure of leaf mesophyll, which affects reflectance at near infrared wavelengths (Lowe et al., 2017).

1.2. Proximal sensing

The use of hyperspectral technology for close-range assessment of various characteristics of plants has become increasingly widespread in recent years. Although this technique is very promising, it is still facing some major challenges that are mainly related to the technical challenges associated with setup, data processing, and sample type. These technical challenges related to proximal sensing of plants have been discussed in a number of review papers (Liu et al., 2020b; Mishra et al., 2020, 2017). There are several hardware configurations behind hyperspectral technology and thus, measurements can be made in various ways. However, a critical component of a stress monitoring system is the sensor's ability to detect abiotic stress-induced changes in the spectral response of plants. Typically, the visible spectrum is the most important range for assessing plant stress, but other parts of the spectrum can also be affected (Zubler and Yoon, 2020). It is possible to apply the same sensor in an indoor or outdoor setting, and it may be installed at various distances from the sample, thereby providing different sensing scales. For the purpose of proximal sensing, both portable and fixed spectrometers can be used to capture spectra at leaf and canopy scales in laboratory and outdoor environments. Using proximal imaging, leaf stress characteristics such as pigment variations and the spatial distribution of leaf stress in a canopy may be examined. A common practice is to use proximal sensing for calibrating stress assessment methods that are designed to be incorporated into applications using airborne or satellite imaging spectroscopy (Laroche-Pinel et al., 2021). To avoid environmental interference, a non-imaging sensor (leaf-clip) that is equipped with an internal light is the ideal choice for measurements. The use of proximal hyperspectral technologies at canopy scales makes it possible to establish a link between leaf and large-scale measurements.

A variety of acquisition areas can be used to study canopy reflectance on a range of scales, from a single plant to multiple plants (Lassalle, 2021). Research studies often involve the exposure of plants to stressors in controlled environments that are reproducible and can be used to evaluate the intensity and duration of exposure to a single or multiple stressors (Mirzaei et al., 2019; Nguyen et al., 2020a; Tirado et al., 2021). Several stress exposure situations cannot be replicated in an experimental setting, whether the stressor is hard to manipulate or the species are particularly challenging (Cui et al., 2019; Grieco et al., 2022a). Therefore, measurements of leaf or canopy reflectance in the field may be conducted to adapt controlled environment methods or to obtain calibration data to test airborne and satellite-based imaging procedures (Laroche-Pinel et al., 2021). In many field applications, sensors mounted on land-based devices can achieve a high spatial resolution, allowing them to measure plant parameters at the leaf or canopy scale, with spatial resolutions of up to one centimeter (Grieco et al., 2022a; Jiang et al., 2020; Zhu et al., 2021). An overview of different setups used for proximal hyperspectral sensing of abiotic stress from 2019 to 2022 can be found in Fig. 2.

1.3. Data processing

Reflectance differences are able to reveal physiological characteristics of plants as well as assess a genotype's response to abiotic stressors using appropriate spectral analysis. While hyperspectral data are not always processed according to a standard procedure, in general, it comprises of four steps: (i) preprocessing, (ii) segmentation, (iii) variable extraction, and (iv) data analysis (Liu et al., 2020b). An appropriate data preprocessing method can improve spatial contrast, reduce interference signals, highlight objects, and thereby facilitates subsequent analysis. Using image segmentation, certain features of an image can be identified, including the main subject and the surrounding area. It can be employed for practical agricultural purposes to minimize errors caused by background noise. In particular, cluster-based methods, such as k-means, provide useful information regarding stressed areas of a plant (Mishra et al., 2021). The complete reflectance spectrum may be employed to assess plant health and can be integrated directly into machine learning algorithms. Since reflectance measurements are typically conducted at many wavelengths, a considerable amount of information may be redundant within a particular range of wavelengths, complicating the identification of optimal wavelengths to employ for monitoring a particular stressor. Therefore, spectral signatures must often be converted into abstract variables, such as principal components, to reduce dimensionality or select features. Many of the proximal HSI studies have successfully applied spectral reflectance indices (SRIs) that are directly related to plant characteristics, such as chlorophyll *a*nd water content, and are then used for subsequent analyses to assess plant status (El-Hendawy et al., 2019c; Ma et al., 2021a; Wang et al., 2020a). The SRIs are formed by combining a number of wavelengths corresponding to certain physiological properties that serve to describe abiotic stress reactions in plants (Żelazny and Lukáš, 2020). Reflectance-physiology relationships shown in Fig. 3 enable the rapid phenotyping of plants by computing SRIs based on their physiological characteristics and using predictive models developed by PLS (Mertens et al., 2021). Based on index-based linear regression models, the SRIs were assessed for drought detection and predicting physiological responses. The indices are dependent on WC, photosynthetic efficiency, pigment content, and red/NIR reflectance, and their models were compared to PLS ones to determine which one is better at monitoring drought effects. Because PLS uses all available wavelengths, there could be additional noise produced by some wavelengths. Therefore, SRI-based models with comparable accuracy to PLS models could be useful for predicting physiological traits based on hyperspectral data.

An effective method of monitoring plant stress involves evaluating the plant's spectral signature to help identify the level of stress at which the plant has been exposed. Conventionally, this evaluation was derived from a graphical analysis of leaf and canopy spectra. Later, data analysis is divided according to three general approaches: statistical analysis, prediction models, and classification models (Lassalle, 2021). In statistical analysis,

Fig. 2. Various proximal hyperspectral sensor setups for monitoring abiotic stress in plants under laboratory and field conditions. (a) personal photograph, (b) (Moroni et al., 2019), (c) (Pan et al., 2022), (d) (Ryckewaert et al., 2022), (e) (Żelazny and Lukáš, 2020), (f) (Bloem et al., 2020), (g) (Zhang et al., 2019b), (h) (Weksler et al., 2021), (i) (Grieco et al., 2022b), (j) (Jiang et al., 2020), (k) (Singh et al., 2020), (l) (Ma et al., 2021a).

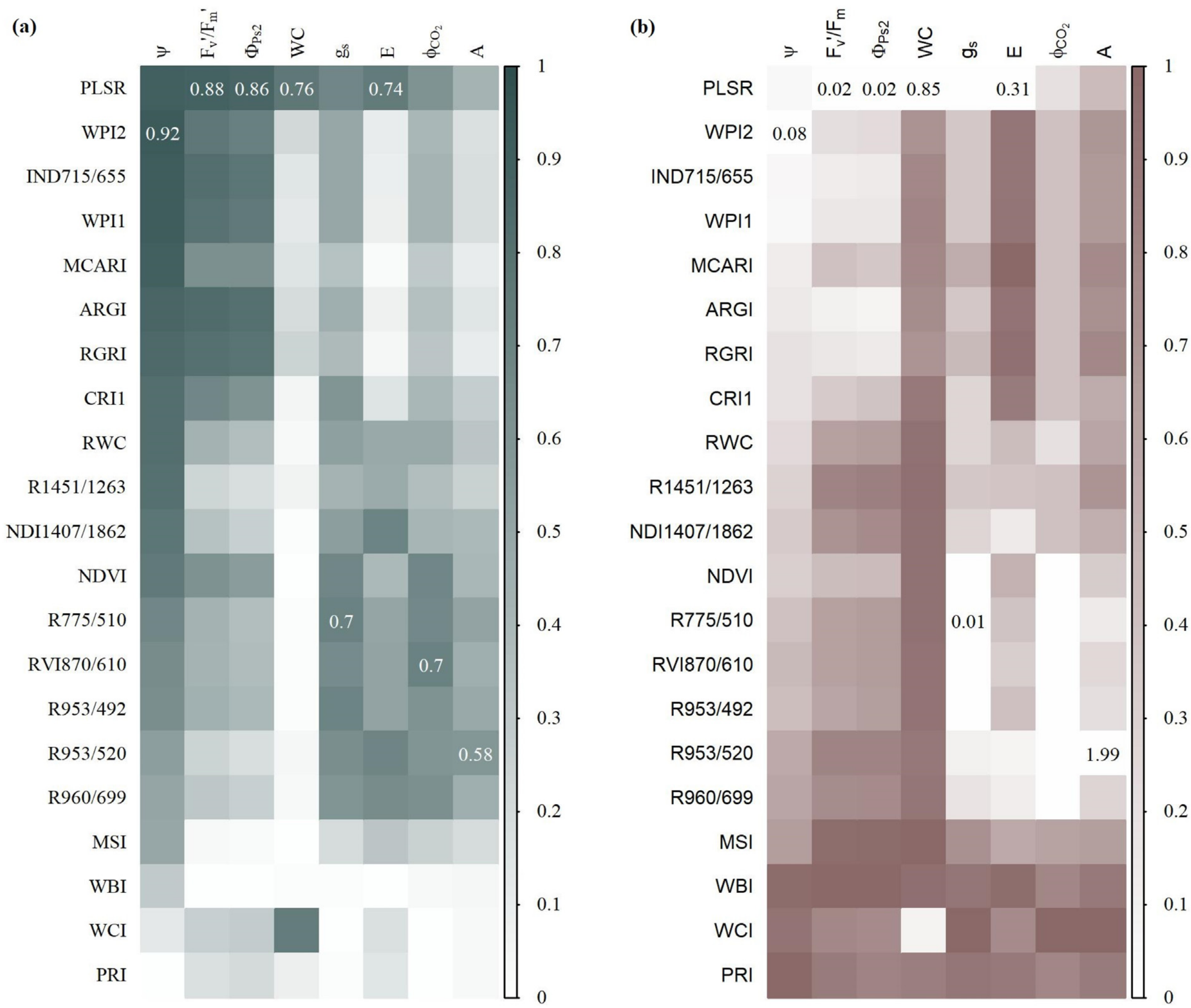

Fig. 3. Heatmap of R^2 values (a) and scaled RMSE values (b) to compare the prediction accuracy of SRI and PLS-based models (Mertens et al., 2021).

reflectance metrics are used to identify stressed and healthy plants (Weksler et al., 2020). A lack of relevancy between this method and newly developed reflectance measurements used to assess plant stress results in its inapplicability outside the study context, which severely limits its applicability. Prediction models that combine one or more input variables can calculate a continuous output variable, including the stressor directly or the biological or physiological symptoms associated with plant stress (Kumagai et al., 2022). Furthermore, classification models aim to develop a procedure that maps input data to categorical outputs which can be used to assess plant health (Zhang et al., 2019c). Inversion of radiative transfer models is common in remote sensing applications to extract key physiological parameters from spectra (Jin et al., 2019; Proctor et al., 2021). A number of characteristics, such as chlorophyll, moisture, and canopy structure, are obtained in models based on look-up tables or machine learning algorithms. However, this model is not appropriate for proximal hyperspectral technologies due to its lack of adaptability to specific illumination issues (Mohd Asaari et al., 2018).

According to our literature search, the most relevant review article is the meta-review conducted by Lassalle et al. (2021). This paper reviews the research works in which hyperspectral remote sensing was applied to monitor natural and anthropogenic plant stressors, in the period of 1970 to 2020, mainly from a statistical perspective. The survey was conducted using close-range and remote hyperspectral sensing approaches for studying both abiotic and biotic stresses in plants, at leaf and canopy scales. However, our review focuses more deeply and in greater detail on only close-range (proximal) hyperspectral sensing and all abiotic stresses. We also discuss the ability of the hyperspectral technology to detect the abiotic stresses, challenges, advantages, limitations, and so on, as well as interactions between the spectral reflectance and the stresses in detail. Furthermore, there are a few other review papers available, however they are not comprehensive enough to address all of the abiotic stresses that plants face in the natural environment (Galieni et al., 2021; Liu et al., 2020b; Mishra et al., 2020, 2017; Paulus and Mahlein, 2020). The studies provide an overview of lighting correction, machine learning techniques, and guidelines for applying hyperspectral imagery to plant phenotyping, from satellites to ground-based platforms.

All the applications considered in this review were conducted from 2019 to 2022, in seven different areas related to abiotic stressors in plants: nutrient deficiency, drought, salinity, heavy metal, herbicide, high and low temperatures and other environmental stresses. A total of 340 articles were published between 2010 and 2022, of which 182 articles were published in the period between 2019 and 2022 (Fig. 4). The articles described the use of proximal hyperspectral technologies for assessing abiotic stresses on plants in laboratory and field experiments. The following sections address applications of proximal hyperspectral technologies to each of the seven categories of abiotic stress, and in addition, full details of the studies from 2019 to 2022 are presented in Tables 1–7 for each stressor. The tables provide detailed information regarding each study, including study scale, stress type, plant, hyperspectral sensor, spectral range, sensor distance from target, measurement environment, data preprocessing, modeling approaches, and optimal performance. The modeling approaches column includes a list of different models used for prediction or classification, as

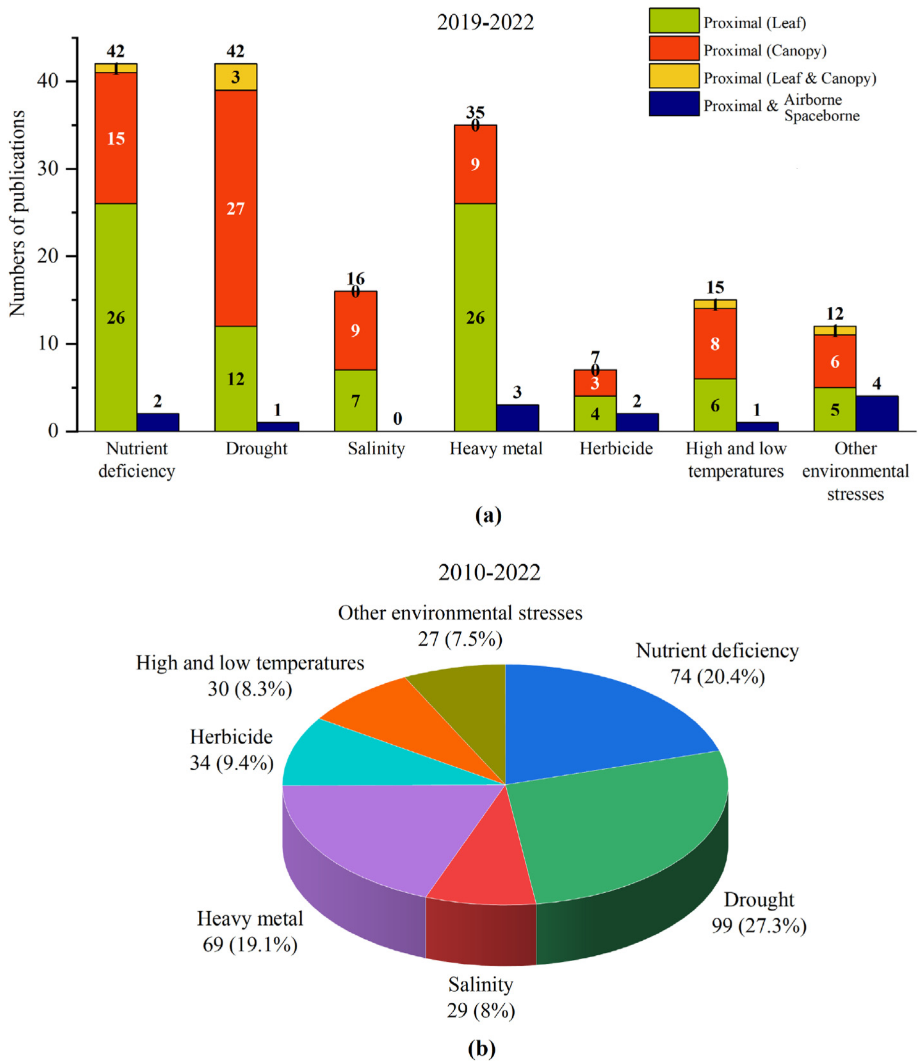

Fig. 4. Distribution of the number of publications in the field of monitoring plant abiotic stressors using proximal hyperspectral remote sensing during the years (a) 2019-2022 (b) 2010-2022.

well as techniques for selecting variables, spectral reflectance indices, and statistics if such approaches were employed.

2. Applications of proximal hyperspectral sensing

It has been demonstrated that leaf-scale hyperspectral measurements are less sensitive to external conditions such as lighting, climate, and humidity when compared to canopy-scale measurements. Basic laboratory research can benefit from this approach, since it can provide insight into the slight changes that occur in plants during stressful conditions. However, measurements made at the leaf level are not suited to practical use in the field due to their low throughput. By acquiring proximal hyperspectral images at canopy scale in the field, high spatial resolution can be achieved and measurement throughput is significantly increased. As well as its high accuracy, data collected this way is less likely to be adversely influenced by environmental factors due to its close proximity to the plant being studied. However, due to its limited capacity for detecting vegetation, it is insufficient to detect plant stress on a large scale (Pérez-Bueno et al., 2022). It is possible to identify different aspects of stress using different hyperspectral measurement scales. Specifically, leaf scale measurements reflect the effect on leaf biochemical characteristics. On the other hand, canopy scale studies can also be used to assess the effect on the structure of plants. Thus, leaf scale spectral indices may not be highly effective in detecting canopy scales due to the inherent bias associated with their transferrable characteristics (Li et al., 2019b).

In general, multiscale spectral indices would be more appropriate for practical purposes, as compared to indices based on a single scale. Stress-sensitive wavelengths at different scales have common characteristics, and are mostly found in the green, red, and near infrared wavelength ranges. As an example, changes in the structure and moisture content of leaves are associated with a reduction in reflection in the NIR region, which is also regarded as a reliable predictor of changes to canopy structure (Franke and Menz, 2007). The following stressors in plants have been considered: 1. nutrient deficiency, 2. drought, 3. salinity, 4. heavy metal, 5. herbicide, 6. high and low temperatures and 7. other environmental stresses. Several cases of leaf and canopy scale measurements under abiotic stress are discussed in the following sections.

2.1. Nutrient deficiency

Nitrogen poses the greatest restriction on crop growth since it has a direct correlation with photosynthesis and overall yields. Phosphorus, potassium, and micronutrients are also vital to the growth of plants and become deficient when plants are unable to properly absorb one or more of the aforementioned compounds (Lassalle, 2021). Nutrient deficiency may affect old or young leaves, resulting in limited growth of the plant and

Table 1
Research studies performed from 2019 to 2022 to detect nutrient deficiency using proximal hyperspectral technologies.

Scale	Stress type	Plant	HSI sensor	Spectral range (nm)	Distance to target (m)	Measurement environment	Data preprocessing	Modeling approaches	Optimal performance	Refs
Leaf	Nitrogen	Rice	Not mentioned	400-1000	0 (leaf clip)	Field	Not mentioned	DWMD, PCA, SPA, IRIV Prediction: PLS, ELM, GA-ELM	$R_p^2 = 0.683$	(Yu et al., 2020)
	Nitrogen	Rice	Fixed: ImSpector V10E (Spectral Imaging Ltd., Oulu, Finland)	400–1000	Not mentioned	Controlled environment	–	Visualization Classification: CNN	Accuracy $rate_p$ = 99.56 %	(Zhu et al., 2022)
	Potassium	Rice	Portable: FieldSpec Pro (ASD, Boulder, CO, USA)	350–2500	0 (leaf clip)	Field	1st Der	SRIs, correlation analysis Prediction: Linear regression	$R_p^2 = 0.77$	(Lu et al., 2020)
	Phosphorus	Rice	NH-7 (EBA JAPAN Co., Ltd.); SIS-I (EBA JAPAN Co., Ltd.)	500-1650	Not mentioned	Controlled environment, Field	SG, 1st Der-SG, 2nd Der-SG, SNV-SG, SNV- 1st Der-SG, SNV-2nd Der-SG	Visualization Prediction: PLS, RF	$R_p^2 = 0.75$	(Takehisa et al., 2022)
	Phosphorus	Cucumber	Fixed: ImSpector NI7E, Spectral Imaging Ltd., Oulu Finland	870–1770	Not mentioned	Controlled environment	–	PCA, ICA Classification: PCA, HCA, KNN, ANN	Accuracy $rate_p$ = 97.5 %	(Shi et al., 2022)
	Various nutrients	Orange	Portable: FieldSpec 2 (ASD, USA)	380 -1020	Not mentioned	Field	1st Der	Relief-F Prediction: DT, RF, KNN, ANN, SVM, RR, Lasso Regression	R_p^2 = 0.912-0.727	(Osco et al., 2020)
	Potassium	Peach	Portable: HSC-2 (Senop, Helsinki, FI)	500-900	0.3	Controlled environment	SG-1st Der, SG-2nd Der, MSC, SNV	PCA Prediction: PLS	$R_p^2 = 0.81$	(Abenina et al., 2022)
	Nitrogen	Olive	Portable: FieldSpec 4 (ASD, USA)	350- 2500	Not mentioned	Field	SG, SNV, 1st Der, 1st Der-SNV, 1st Der-SNV-SG, 2nd Der, 2nd Der-SNV, 2nd Der-SNV-SG	SRIs Prediction: Linear regression, PLS	R_v^2 = 0.71-0.56	(Rubio-Delgado et al., 2021)
	Nitrogen	Lettuce	Fixed: Specim FX-10 (Specim, Spectral Imaging Ltd., Oulu, Finland)	400–1000	Not mentioned	Controlled environment	1st Der	SRIs Prediction: linear regression, PLS, PCR	R_v^2 = 0.81 -0.97	(Eshkabilov et al., 2021)
	Nitrogen, drought	Spinach	Portable: CompactSpec dual-channel diode array spectrometer	305–2205	0.01	Field	2nd Der-SG	SRIs, CARS Prediction: PLS	$R_v^2 = 0.47$	(Rubo and Zinkernagel, 2022)
	Magnesium	Cucumber	Fixed: ImSpector V10E (Spectral Imaging Ltd., Oulu, Finland)	400–900	0.18	Controlled environment	–	Visualization Prediction: PLS, iPLS, SA-iPLS	$R_p^2 = 0.894$	(Shi et al., 2019)
	Nitrogen	Cucumber	Fixed: FSR, Fanavaran Physics Noor Co., Tehran, Iran	400–1000	1	Controlled environment	–	ANN-SA Prediction: ANN-PSO, CNN, PLS	$R_p^2 = 0.986$	(Sabzi et al., 2021a)
	Nitrogen	Cucumber	Fixed: FSR, Fanavaran Physics Noor Co., Tehran, Iran	400 -1100	1	Controlled environment	SNV-SG	ANN-ABC Classification: ANN-ICA	Accuracy $rate_p$ = 96.11 %	(Sabzi et al., 2021b)
	Nitrogen	Cucumber	Fixed: FSR, Fanavaran Physics Noor Co., Tehran, Iran	400–1100	1	Controlled environment	MSC, SG	CNN	$R_p^2 = 0.968$	(Pourdarbani et al., 2021)
	Nitrogen, magnesium, potassium	Cucumber	Fixed: FSR, Fanavaran Physics Noor Co., Tehran, Iran	400 -1100	1	Controlled environment	SNV	Visualization Prediction: PLS, iPLS, SiPLS, and GA-iPLS Classification: KNN	$R_p = 0.909$ Accuracy $rate_p$ = 96.67 %	(Shi et al., 2021)
	Nitrogen	Maize	Portable: LeafSpec, developed by the Purdue Phenotyping Lab group	450–900	0 (leaf clip)	Controlled environment, Field	–	SRIs, Visualization Prediction: AdaBoost, Logistic Regression, PLS, RF	R_p^2 = 0.771-0.880	(Ma et al., 2020; Wang et al., 2020c)
	Nitrogen, phosphorus, potassium, drought	Maize	Portable: FieldSpec 4 (ASD, USA)	350- 2500	0 (leaf clip)	Field	SG	SRIs, Correlation analysis Prediction: PLS, SVM	$R^2 > 0.85$	(Ge et al., 2019)

ARTICLE IN PRESS

	Nitrogen, phosphorus, potassium, drought	Maize	Portable: FieldSpec 2 (ASD, USA)	350- 2500	0 (leaf clip)	Controlled environment, Field	SG-1st Der	Prediction: PLS, SVM, RF, KNN, ANN, GDboost	$R_v^2 = 0.78$	(Singh et al., 2022b)
	Phosphorus	Maize	Portable: FieldSpec 3 (ASD, USA)	450-1000	0 (leaf clip)	Field	–	PCA Classification: LDA	Accuracy $rate_p = 85$ %	(de Oliveira et al., 2022)
	Nitrogen	Wheat	Portable: FieldSpec 2 (ASD, USA)	400- 2400	0 (leaf clip)	Field	SG-1st Der	Prediction: SVM, RF, KNN, ANN, GDboost	$R^2 > 0.85$	(Singh et al., 2022a)
	Nitrogen, phosphorus, potassium	Woody plants, shrubs and grasses,	Portable: FieldSpec 2 (ASD, USA)	350 -1000	0 (leaf clip)	Field	1st Der, Nor	SRIs, correlation analysis Prediction: Linear regression	$R_p^2 =$ 0.5–0.8	(Peng et al., 2020)
	Nitrogen, Iron	Avocado	Fixed: SVC HR-1024I (Spectra Vista Corp., USA)	400–970	0.50	Controlled environment	Nor	Correlation analysis Classification: FDA	Accuracy $rate_p = 100$ %	(Hariharan et al., 2019)
	Nitrogen, potassium, magnesium	Grapevine	Fixed: Pika XC2 HS benchtop (Resonon Inc., Bozeman MT, USA),	380–1000	0.57	Controlled environment	1st Der	SRIs, Classification: SVM	Accuracy $rate_p =$ 93.19 %	(Debnath et al., 2021)
	Various macronutrient	Oil palm	Portable: FieldSpec 4 (ASD, USA)	400-2500	0 (leaf clip)	Field	–	CFS Classification: NB, LMT	Accuracy $rate_p =$ 76.13-100 %	(Amirruddin et al., 2020)
	Nitrogen	Tea	Portable: FieldSpec 4 (ASD, USA)	400-2500	0 (leaf clip)	Controlled environment, Field	1st Der, SNV, MSC, DT, CR	GA, sensitivity analysis Prediction: RF, SVM, Cubist, SGB, KELM	$R_p^2 < 0.85$	(Yamashita et al., 2020)
Leaf & Canopy	Nitrogen	Wheat	Portable: FieldSpec 3 (ASD, USA); Fixed: WIWAM (FX10+ SWIR), Labscanner (FX10e) (Specim, Oulu, Finland)	350-2500	0 (leaf clip) and 1.4	Controlled environment	SG	SRIs Prediction: PLS	$R_v^2 =$ 0.75-0.86	(Liu et al., 2020c)
Canopy	Potassium	Pepper	Fixed: Specim FX-10 (Specim, Spectral Imaging Ltd., Oulu, Finland)	400–1000	2	Controlled environment	SG -SNV	SRIs Correlation analysis	–	(Weksler et al., 2020)
	Various nutrients	Barley	Fixed: HySpex SWIR 384, Norsk Elektro Optikk, Norway	1000-2500	1	Field	SNV, Nor	Prediction: PLS, MLP, RBF	$R_v^2 = 0.9$	(Grieco et al., 2022b)
	Various macronutrient	Bok choy, spinach	Fixed: OCI Imager (OCI-UAV-D1000), BaySpec Inc	460-983	1.5	Controlled environment	1st Der	Correlation analysis Classification: LDA	Accuracy $rate_p = 80$ %	(Nguyen et al., 2020b)
	Phosphorus	Sugar beet, celery, strawberry	Fixed: ImSpector V10E and N25E 2/3″	400–1000, 1000–2500	0.20	Controlled environment	2nd Der- SG	CFS Classification: ANN, SVM, NB, RF	Accuracy $rate_v =$ 45-100 %	(Siedliska et al., 2021)
	Various nutrients	Strawberry	Fixed: Resonon Pika XC2 (Resonon Inc., USA)	400-1000	Not mentioned	Controlled environment	–	Classification: Deep learning,	Accuracy rate = 100 %	(Yang, 2022)
	Nitrogen	Wheat	Portable: FieldSpec Pro (ASD, Boulder, CO, USA)	350–1075	1	Field	–	SRIs, correlation analysis Prediction: Linear regression	$R_v^2 = 0.861$	(Song et al., 2021)
	Nitrogen, drought	Maize	Portable: FieldSpec 2 (ASD, USA)	395–1004	0.1-0.6	Field	–	SRIs, PCA, correlation analysis Prediction: MLR	$R_v^2 = 0.57$	(Sellami et al., 2022)
	Potassium, salinity	Pepper	Fixed: FX10 (Specim, Spectral Imaging Ltd., Oulu, Finland)	400–1000	Not mentioned	Controlled environment	SNV-SG-1st Der	Classification: XGBoost, SVM Prediction: XGBoost	Accuracy $rate_v = 80$ % $R_v^2 = 0.75$	(Weksler et al., 2021)
	Nitrogen, phosphorous, potassium	Winter oilseed rape	Portable: PSR-3500 (Spectral Evolution, Lawrence, MA, USA); Portable: FieldSpec Pro (ASD, Boulder, CO, USA)	400-2300	1	Field	–	RF score Classification: RF, SVM, ANN	Accuracy $rate_v =$ 80.76 %	(Liu et al., 2020d)
	Nitrogen, phosphorous,	Radiata pine	Fixed: FX10 (Specim, Spectral Imaging Ltd., Oulu, Finland)	400–1000	2	Controlled environment	SG-1st Der	SRIs, correlation analysis, PROSAIL (Radiative transfer), RF	$R_v^2 = 0.80$	(Watt et al., 2020a, 2020b)

(continued on next page)

Table 1 (*continued*)

Scale	Stress type	Plant	HSI sensor	Spectral range (nm)	Distance to target (m)	Measurement environment	Data preprocessing	Modeling approaches	Optimal performance	Refs
								Prediction: gnls		
	Nitrogen	Maize	Fixed: MSV-101-W, Middleton Spectral Vision, Middleton, WI, USA	376–1044	7	Field	–	SRIs, Prediction: ANN, PLS	$R_v^2 = 0.822$	(Ma et al., 2021a, 2021b)
	Nitrogen, phosphorus	Grass–legume polycultures	Fixed: FX10, SWIR (Specim, Spectral Imaging Ltd., Oulu, Finland)	400-1000, 1000-2600	1.4	Controlled environment	SG	Prediction:PLS	$R_v^2 = 0.93$	(Ball et al., 2022)
	Various nutrients	Chamomile	Fixed: BaySpec OCI™-F Series (USA San Jose, California)	400-1000	1.5	Field	–	SRIs, correlation analysis, PCA	–	(Singh et al., 2020)

branching. Plant leaves become discolored and disfigured due to inadequate nutrition, whereas spectral reflectance can serve as an indicator that allows identification of nutritional status. The effects of nutritional deficiencies typically have an impact in the visible region owing to pigmentation changes and the yellowing of leaves leads to higher reflectance in the green-red region (Li et al., 2020). Moreover, it has been demonstrated that necrosis associated with various nutrient deficiencies increases reflectance, while in non-necrotic areas, the reflectance decreases (Lassalle, 2021). So, the use of hyperspectral images can be an effective method for determining crop nutrition in situ, allowing for consideration of its spatial and temporal variability. Studies conducted using proximal hyperspectral technologies to detect nutrient deficiencies are presented in Table 1.

2.1.1. Leaf scale

Rice production systems require a reliable method of nitrogen testing in order to ensure the proper and timely application of fertilizers. HSI was used by Yu et al. (2020) to overcome rice's nitrogen deficiency to achieve precise fertilization without affecting yield. The spectral reflectance and nitrogen content data were collected to determine the standard nitrogen content and reflectance in order to maximize yields. Data were reduced in dimensionality and they were used to establish regression models to evaluate the nitrogen content in japonica rice. It was determined that the GA-ELM prediction model treated by the DWMD demonstrated superior performance with the R^2 of training and validation sets higher than 0.68.

There is a similarity between the symptoms that occur during the early growth of leaves under phosphorus deficiency and those that affect healthy leaves during the early stages of senescence. As a result, it is difficult to detect them visually or through computer imaging. In a study performed by Shi et al. (2022), spectral images of cucumber leaves were captured, and a set of P deficiency characteristic signals were identified from the NIR. In this work, PCA and ICA methods were used to extract information from HSI images of leaves and it was found that ICA was effective in identifying water-stained plaques that result from P deficiencies. Also, PCA and HCA confirmed that the invisible symptoms were related to an early P deficiency through similarities in spectra between different regions of leaves. Based on that, it was possible to diagnose P deficiency 15 to 24 days in advance compared with other methods.

Analysis of macro- and micronutrients in situ is essential for the proper management of citrus plants, as an optimal nutrient content is the key to maximize profitability. Based on hyperspectral analysis of Valencia orange leaves, Osco et al. (2020) proposed a machine learning approach for quantifying macro- and micronutrient composition (N, P, K, Mg, S, Cu, Fe, Mn, and Zn). Several algorithms were employed, and the random forest model showed the best performance. For the purpose of determining responsible wavelengths, the Relief-F algorithm was used. The results demonstrated good prediction (R^2) for nutrients between 0.912 and 0.727.

For olive trees growing in semi-arid environments, nitrogen is one of the major limiting factors, so its measurement is necessary to determine the most appropriate fertilization method. The spectral properties of olive leaves were analyzed by Rubio-Delgado et al. (2021) to estimate their nutritional status using hyperspectral data. The vegetation indices, consisting of multiple wavelengths, as well as PLS models, were built and evaluated in terms of their prediction performance, while the reflectance curves were preprocessed to reduce noise. It was determined that wavelengths corresponding to N variation could be found in the visible and short-wave infrared wavelength ranges, representing chlorophyll a and b as well as nitrogen. The PLS models were more accurate than vegetation indices, although they were subject to higher levels of error due to the noise incorporated with the hyperspectral data.

There is a close relationship between leaf nitrogen content and the chlorophyll level of green leaves. The purpose of the study was to investigate variations in hyperspectral data to quantify nitrogen and chlorophyll concentrations (Fig. 5) (Yamashita et al., 2020). It was done to identify the nitrogen content of leaves in tea plants, which are large feeders and require large quantities of nitrogen to grow. Various machine learning and preprocessing methods were used to develop regression models. By using leaf

Table 2
Research studies performed from 2019 to 2022 to detect drought using proximal hyperspectral technologies.

Scale	Plant	HSI sensor	Spectral range (nm)	Distance to target (m)	Measurement environment	Data preprocessing	Modeling approaches	Optimal performance	Refs
Leaf	Soybean	Portable: FieldSpec 3 (ASD, USA)	350- 2500	0 (leaf clip)	Field	–	Stepwise procedure Classification: PCA, LDA	Accuracy $rate_p$ = 50-100 %	(Crusiol et al., 2021)
	Lemon	Portable: PSR-3500 (Spectral Evolution, Lawrence, MA, USA)	350- 2500	0 (leaf clip)	Controlled environment	–	SRIs Prediction: SVM, RF, GDboost, Adaboost	R_p^2 = 0.88-0.92	(Zhou et al., 2021c)
	Vine	Portable: FieldSpec 4 (ASD, Malvern Panalytical Ltd., Malver, UK)	350- 2500	0 (leaf clip)	Field	–	SRIs Prediction: Extra Trees, Linear regression	R_p^2 = 0.62	(Laroche-Pinel et al., 2021)
	Six agronomic species	Portable: PSR-3500 (Spectral Evolution, Lawrence, MA, USA)	350- 2500	0 (leaf clip)	Controlled environment, Field	–	VIP Prediction: PLS Classification: LDA, PLS-DA	R_p^2 = 0.49-0.87 Accuracy $rate_p$ = 66 %	(Burnett et al., 2021)
	Rice	Portable: FieldSpec 3 (ASD, USA)	350–2500	0 (leaf clip)	Controlled environment	–	SRIs Correlation analysis Prediction: PLS-MLR, PLS-ANN, SVM, RF, PLS, ANN	R_v^2 = 0.97	(Krishna et al., 2019)
	Lettuce	Portable: FieldSpec Pro (ASD, Boulder, CO, USA)	325–1075	Not mentioned	Controlled environment	–	Correlation analysis Classification: ANN, DT, SVM, RF, NB, Logistic Regression	Accuracy $rate_p$ = 93 %	(Osco et al., 2019)
	Soybean	Portable: FieldSpec 3 (ASD, USA)	325–1075	0.120	Controlled environment	1st Der	SRIs Correlation analysis Prediction: Linear regression	R_p = 0.736-0.860	(Kovar et al., 2019)
	Soybean	Portable: FieldSpec 3 (ASD, USA)	350–2500	0 (leaf clip)	Controlled environment	–	PCA Classification: LDA	Accuracy $rate_p$ = 84-100 %	(Guilherme Teixeira Crusiol et al., 2021)
	Radiata pine	Portable: FieldSpec 3 (ASD, USA)	400–2500	0.009–0.01	Controlled environment	–	SRIs Correlation analysis Prediction: Linear regression	R_p^2 = 0.86-0.90	(Watt et al., 2021)
	Tea	Fixed: Gaia field pro-v10, Finland	400–1100	0.38	Controlled environment	MSC-1st Der-SG, MSC-2nd Der-SG,	SPA, UVE, CARS Prediction: SVM, RF, PLS	R_p = 0.81-0.95	(Chen et al., 2021)
	Maize	Not mentioned	862.9-1704	Not mentioned	Controlled environment	–	PCA, KLD Prediction: SVM-PSO	R_p = 0.768	(Gao et al., 2019a)
	Wild rocket	Portable SPECIM IQ camera (Spectral Imaging Ltd., Oulu, FI)	400–1000	Not mentioned	Controlled environment	–	SRIs, Visualization Classification: ANN	Accuracy $rate_p$ = 73.3 %	(Navarro et al., 2022)
Leaf & Canopy	Maize	Portable: FieldSpec 4 (ASD, USA)	350–2500	0 (leaf clip) and 1.4	Field	–	SRIs, Correlation analysis, PROSPECT (Radiative transfer),	–	(Li et al., 2021d)
	Oak	Fixed: SVC HR-1024I (Spectra Vista Corp., USA)	400–2400	Not mentioned, 0.40	Controlled environment	–	Classification: PLS-DA	Accuracy $rate_p$ = 77.9 %	(Fallon et al., 2020)
	Haloxylon ammodendron	Portable: FieldSpec 4 (ASD, USA)	350-2500	0 (leaf clip) and 1	Field	1st Der	SCOPE (Radiative transfer), SRIs Prediction: polynomial regression	R_v^2 = 0.96	(Jin et al., 2019)
Canopy	*Bromus inermis* grass	Fixed: Headwall Photonics VNIR A-Series, USA	400 -1000	0.45	Controlled environment	1st Der	SRIs Classification: ANN, SVM, RF	Accuracy $rate_p$ = 100 %	(Dao et al., 2021)
	Bromus inermis grass	Fixed: Headwall Photonics VNIR A-Series, USA	400 -1000	0.50	Controlled environment	–	PROCOSINE, PROSPECT (Radiative transfer), sensitivity analysis	–	(Proctor et al., 2021)
	Arabidopsis thaliana	Fixed: HySpex VNIR-1800 (Norsk Elektro Optikk, Oslo, Norway)	407–997	1	Controlled environment	SG-Nor-SNV	PCA, deep learning, k-means	–	(Mishra et al., 2021)
	Oak	Fixed: Headwall Photonics, Fitchburg, MA, USA	545–1700	Not mentioned	Controlled environment	–	SRIs Prediction: Linear regression	R_p^2 = 0.66	(Mazis et al., 2020)
	Soybean, Maize	Fixed: Cubert UHD 185 camera (UHD; Cubert GmbH, Ulm, Germany)	450- 950	2	Controlled environment	SNV	SRIs, VIP Prediction: PLS	R_v^2 = 0.77–0.92	(Sobejano-Paz et al., 2020)
	Maize	Fixed: ImSpector V10E and N25E (Spectral Imaging Ltd., Oulu, Finland)	400–1000, 970–2500	1.5	Controlled environment	–	SRIs, VIP Prediction: PLS	R_v^2 = 0.86-0.92	(Mertens et al., 2021)
	Maize	Fixed: MSV-500 (Middleton Spectral Vision Co., USA)	380–1017	2.3	Controlled	–	SRIs, Visualization	–	(Zhang et al., 2019b)

(continued on next page)

Table 2 (*continued*)

Scale	Plant	HSI sensor	Spectral range (nm)	Distance to target (m)	Measurement environment	Data preprocessing	Modeling approaches	Optimal performance	Refs
					environment				
	Maize	Fixed: MSV-500 (Middleton Spectral Vision Co., USA)	370–1030	Not mentioned	Controlled environment	MSC	Prediction: CNN, PLS, SVM	$R_p^2 = 0.872$	(Rehman et al., 2020)
	Maize	Fixed: ImSpector V10E (Spectral Imaging Ltd., Oulu, Finland)	400-1000	Not mentioned	Controlled environment	SNV	SRIs	–	(Asaari et al., 2019)
	Maize	Portable: FieldSpec 3 (ASD, USA)	350–2500	1–1.3	Field	–	SRIs, Correlation analysis Prediction: Linear regression	$R_v^2 = 0.791$	(Zhang and Zhou, 2019)
	Maize	Fixed: ImSpector V10E (Spectral Imaging Ltd., Oulu, Finland)	400–1000	1.2	Controlled environment	SNV	Visualization Prediction: PLS, GPR, RR	$R^2 > 0.82$	(Mohd Asaari et al., 2022)
	Maize, sorghum	Fixed: Headwall Nano-Hyperspec (VNIR) imager (Headwall Photonics, Inc., Bolton, MA, USA)	400-1000	1.2	Controlled environment	1st Der	SRIs, PCA	–	(Manley et al., 2019)
	Rice	Portable: FieldSpec 3 (ASD, USA)	350–2500	0 (leaf clip)	Field	–	SRIs Prediction: PLS	$R_v^2 = 0.71$	(Krishna et al., 2021)
	Wheat	Portable: FieldSpec 3 (ASD, USA)	350–2500	1	Controlled environment	–	Correlation analysis, PLS, SPA Prediction: MLR, SMLR	$R_v^2 = 0.637$	(Xie et al., 2020a)
	Wheat	Portable: FieldSpec Pro (ASD, Boulder, CO, USA)	350–2500	0.15	Controlled environment	–	SRIs	–	(Li et al., 2022b)
	Peanut	Portable: FieldSpec 2 (ASD, USA)	325-1075	Not mentioned	Controlled environment	–	SRIs, Correlation analysis	–	(Chen et al., 2020)
	Potato	Fixed: 710 VP (Surface Optics Corp, San Diego, CA, USA)	400–1000	3	Controlled environment	–	Classification: RF, ANN, CNN, SVM, XGB, AdaBoost	Accuracy $rate_p$ = 100 %	(Duarte-Carvajalino et al., 2021)
	Oilseed rape	Fixed: Rikola, Senop, Oulu, Finland	503-903	0.70	Controlled environment	SG, MSC	SRIs, PCA	–	(Želazny and Lukáš, 2020)
	Grapevine	Fixed: HySpex VNIR-1600 and SWIR-384 (Norsk Elektro Optikk, Norway)	400-2500	Not mentioned	Field	SG, 2nd Der	VIP Classification: PLS-DA, SVM	Accuracy $rate_p$ = 97 %	(Zovko et al., 2019)
	Grapevine	Portable: FieldSpec 2 (ASD, USA)	325-1075	0.30	Field	–	SRIs Classification: RF, BT, GPR, VH-GPR	Accuracy $rate_p$ = 79- 100 %	(Pôças et al., 2020)
	Grapevine	Portable: SPECIM IQ camera (Spectral Imaging Ltd., Oulu, FI)	400-1000	1	Field	–	Prediction: PLS, SO-PLS	$R_p^2 = 0.699$	(Ryckewaert et al., 2022)
	Grapevine	Fixed: Headwall Photonics VNIR A-Series, USA	372-1006	1.4	Field	–	SRIs Classification: RF, ANN	Accuracy $rate_p$ = 73 %	(Thapa et al., 2022)
	Tomato	Fixed: HySpex VNIR-1600 and SWIR-384 (Norsk Elektro Optikk, Norway)	400-2500	3	Controlled environment	SG, 2nd Der	VIP Classification: PLS-DA, SVM	Accuracy $rate_p$ = 100 %	(Žibrat et al., 2019)
	Three species of Mediterranean shrubland	Portable: FieldSpec 4 (ASD, USA)	350–2500	0.1	Field	–	SRIs, VIP, Correlation analysis Classification: PLS-DA	–	(Mevy et al., 2022)
	Green roof plants	Portable: FieldSpec 4 (ASD, USA)	350–2500	0.15	Controlled environment	–	SRIs	–	(Moroni et al., 2019)
	Tall fescue	Portable: PSR-1100F (Spectral Evolution, Lawrence, MA, USA); Crop Circle ACS-430 (Holland Scientific, Inc., Lincoln, NE, USA)	320-1100	0.46	Field	–	SRIs, Correlation analysis Prediction: logistic regression	$R_p = 0.79$	(Badzmierowski et al., 2019)

Table 3
Research studies performed from 2019 to 2022 to detect salinity using proximal hyperspectral technologies.

Scale	Plant	HSI sensor	Spectral range (nm)	Distance to target (m)	Measurement environment	Data preprocessing	Modeling approaches	Optimal performance	Refs
Leaf	Rice	Portable: GER 1500, Spectra Vista Corp., Poughkeepsie, New York	282-1097	Not mentioned	Field	SG	SRIs, PCA, PLS Prediction: PLS, ELNET, SVM, GPR, MARS, RF, XGB, GAM, KNN	R_v = 0.823-0.934	(Das et al., 2020)
	Pomegranate	Portable: FieldSpec 4 (ASD, USA)	400–2400	0 (leaf clip)	Controlled environment	–	SRIs Prediction: Linear regression Classification: PLS-DA	R^2_v = 0.61–0.79 Accuracy $rate_p$ = 80-90 %	(Calzone et al., 2021)
	Lettuce	Portable: SVC HR-1024I (Spectra Vista Corp., USA)	350–2500	0 (leaf clip)	Controlled environment	–	SRIs, VIP Prediction: PLS Classification: PCA + PLS-DA	R^2_v = 0.70–0.84 Accuracy $rate_p$ = 0.33-0.91 %	(Cotrozzi and Couture, 2020)
	Tomato	Fixed: Gaia Field-Pro-V10 microscopic	400–1000	Not mentioned	Controlled environment	SNV, Nor MSC, detrending, SG	SPA, VISSA, VCPA Prediction: PLS, PCR	R_v = 0.81	(Wu et al., 2022)
	Olive	Portable: FieldSpec 3 (ASD, USA)	350–2500	0 (leaf clip)	Controlled environment	Nor-1nd Der-SG	SRIs Prediction: PCR, PLS Classification: Correlation analysis + LDA	R^2_v = 0.938 Accuracy $rate_p$ = 64.58-84.88 %	(Boshkovski et al., 2022)
	Barley	Fixed: Hyperspec UV-VIS-line scanner (Headwall Photonics, Bolton, MA, USA)	240–500	0.40	Controlled environment	–	Comparison analysis with non-imaging UV-spectrometer	–	(Brugger et al., 2019)
	Rosemary	Portable: FieldSpec 4 (ASD, USA)	350–2500	Not mentioned	Controlled environment	–	SRIs, Correlation analysis	–	(Atun et al., 2020)
Canopy	Wheat	Fixed: Resonon Pika XC2 (Resonon Inc., USA)	400–1000	10	Field	SG	SRIs, VIP-PLS-MIR Prediction: linear, quadratic, exponential models	$R^2_p \geq 0.63$	(Zhu et al., 2021)
	Spartina alterniflora	Fixed: Headwall Photonics VNIR E-Series, USA	400 -1000	Not mentioned	Controlled environment, Field	SG, 1st Der, 2nd Der,	SRIs Prediction: ELNET, stepwise regression	R^2_v = 0.74-0.99	(Goldsmith et al., 2020)
	Okra	Fixed: ImSpector V10E (Spectral Imaging Ltd., Oulu, Finland)	380–1030	0.24	Controlled environment	–	Deep learning Prediction: PLS	R^2_v = 0.588-0.835	(Feng et al., 2020)
	Wheat	Portable: FieldSpec 4 (ASD, USA)	350–2500	1	Field	–	SRIs Prediction: MLR	R^2_v = 0.38-0.79	(El-Hendawy et al., 2021a)
	Wheat	Portable: FieldSpec Pro (ASD, Boulder, CO, USA)	350–2500	0.80	Field	–	Correlation analysis, SRIs, VIP Prediction: PLS, MLR	$R^2_v \geq 0.7$	(El-Hendawy et al., 2019d)
	Wheat	Portable: FieldSpec Pro (ASD, Boulder, CO, USA)	350–2500	0.80	Field	–	Correlation analysis, SRIs Prediction: PLS	R^2_v = 0.63-0.98	(El-Hendawy et al., 2019c)
	Wheat	Portable: FieldSpec Pro (ASD, Boulder, CO, USA)	350–2500	0.80	Field	–	Correlation analysis, SRIs Prediction: linear and quadratic fitting models	R^2_v = 0.50-0.93	(El-Hendawy et al., 2019b)
	Wheat	Portable: FieldSpec 4 (ASD, Boulder, CO, USA)	350–2500	0.80	Field	–	Correlation analysis, SRIs Prediction: MLR	R^2_v = 0.64-0.85	(El-Hendawy et al., 2021b)
	Wheat	Portable: FieldSpec 4 (ASD, Boulder, CO, USA)	350–2500	0.80	Field	–	VIP Prediction: PLS, MLR	R^2_v = 0.43-0.95	(El-Hendawy et al., 2019a)

reflectance measurements from green and albino yellow leaves, data-based sensitivity analysis revealed considerable differences in signal detected for quantifying nitrogen and chlorophyll contents, particularly between 1325 and 1575 nm, indicating a nitrogen content-specific wavelength range.

2.1.2. Canopy scale

Monitoring plant physiological status throughout the day and taking multiple images of plants are crucial aspects for understanding hourly variations and effects. A moving hyperspectral camera was developed by Weksler et al. (2020) in order to collect multiple measurements of the greenhouse throughout the day, which are continuously tracked by physiological sensors. This system provided insight into the correlation between the spectral and physiological characteristics of potassium-treated pepper plants. There were significant correlations between the spectra and momentary transpiration rates using three bands (523, 697, and 818 nm). Obtained results indicate that the time of spectral measurements in relation to the physiological condition of plants can provide important information, which varies across plant types and needs to be considered when acquiring remote sensing data.

The enrichment of plant nutrients has been a key aspect for public health, and is of growing significance to the agricultural industry. To enhance agronomic properties, including nutrient concentration, 25 wild barley accessions have been crossed with the elite cultivar to make HEB-25. A study by Grieco et al. (2022b) investigated the potential of HSI for predicting the concentration of micro and macronutrients in the leaves of the HEB-25 plants collected at different stages of development. The aim was to establish quantitative models to explain leaf nutrient uptake, as well as plant physiology and yield characteristics, to demonstrate the relationship between them. In particular, the predictability of N, P, and K leaf concentrations was high, and a R^2 of 0.90, 0.75 and 0.89 was obtained, respectively. In this way, plant breeders could assess nutrient concentrations in large fields for purposes of selecting plants better adapted to enhance the concentration of nutrients in harvested edible parts.

A novel night-based HSI system was developed by Nguyen et al. (2020b) to assess leaf reflectance of bok choy and spinach under high, medium, and low fertilization conditions. This study has identified spectral bands where leaf reflectance can be used to accurately measure crop response to fertilizers. Moreover, a strong relationship between leaf

Table 4
Research studies performed from 2019 to 2022 to detect heavy metal using proximal hyperspectral technologies.

Scale	Stress type	Plant	HSI sensor	Spectral range (nm)	Distance to target (m)	Measurement environment	Data preprocessing	Modeling approaches	Optimal performance	Refs
Leaf	Copper	Chicory	Portable: FieldSpec Pro (FR, ASD, USA)	350-2500	0 (leaf clip)	Controlled environment	CWT	SRIs, VIP Prediction: PLS	$R_v^2 = 0.848$	(Lin et al., 2021)
	Copper, lead	Maize	Fixed: SVC HR-1024I (Spectra Vista Corp., USA)	350-2500	0.05	Controlled environment	VMD	PCA Classification: SVM	$OA_V = 0.75$-1	(Li et al., 2021a)
	Copper, lead	Maize	Fixed: SVC HR-1024I (Spectra Vista Corp., USA)	350-2500	0.05	Controlled environment	–	Correlation analysis, visualization	–	(Fu et al., 2020)
	Copper, lead	Maize	Fixed: SVC HR-1024I (Spectra Vista Corp., USA)	350-2500	0.05	Controlled environment	CR, FOD	SRIs Classification: NB	Accuracy rate$_p$ = 100 %	(Li et al., 2021b)
	Copper	Maize	Fixed: SVC HR-1024I (Spectra Vista Corp., USA)	350-2500	0.05	Controlled environment	DFT, DWT	Reflectance ratios	–	(Wang et al., 2020d)
	Cadmium	Rice	Fixed: ImSpector V10E (Spectral Imaging Ltd., Oulu, Finland)	400-1000	0.27	Controlled environment	–	GA CARS, Bw Prediction: PLS, SVM, ELM	$R_p = 0.943$	(Shen et al., 2020)
	Cadmium	Rice	Portable: UniSpec, PP systems, Haverhill, MA, USA	300–1150	0 (leaf clip)	Controlled environment	1st Der	Prediction: PLS	$R_v^2 = 0.873$	(Zhou et al., 2019a)
	Cadmium, lead (leaf and soil)	Rice	Portable: UniSpec, PP systems, Haverhill, MA, USA	310–1100	0 (leaf clip)	Field	1st Der, 2nd Der	SRIs Prediction: PLS	$R_v^2 = 0.592$	(Zhou et al., 2019b)
	Cadmium, lead	Lettuce	Fixed: ImSpector V10E (Spectral Imaging Ltd., Oulu, Finland)	400.68–1001.61	0.45	Controlled environment	SG	WT, SCAE Prediction: SVM	$R_p^2 = 0.942$	(Zhou et al., 2020a)
	Cadmium	Lettuce	Fixed: ImSpector V10E (Spectral Imaging Ltd., Oulu, Finland)	380–1030	0.45	Controlled environment	SG, SG-SNV, SG-SNVD, SG-1st, SG-2nd, SG-3rd, SG-4th	SPA, PLS, SAE Prediction: SVM	$R_p^2 = 0.949$	(Xin et al., 2020)
	Cadmium	Lettuce	Fixed: ImSpector V10E (Spectral Imaging Ltd., Oulu, Finland)	431.05- 962.45	Not mentioned	Controlled environment	WT, 1st Der, 2nd Der	PCA, IRIV, VISSA Classification: SVM, GOA-SVM	Accuracy rate$_p$ = 98.57 %	(Zhou et al., 2019)
	Cadmium	Lettuce	Fixed: ImSpector V10E (Spectral Imaging Ltd., Oulu, Finland)	480-1010	Not mentioned	Controlled environment	–	WT, PCA Classification: SVM, CS-SVM	Accuracy rate$_p$ = 94.19 %	(Zhou et al., 2021b)
	Cadmium	Lettuce	Fixed: ImSpector V10E (Spectral Imaging Ltd., Oulu, Finland)	431–961	0.45	Controlled environment	SG–SNV	PSA Prediction: PLS, SVM, PSO-DBN	$R_p^2 = 0.923$	(Sun et al., 2019)
	Cadmium	Lettuce	Fixed: ImSpector V10E (Spectral Imaging Ltd., Oulu, Finland)	400-1000	Not mentioned	Controlled environment	SNV, 1st Der, 2nd Der, 1st Der-SNV, 2nd Der-SNV	IRIV, WT Prediction: SVM	$R_p^2 = 0.884$	(Zhou et al., 2021a)
	Lead	Lettuce	Fixed: ImSpector V10E (Spectral Imaging Ltd., Oulu, Finland)	478–978	Not mentioned	Controlled environment	–	CARS Classification: PLS-DA, SVM, DBN	Accuracy rate$_p$ = 96.67 %	(Sun et al., 2021)
	Lead	Lettuce	Fixed: ImSpector V10E (Spectral Imaging Ltd., Oulu, Finland)	480.46-1001.61	0.45	Controlled environment	SNV, 1st Der, 2nd Der, 3rd Der, 4th Der	WT, MC, SAE Prediction: SVM	$R_p^2 = 0.947$	(Zhou et al., 2022c)
	Lead	Lettuce	Fixed: ImSpector V10E (Spectral Imaging Ltd., Oulu, Finland)	400.68-1001.61	Not mentioned	Controlled environment	SG, SNV, 1st Der, 2nd Der,	WT, SAE Prediction: SVM	$R_p^2 = 0.959$	(Zhou et al., 2020b)
	Lead	Tea	Portable: FieldSpec 4 (ASD, USA)	350-2500	0 (leaf clip)	Controlled environment	–	CFS, PLS, Correlation analysis Prediction: PLS, RBF Classification: LDA	$R_p = 0.952$ Accuracy rate = 91.67 %	(Sanaeifar et al., 2022a)
	Lead	Tea	Portable: FieldSpec 4 (ASD, USA)	350-2500	0 (leaf clip)	Controlled environment	SNV, detrending, Nor, MSC	SPA, CARS, CARS-SPA, Correlation analysis Prediction: PLS, PCR Classification: PLS-DA	$R_p = 0.931$ Accuracy rate = 97.9 %	(Sanaeifar et al., 2022b)
	Cadmium	Tomato	Fixed: ImSpector V10E (Spectral	431.05-962.45	Not	Controlled	OSC, SNV, SNV	WT	$R_p^2 = 0.893$	(Jun et al., 2019)

			Imaging Ltd., Oulu, Finland)		mentioned	environment	detrending, 1st Der, 2nd Der	Prediction: SVM		
	Lead	Oilseed rape	Fixed: ImSpector V10E (Spectral Imaging Ltd., Oulu, Finland)	400.68-1000.61	0.45	Controlled environment	1st Der	CARS, MRF Prediction: SVM, HHO-SVM	$R_p^2 = 0.943$	(Cao et al., 2021)
	Zinc	Oilseed rape	Fixed: ImSpector V10E (Spectral Imaging Ltd., Oulu, Finland)	431.04–962.45	0.4	Controlled environment	MSC	Deep learning, SPA, VISSA Prediction: SVM	$R_p^2 = 0.957$	(Fu et al., 2022)
	Various heavy metals	Peach	Portable: FieldSpec 4 (ASD, USA)	350–2500	0.05–0.10	Field	1st Der	SRIs Prediction: Linear regression	$R_p^2 > 0.8$	(Liu et al., 2021b)
	Various heavy metals	Grapevine	Portable: FieldSpec3 (ASD, Inc., USA)	350–2500	Not mentioned	Controlled environment	Nor	SRIs, PLS Prediction: SVM, Linear regression	$R_p^2 = 0.56\text{-}0.86$	(Mirzaei et al., 2019)
	Cadmium	*Miscanthus sacchariflorus*	Fixed: ImSpector V10E (Spectral Imaging Ltd., Oulu, Finland)	380–1030	0.263	Controlled environment	WT	SRIs, SPA, CARS Prediction: PLS, SVM	$R_p^2 = 0.91$	(Feng et al., 2019)
	Copper	*Jatropha curcas* L. (stem and root)	Fixed: Headwall Photonics SWIR M series, Fitchburg, MA, USA	900-2500	Not mentioned	Controlled environment	SG, SG-SNV, SG-MSC, SG-1st, SG-2nd, SG-MSC-1st, SG- MSC-2nd, SG-SNV-1st	Classification: PCA, LDA	Accuracy $\text{rate}_c = 83.93$ %, sensitivity_v and specificity_v (>0.70)	(García-Martín et al., 2020)
Canopy	Cadmium	Basil, kale	Fixed: Middleton Spectral Vision (Middleton, Wisconsin, USA)	400-998	Not mentioned	Controlled environment	–	SRIs, visualization	–	(Zea et al., 2022)
	Copper, cesium	*Arabidopsis thaliana*	Fixed: Headwall Photonics VNIR *E*-Series, USA	400-1000	0.305	Controlled environment	–	MCR, visualization	–	(Ruffing et al., 2021)
	Copper	Seriphidium terrae-albae	Portable: FieldSpec3 (ASD, Inc., USA)	350-2500	0.20	Field	SG, 1st Der	SRIs Prediction: Linear regression	$R_p^2 = 0.55$	(Cui et al., 2019)
	Copper	Wheat	Portable: AvaSpec-ULS2048FT-SPU Spectrometer, Netherlands Avantes	350–1000	0.5	Field	1st Der	SRIs Prediction: Linear regression	$R_p^2 = 0.65\text{-}0.72$	(Wang et al., 2020a)
	Cadmium, lead	Rice	Portable: FieldSpec3 (ASD, Inc., USA)	350-2500	0.30	Controlled environment	Nor-SG-1st, SG- Nor-1st, SG- Nor-2nd, SG-Sta-1st, SG-Sta-2nd, Nor-Sta-SG-1st, Nor-Sta-SG-2nd, Nor-SG-Sta-1st, Nor-SG-Sta-2nd, Sta-SG- Nor-1st	Significant bands Prediction: PLS, SVM	$R_p^2 = 0.7$	(Zhang et al., 2020b)
	Cadmium, lead	Rice	Portable: FieldSpec3 (ASD, Inc., USA)	350-2500	Not mentioned	Controlled environment	SG-2nd, Nor-1st	Significant bands, RF Classification: SVM	Accuracy $\text{rate}_p > 0.6$	(Zhang et al., 2019c)
	Cadmium, lead	Rice	Portable: FieldSpec3 (ASD, Inc., USA)	350-2500	0.20	Controlled environment	SG, Sta, 1st Der	Significant bands, RF, SRIs Classification: SVM	Accuracy $\text{rate}_p = 0.85\text{-}0.96$	(Zhang et al., 2021a)
	Mercury	Tobacco	Fixed: ImSpector V10E (Spectral Imaging Ltd., Oulu, Finland)	400–1000	0.260	Controlled environment	–	PCA, CARS Classification: PLS-DA, SVM	Accuracy $\text{rate}_p = 51.11\text{-}66.67$ %	(Yu et al., 2021)
	Copper	B. megistophylla, *B. microphylla*, *R. willmottiae*	Portable: FieldSpec Pro (FR, ASD, USA)	400-2500	0.90	Controlled environment	–	SRIs, Correlation analysis	–	(Zhao et al., 2020)

Table 5
Research studies performed from 2019 to 2022 to detect herbicide stress using proximal hyperspectral technologies.

Scale	Stress type	Plant	HSI sensor	Spectral range (nm)	Distance to target (m)	Measurement environment	Data preprocessing	Modeling approaches	Optimal performance	Refs
Leaf	Glyphosate	Maize	Fixed: Resonon Pika XC2 (Resonon Inc., USA)	400–900	1	Field	–	SPA, sensitivity analysis Classification: KNN, RF, SVM	Accuracy $rate_p$ = 75 %	(Zhang et al., 2021b)
	Glyphosate	Johnsongrass	Portable: FieldSpec Pro (ASD, Boulder, CO, USA)	325–1075	0.1	Controlled environment	–	SPA Classification: KNN, RF, SVM, LDA	Accuracy $rate_p$ = 77 %	(Huang et al., 2022)
	Dicamba	Soybean	Fixed: Resonon Pika XC2 (Resonon Inc., USA)	400–900	1	Field	–	SRIs, sensitivity analysis Classification: NB, RF, SVM	Accuracy $rate_p$ = 94 %	(Zhang et al., 2019a)
	56 % MCPA-Na, Mesosulfuron-methyl, Isoprouron	Wheat	Fixed: ImSpector V10E (Spectral Imaging Ltd., Oulu, Finland)	400-1000	Not mentioned	Controlled environment	1st Der-SG	SCNN-FS Classification: SCNN	Accuracy $rate_p$ = 96 %	(Chu et al., 2022b)
Canopy	Quinclorac	Rice	Fixed: FX10 (Specim, Spectral Imaging Ltd., Oulu, Finland)	380–1030	0.35	Controlled environment	WT-SG	Visualization, PCA Classification: SVM	Accuracy $rate_p$ =85-100 %	(Wang et al., 2020b)
	Glyphosate	Rolled grass sod	Fixed: SVC HR-1024I (Spectra Vista Corp., USA); Portable SPECIM IQ camera (Spectral Imaging Ltd., Oulu, FI)	350–2500	0.80, 0.36	Controlled environment	SG	SRIs, visualization Prediction: Linear regression	$R^2 > 0.86$	(Bloem et al., 2020)
	Triclopyr, diquat	*Pinus contorta* (Douglas)	Fixed: FX10 (Specim, Spectral Imaging Ltd., Oulu, Finland)	400-1000	2	Controlled environment	–	SRIs, visualization Prediction: SVM, PLS, ELNET	$R_v^2 = 0.65$	(Scholten et al., 2019)

reflectance and nutrient content was also found. It was found that leaf reflectance measurements can be used to determine fertilization levels with 75 % and 80 % accuracy for bok choy and spinach, respectively. A major purpose of the research was to explore the potential of remote sensing techniques to assess crop nutrition after sunset, without affecting operations.

Siedliska et al. (2021) developed discrimination models to analyze phosphorus content during different growth stages of wild celery, strawberry and sugar beet crops under differing fertilization regimes. Measurements from hyperspectral imaging were incorporated into supervised machine learning algorithms to classify plants based on four P fertilization levels. It is feasible to accurately see how much phosphorus is present at the beginning of the growth process. However, the accuracy of the classification increases as the plant grows.

2.2. Drought

Drought is a natural occurrence caused by a lack of rain over an extended period of time that contributes to water shortages. Drought occurs in all climates, which is characterized by a wide range of negative effects reducing plant growth, crop yield, and food quality (Jiao et al., 2021). Plants that are exposed to water stress undergo a series of physiological and biochemical reactions that vary with severity and duration. Lack of water can result in reduced levels of photosynthesis in the plant as a result of the closing of the stomata. Symptoms of a severe drought include the loss of leaf moisture, wilting and curling of leaves, and drooping of branches, followed by the degradation of chlorophyll levels and an overall reduction in leaf surface area. In addition, minor to moderate drought conditions can affect the concentration of carotenoids in plants (Lassalle, 2021). Water stress has a direct impact on the reflectance of vegetation. Reduced chlorophyll on leaves increases reflectance in the visible region and changes the position of the red edge. Due to changes in leaf moisture content, an increase in reflectance can also be found at wavelengths associated with water absorption (Fallon et al., 2020). Water stress can be irreversible before visible symptoms become apparent, which is why identifying plant physiological changes at an early stage is important for preventing crop losses (Gerhards et al., 2019). The continuous spectral data available from hyperspectral imagery may provide greater insight into how plants respond to water stress. Table 2 presents studies conducted using proximal hyperspectral technologies to detect drought.

2.2.1. Leaf scale

Genetic variation in soybeans should be studied for a variety of reasons, including intellectual property protection, increasing agricultural production efficiency, and improving seed breeding practices. Crusiol et al. (2021) examined hyperspectral technology for developing classification of soybean genotypes subjected to a wide range of water availability conditions during various stages of plant development. In PCA, 94 % of the spectral variance of soybean genotypes can be explained by the first three principal components, mainly SWIR wavelengths. Up to 138 spectral bands were selected in a stepwise process for soybean genotype discrimination. The LDA was carried out using measurements from samples grown under various water conditions and at various stages of physiological development, showing an accuracy of between 50 % and 100 % in the validation set.

A comprehensive assessment of drought impacts on fruit trees are essential for effective farming and understanding their physiological characteristics, together with yield predictions. Zhou et al. (2021c) investigated the application of hyperspectral data for the early detection of drought and leaf photosynthetic properties in citrus trees under greenhouse conditions. Studies of citrus physiology using gas exchange techniques were complemented by measurements of hyperspectral reflectance of leaves, which were undertaken on citrus grown under various drought conditions.

Table 6
Research studies performed from 2019 to 2022 to detect temperature-induced stress using proximal hyperspectral technologies.

Scale	Stress type	Plant	HSI sensor	Spectral range (nm)	Distance to target (m)	Measurement environment	Data preprocessing	Modeling approaches	Optimal performance	Refs
Leaf	Frost	Wheat	Fixed: Resonon Pika XC2 (Resonon Inc., USA)	392–889	0.20	Controlled environment	–	SRIs	–	(Murphy et al., 2020)
	Frost	Blueberry bud	Fixed: Micro-Hyperspec VNIR (X-Series, Headwall Photonics, Fitchburg, MA, USA)	517–1729	0.348	Controlled environment	Nor	PCA, SPA Classification: PLS-DA, QDA	Accuracy $rate_p$ = 64-82 %	(Gao et al., 2019, 2021)
	Frost	Tea	Not mentioned	871–1766	Not mentioned	Controlled environment	Nor	Prediction: PLS, PCR, Linear regression	$R_v^2 = 0.968$	(Asante et al., 2021)
	Drought, heat	Cotton	Portable: FieldSpec 3 (ASD, USA)	350-2500	0 (leaf clip)	Field	–	PCA, HCA, SRIs Prediction: PLS	$R^2 > 0.70$	(Melandri et al., 2021)
	Heat	Soybean	Portable: FieldSpec 4 (ASD, USA)	400-2500	0 (leaf clip)	Field	–	SRIs Prediction: PLS, RR, LASSO, SVM, linear regression	R_p^2 = 0.48-0.65	(Kumagai et al., 2022)
Leaf & Canopy	Frost	Wheat	Portable: FieldSpec 3 (ASD, USA); Spectral Libraries	350–2500	0 (leaf clip), 1.5, 0.40, 0.15	Field	–	SMA, SRIs	R^2 = 0.58–0.75	(Fitzgerald et al., 2019)
Canopy	Frost	Loblolly pine	Fixed: Resonon Pika XC2 (Resonon Inc., USA)	390–1000	Not mentioned	Controlled environment	–	SPA Prediction: PLS Classification: SVM, LDA	$R_p^2 = 0.78$ Accuracy $rate_p$ = 97 %	(Lu et al., 2021b, 2021a)
	Frost	Wheat	Portable: FieldSpec 3 (ASD, USA)	350–2500	0.30, 1	Controlled environment, Field	–	SRIs, Correlation analysis, SPA Prediction: MLR, PCR	$R_v^2 = 0.841$	(Xie et al., 2020b)
	Frost	Maize	Fixed: Resonon Pika XC2 (Resonon Inc., USA)	395-885	Not mentioned	Controlled environment	SG-1st Der	Classification: CNN	Accuracy $rate_p$ = 41.8 %	(Yang et al., 2019)
	Heat	Ginseng	Fixed: VIS/NIR, SWIR (Headwall Photonics, Fitchburg, MA, USA)	400–1800	0.26	Controlled environment	–	VIP-SPA, Visualization Classification: PLS-DA,	Accuracy $rate_p$ = 98.9 %	(Park et al., 2021)
	Heat	Rice	Portable: FieldSpec Pro (ASD, Boulder, CO, USA)	350–2500	1	Field	–	Correlation analysis, SRIs Prediction: linear regression	$R_p^2 = 0.83$	(Xie et al., 2019)
	Heat, drought	Strawberry	Fixed: Headwall Photonics VNIR A-Series, USA	397-1003	Not mentioned	Controlled environment	–	Correlation analysis, SRIs Classification: SVM, RF, DT, Adaboost, XGB	Accuracy $rate_p$ = 94 %	(Poobalasubramanian et al., 2022)
	Heat, frost, salinity	Maize	Fixed: Specim V10 (Specim Spectral Imaging Oy Ltd., Oulu Finland)	400–1000	Not mentioned	Controlled environment	–	PCA Classification: SVM	Accuracy $rate_p$ = 84 %	(Tirado et al., 2021)

A significant decrease in photosynthetic parameters was observed during drought, and this trend was most apparent within the top layer of the plants. Four machine learning models were evaluated for the prediction of photosynthetic parameters from leaf reflectance spectra, and the RF algorithm showed the highest ability to predict photosynthetic parameters (R^2 was from 0.88 to 0.92).

The most significant challenge facing winegrowers in the Mediterranean region is the management of water. Climate change has led to frequent and severe droughts, which has resulted in reduced yields for wine producers. As a result, the productivity of the vineyards is compromised, affecting the alcohol content. Using hyperspectral data, Laroche-Pinel et al. (2021) evaluated the results from several vine plots consisting of three grape varieties with varying growth stages and irrigation methods. Regression methods were used to examine correlations between leaf reflectance and vine water status as determined by stem water potential. The findings revealed the most effective spectral domains and vegetation indices for assessing vine water availability. Short Wave Infrared domain was directly affected by water content and Near Infrared and Red-Edge bands were indirectly correlated with water status by affecting chlorophyll concentration and cellular morphology. Their study aimed to determine whether vine water status could be monitored over a landscape with the help of multispectral satellite spectral bands, such as Sentinel-2 data.

Using hyperspectral leaf reflectance, Burnett et al. (2021) examined metabolism-driven responses to drought in the early stages before any visible signs are present rather than relying solely on incomplete drought indices. The physiology, biochemistry, and spectral responses to drought conditions were determined in six glasshouse-grown plants. PLS model used for prediction of metabolite content, with validation R^2 values of 0.49 to 0.87. LDA and PLS-DA were also used to distinguish between plants that are watered and those that are affected by drought through the measurement of spectral characteristics and traits. Finally, the models developed by the greenhouse were validated in an independent field study.

2.2.2. Canopy scale

Spectral indices are derived from few bands without considering the effects of drought on other parts of the spectrum. Using machine learning and advanced computing capabilities, full spectra can be used to gain a deeper understanding of the effects of drought. The study of Dao et al. (2021) evaluated the performance of ANN, SVM, and RF in monitoring droughts with traditional spectral indices. Using close-range HSI technology, full spectra were processed with the models to assess the effects of drought on *Bromus inermis* grass grown under different treatments. Most of the spectral indices were not able to distinguish between short- or long-term drought stress.

Table 7
Research studies performed from 2019 to 2022 to detect other environmental stresses than those previously considered using proximal hyperspectral technologies.

Scale	Stress type	Plant	HSI sensor	Spectral range (nm)	Distance to target (m)	Measurement environment	Data preprocessing	Modeling approaches	Optimal performance	Refs
Leaf	Rare earth mining areas	Three types of reclaimed vegetation	Portable: FieldSpec 4 (ASD, USA)	350–2500	Not mentioned	Field	1st Der	Correlation analysis, SRIs Prediction: PLS, SAE, ANN	$R_v^2 = 0.981$	(Li et al., 2022a)
	Rare earth mining areas	Six types of reclaimed vegetation	Portable: FieldSpec 4 (ASD, USA)	350–2500	Not mentioned	Field	1st Der	SRIs, sensitivity analysis Classification: ANN, Fisher and stepwise discrimination	Accuracy $rate_p = 93.6$ %	(Zhou et al., 2022b)
	Waterlogging	Oilseed rape	Fixed: Resonon Pika XC2 (Resonon Inc., USA)	400–1000	0.35	Field	SG	SPA, PCA, Visualization Classification: QDA, KNN, SVM	Accuracy $rate_p = 100$ %	(Xia et al., 2019)
	Oil	Five species	Portable: FieldSpec 4 (ASD, USA)	400-2500	0 (leaf clip)	Field	–	Correlation analysis, PROSPECT (Radiative transfer) Prediction: Univariate regression	$R_v^2 \geq 0.74$	(Lassalle et al., 2019b)
	Ozone	Soybean	Portable: PSR-3500 (Spectral Evolution, Lawrence, MA, USA)	350- 2500	0 (leaf clip)	Field	–	Correlation analysis, SRIs Prediction: linear regression	$R_v^2 = 0.64$	(Gosselin et al., 2020)
Leaf & Canopy	Oil	*Rubus fruticosus* L. (bramble)	Portable: FieldSpec 4 (ASD, USA)	350-2500	0 (leaf clip), 0.05 and 0.2	Controlled environment	SG	SRIs Prediction: Logistic Regression; Classification: RLR	$R^2 > 0.7$ Accuracy $rate_p = 90$ %	(Lassalle et al., 2019c)
Canopy	Natural gas leakage	Various plant species	Portable: SVC HR-1024I (Spectra Vista Corp., USA); Fixed: SOC710VP (SOC, USA)	350–2500; 400 – 1000	1 and 5	Field	SG	SRIs, Correlation analysis, Visualization	–	(Jiang et al., 2020; Pan et al., 2022; Ran et al., 2022, 2020)
	Carbon dioxide	Wheat	Portable: FieldSpec 3 (ASD, USA)	350-2500	1.2	Field	1st Der	Correlation analysis Prediction: linear regression	$R_v^2 > 0.8$	(Liu et al., 2021a)
	Hailstorm	Cotton	Portable: FieldSpec 2 (ASD, USA)	325-1075	0.5	Field	SG	Correlation analysis, SRIs, VIP Prediction: PLS, SVM, ANN	$R_v^2 = 0.85$	(Wang et al., 2021)

Using pre-processed spectra and machine learning algorithms, drought detection was achieved with up to 100 % accuracy.

It is essential to choose plants based on their appropriate characteristics in forest development plans and to ensure that forests are managed sustainably. In a study done by Mazis et al. (2020), images captured by RGB and hyperspectral cameras were used to assess oak seedlings' biophysical traits and their response to drought under controlled conditions. Images of plants acquired with high throughput were obtained by low throughput tests, involving measurements of gas exchange, leaf spectrum analysis, and physiological characteristics. The chosen traits were relevant for forest breeding and monitoring species health in drought-prone areas. The results of image analysis and observed morphological characteristics were highly correlated in both well-watered and dry-down environments. This study demonstrated that vegetation indices were an effective tool for assessing the health and productivity of oak seedlings.

For distinguishing phenology effects related to drought, Sobejano-Paz et al. (2020) studied soybean and maize crops using hyperspectral and thermal images under controlled conditions, which included a variety of photosynthetic pathways and soil water levels. It was determined the potential of this approach to detect changes in leaf physiology under three soil moisture regimes and evaluate physiological, morphological, biochemical and remote sensing responses to water stress. Moreover, PLS-determined important spectral bands associated with drought were not found at the same wavelengths as the studied vegetation indices, indicating the value of having a full spectrum to describe leaf function and suggest crop-specific wavelengths.

The study conducted by Krishna et al. (2021) to assess the response of ten different rice genotypes in drought conditions was based on the use of thermal images to evaluate stress severity and genotype responses, as well as to calculate the Crop Water Stress Index (CWSI). Additionally, canopy reflectance measurements from the same genotype fields were collected simultaneously with thermal imaging. A significant correlation was observed between relative water content (RWC) measured in the laboratory and CWSI ($R^2 = 0.63$). PLS model was used to develop a relationship between CWSI and canopy hyperspectral data, and the ten most significant wavelengths for detecting drought stress in plants were identified.

2.3. Salinity

Growing plants under saline conditions limits crop productivity, resulting in substantial yield losses. The losses can be mitigated by choosing salt-tolerant crops, which provide improved irrigation options and decrease freshwater consumption (Morton et al., 2019). The deposition of salt occurs naturally due to wind and rainfall, as well as irrigation with saltwater and

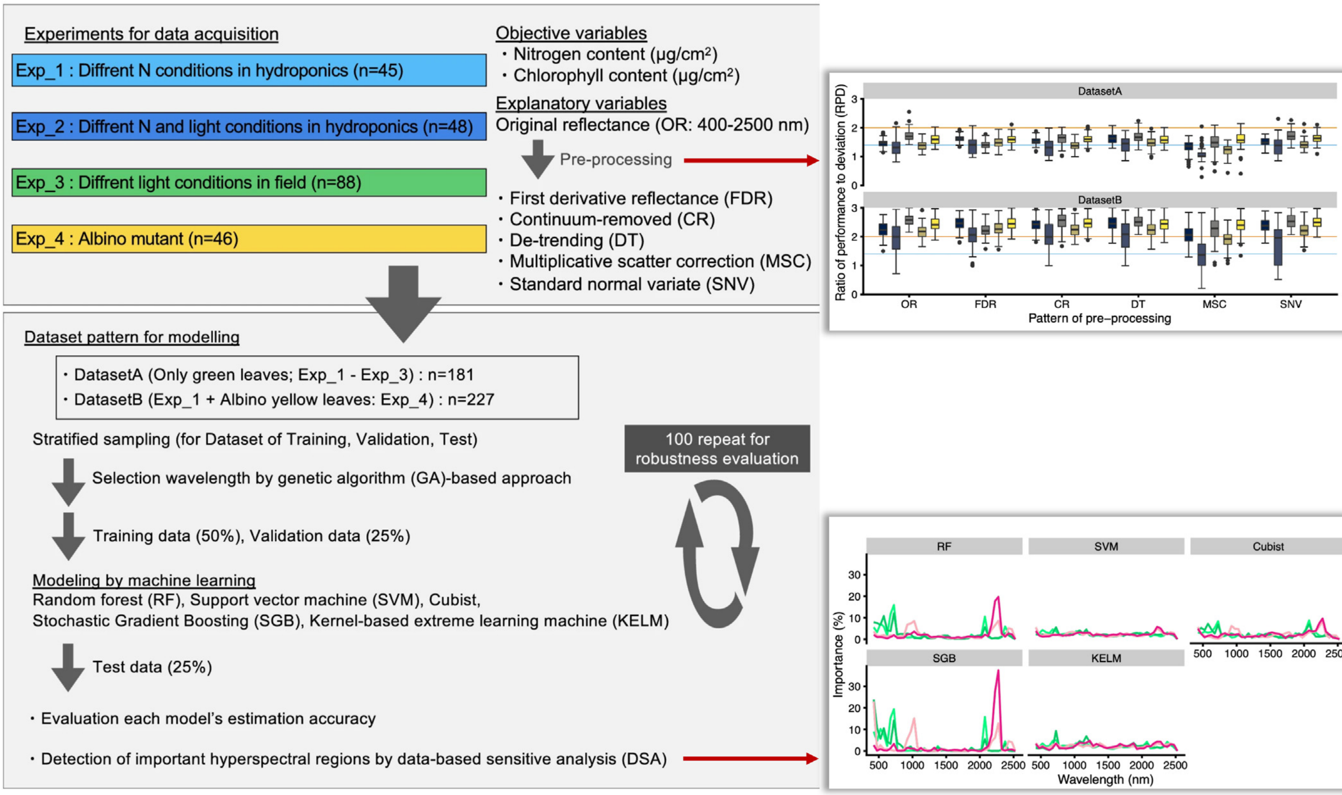

Fig. 5. Procedure for the detection of hyperspectral regions corresponding to nitrogen content (Yamashita et al., 2020).

soil amendments. It has become a global environmental concern most prevalent in arid regions. The majority of crops cannot tolerate this stressor which affects them in multiple ways. Accumulation of salt causes degeneration of leaf tissue, as well as changes in the interactions between plants and water and nutrients, resulting in a reduction of chlorophyll and disease resistance (Lassalle, 2021). A variety of symptoms of salinity stress can occur, including subtle discoloration or yellowing of the leaves. However, as with most stresses in plants, these symptoms are commonly observed as increased reflectivity in green areas as chlorophyll levels are reduced (Goldsmith et al., 2020). On the other hand, changes in reflectance between species with different leaf morphologies may differ significantly. As a result, salinity stress in plants can be measured and assessed using hyperspectral data. Salinity detection studies using proximal hyperspectral technologies are presented in Table 3.

2.3.1. Leaf scale

The productivity of salty soils can be enhanced through the selection of salinity-tolerant varieties and genotypes. Das et al. (2020) used the hyperspectral technology to monitor salinity stress across 56 rice genotypes to determine their salinity tolerance and sensitivity. In this study, a comparison was made of PCA and PLS combined modeling strategies to predict leaf nutrients under salinity stress. It was shown that the combined approach gives more accurate results than simple ones. PLSR-combined models produced the best performance in selecting salt-tolerant rice genotypes based on leaf nutrition.

Calzone et al. (2021) identified and monitored two varieties of pomegranate during salt treatment for 35 days. PLS models were built based on the spectra to predict a wide range of leaf parameters critical to understand plant-salinity relationships. It was possible to analyze spectral signatures even without seeing any symptoms 14 days after salt treatment, but it was not possible to determine the tolerance levels between cultivars.

The use of optical techniques can detect plant stress before visible symptoms develop. However, there is a lack of testing for multiple environmental factors, as well as an insufficient level of data analysis. The potential of HSI was investigated by Cotrozzi and Couture (2020) in the context of characterizing crop leaf reactions to multiple stresses before the development of visible symptoms. In addition to reflectance spectra, physiological and biochemical responses were measured on lettuce leaves under the combination of different light intensities and types, fertilization, and salinity conditions. Multiple stress conditions, independently and in combination, were characterized by PLS, PLS-DA, and spectral indices. It was found that spectral data were well suited to predict the osmotic potential, chlorophyll and phenol levels with a validation R^2 between 0.70 and 0.84. It was observed that lettuce yields and quality were improved under high intensity sodium lighting with high fertilization and without salinity.

The study by Boshkovski et al. (2022) examined photosynthesis and antioxidant activity in olive plants exposed to drought and salt treatment, and their relationship with spectral reflectance. The relationship between spectral data and biochemical characteristics was studied using PCR, PLS, and LDA. Plants under stress developed a reduction in photosynthesis and water content, and an increase in enzyme activity. Significant wavelength ranges were determined based on enzyme activity and specific vegetation indices. The results of this study may enable farmers to identify stress effectively in large olive trees and may assist them in optimizing crop growth, productivity, and sustainability.

2.3.2. Canopy scale

Salinity varies along the soil profile due to the downward flow of water in the soil. Due to this, in order to determine the extent of soil salinity stress on crops caused by irrigation with salt water, soil salinity must be measured at different depths. An experiment was performed on six winter wheat plots under three levels of salinity irrigation, to determine how vegetation indices correlate with salinity at four depths (Zhu et al., 2021). Because the grain filling stage is highly sensitive to salinity, HSI vegetation indices at this stage were correlated with salinity at different soil depths. Results from this study suggested that the optimal indices incorporating salt-affected blue, red-edge, and near-infrared wavebands are more effective for estimating soil salinity, especially at 30 cm depth (R^2 = 0.81). To solve this practical problem, linear or quadratic models based on vegetation indices were suitable for determining soil salinity at multiple depths and identifying salt stress in wheat. An evaluation of local saline water irrigation systems could be achieved using this technique.

In coastal areas, climate change, increased soil fertility, insufficient rainfall, and excessive harvesting have caused rapid changes in the environment, resulting in increased stress on coastal salt marsh plants. Because marsh state can quickly change due to these drivers, it is crucial to detect stressors early. However, barrier access and the vulnerability of coastal salt marshes make fieldwork difficult. Using hyperspectral imagery, Goldsmith et al. (2020) investigated the effects of three major stressors (nitrogen, salinity, and oxidation-reduction potential) on *Spartina alterniflora* in the field. Models of spectral response were consistent with salinity and foliar nitrogen within greenhouse and field experiments, however, they could not be adapted to the field because of the insufficient factors examined in greenhouses and the multiple stresses encountered in the field.

Feng et al. (2020) used HSI to characterize 13 okra genotypes after salt treatment for two and seven days as well as assess the physiological and biochemical characteristics of the crop, which is a laborious process. Algorithms were developed for segmenting leaves and plants from RGB images derived from HSI images and they can be used to measure okra's physiological responses to salinity stress. The relationship between leaf spectral reflectance data and physiological traits was analyzed using PLS models with correlation coefficients in the range of 0.588–0.835.

Using robust and nondestructive approaches, stress tolerance indices (STIs) can be employed along with early grain yield (GY) estimation methods to assist breeders in developing improved genotypes that are tolerant to various environmental conditions. In the study by El-Hendawy et al. (2021a), the spectral reflectance indices were assessed for their ability to predict GY and STI properties of different wheat genotypes under salinity and control treatments. As a result of the MLR model, three spectral indices were identified as the most significant factors affecting GY.

2.4. Heavy metal stress

A major source of hazardous contaminants in plants is the presence of heavy metals which are present in the nature, industrial wastes and environmental pollution in the air, water and soil. Heavy metals are easily absorbed by plants and have long-lasting effects, which can inhibit the growth of plants. Moreover, the pollutants can also make their way into the food chain, potentially posing grave health risks (Wang et al., 2018). Global economic growth and rapid industrialization have led to increase the problem, especially in developing countries with large populations. Some metals, such as iron, copper, and zinc, are essential to plants but are poisonous if they exceed a certain concentration, whereas other elements (such as lead, arsenic, cadmium, and mercury) are toxic to plants even at low concentrations (Küpper and Andresen, 2016). Metallic stress adversely affects a wide range of essential functions, such as metabolism, mineral nutrient transport, and water uptake, and can alter pigmentation and leaf structure (Ruffing et al., 2021). The level of heavy metals in agricultural areas, therefore, should be closely monitored to ensure that they do not advance to harmful levels. As a potentially viable alternative to conventional methods of monitoring heavy metal contamination in plants, it is necessary to deeply evaluate the capabilities of hyperspectral sensing. In Table 4, we present studies conducted using proximal hyperspectral technologies to detect heavy metals.

2.4.1. Leaf scale

A combination of maize leaf spectra under different levels of Cu and Pb stress and time-frequency analysis was conducted to convert pollution features based on spectral data into frequency information. As a result, weak difference information can be significantly enhanced. With the use of a PCA diagram along with an SVM classifier, the pollutant characteristics could be identified, and the red edge was found to be the most effective region of the spectrum to discriminate Cu from Pb (Li et al., 2021a). Lin et al. (2021) developed an efficient method for monitoring Cu concentrations in chicory using hyperspectral data. The relationship between leaf Cu levels and hyperspectral measurements during growth stages was investigated using CWT and PLS methods. Effective wavelengths that reliably track leaf Cu concentration changes were selected, and accurate detection models were built.

In a comprehensive study conducted by Feng et al. (2019), HSI was used as an alternative for the evaluation of the phytoremediation capability of *Miscanthus sacchariflorus* tissues for Cd contamination (Fig. 6). Chemometric analysis of the complete spectral information enabled the comparison of multiple wavelengths and resulted in an improved model over vegetation indexes. Based on optimal wavelengths, regression models provided the best prediction of Cd concentrations in leaves and roots. As a result, CARS-PLS was the most accurate model for leaves, while CARS-SVM provided the best prediction for roots. Finally, the distribution maps of Cd in plant tissues were derived using the optimal models incorporating the characteristics of each pixel. Toward the development of multispectral imaging systems that are affordable and easy to use in real-time, composition-based visualizations of reduced bands would be beneficial.

The heavy metal stress in rice plants avoids water absorption and ion channel function, as a result of which the plants usually suffer from water shortages and excessive amounts of free proline accumulations (Choudhary et al., 2007). Thus, the free proline content was considered to be able to affect stress responses caused by heavy metal exposure. Shen et al. (2020) proposed a hyperspectral imaging and chemometrics-based approach to quantify free proline in rice leaves exposed to Cd stress. Rice leaves were grown and studied at four different time points and five different Cd concentrations. Based on the spectra and effective wavelengths, prediction models were developed. For the purpose of illustrating the variation in free proline content in rice leaves, the distribution of free proline in leaves was mapped. The best detection of free prolines was based on 27 wavelengths and the R_p of 0.943.

2.4.2. Canopy scale

Cd stress can be evaluated using HSI in two vegetation types, which are significantly different in terms of their vulnerability to Cd stress. Using biochar from hardwoods as a local amendment, Cd stress in these crops was reduced, and Cd uptake into plant tissues was minimized. To optimize the use of HSI, a number of vegetative indices that are sensitive to Cd stress were investigated. The anthocyanin reflectance index (ARI) was the most effective index for assessing plant stress reductions resulting from biochar application. The authors evidenced that HSI could be used to find the soil amendments that are capable of binding Cd, allowing for rapid remedial plans. Additionally, HSI may provide valuable insight into regulating plant growth by biochar amendments (Zea et al., 2022). In another study, *Arabidopsis thaliana* stress signatures corresponding to salt, copper, and cesium were identified using HSI and multivariate curve resolution (MCR) analysis. Despite all stresses having similar physiological effects, hyperspectral imaging yielded distinct fingerprints that allowed differentiation of stress types. To distinguish the cesium stress from other similar stressors, salt and copper were also included in this study. In addition, root anatomy, leaf area, and chloroplast structure were measured to evaluate the impact of stress on the plant. Results of this study indicated that HSI can be used for monitoring environmental chemicals, including radioactive cesium released by nuclear reactors (Ruffing et al., 2021).

In the study of Yu et al. (2021), a proximal HSI technique combined with machine learning techniques was used to determine canopy characteristics of tobacco plants exposed to different levels of Hg. In addition, the structure and appearance of mesophyll tissues were examined in tobacco leaves. To distinguish stressed from unstressed samples, discrimination models were built by using whole spectra and effective wavelengths identified by PCA and CARS. Zhang et al. (2020b) designed a cross-stress experiment involving multiple heavy metals and evaluated the possibility of determining exposure to Cd and Pb from hyperspectral images of the rice canopy. Significant bands are mainly located in the range of 681–776 nm and 1224–1349 nm for Cd stress and 712–784 nm for Pb stress. Cd can be predicted using an R^2 value of 0.7, but Pb cannot be precisely predicted.

Due to differences between laboratory and field conditions, applying spectral data characteristics to all situations can be challenging. Through field experiments, Wang et al. (2020a) developed a methodology to determine copper content within wheat canopy using hyperspectral data collected throughout the growing season. The copper content of the wheat canopy increased with increasing soil stress, and its spectral reflectance changed. Spectral indices and wavelengths were selected according to their ability to predict copper levels in the wheat canopy. In addition, it was found that the sensitive bands identified provided a good indicator of copper content in the wheat canopy during tillering, jointing, and heading.

2.5. Herbicide

The inappropriate use of herbicides can cause direct pollution of the environment, and these pollutants can then enter the food chain. There may be adverse effects on crops and they may interfere with physiological mechanisms (Mohseni-Moghadam et al., 2016). Thus, leaf symptoms may vary depending on the chemical and dosage used. The spectral responses of plants to herbicides have generated increasing interest in the need for regulation and monitoring of these substances. The following sections discuss the application of hyperspectral technologies to assess crop damage from herbicides in agricultural fields in order to provide practical management advice. We also present studies conducted using proximal hyperspectral technologies to detect herbicide stress in Table 5.

2.5.1. Leaf scale

Glyphosate is a non-selective herbicide widely used in crop fields to control weeds. The use of glyphosate can cause drift into unintended areas, causing damage to plants that are not glyphosate-resistant. Through the use of the HSI technique combined with machine learning algorithms, Zhang et al. (2021b) evaluated the damage caused by glyphosate in field experiments and the recovery rate of damaged plants in experiments with different rates of glyphosate application. It was possible to observe the spectral variation pattern among maize plants treated with glyphosate at different concentrations. The spectral differences between recoverable and non-recoverable plants could be observed as early as one week after treatment. Based on spectral sensitivity analysis, two spectral indices were created based on 449 nm, 669 nm, and 771 nm reflective wavelengths that could classify maize plants as recoverable and unrecoverable with an overall accuracy of over 95 %. In addition, this research group (Zhang et al., 2019a) used HSI to investigate soybean plants' responses to dicamba, another commonly used herbicide, which showed promise for predicting their recovery ability and the severity of damage they suffered.

In a study Chu et al. (2022a), HSI combined with shallow convolutional neural networks (SCNNs) was employed to identify the reflectance characteristics of two varieties of wheat plants exposed to different herbicides and stress rates over time in order to detect herbicide stress in its early stages. According to the first-order derivatives, the effects of different herbicides are primarily observed at the wavelengths of 518–531 nm, 637–675 nm, and around 700 nm, reflecting the varying levels of chlorophyll and carotenoids. The proposed approach yielded 96 % accuracy in determining herbicide types and 80 % accuracy in determining stress levels after 48 h in both considered wheat varieties, which have great potential for developing field-based herbicide stress recognition methods.

It was also evidenced that hyperspectral sensing was able to detect symptoms occurring in cotton plants as soon as two days after application of phenoxy herbicides (Suarez et al., 2017). In addition to being highly correlated with yield, the green peak (around 550 nm) and NIR spectrum significantly increased the accuracy of the monitoring of the dose drifted to the crop by >25 %. This finding greatly simplified the analysis of the herbicide impact on cotton through an emphasis on other factors (e.g. the timing of exposure and data gathering) instead of preprocessing.

2.5.2. Canopy scale

As an endogenous hormone, salicylic acid is able of reducing herbicide toxicity by activating antioxidant enzymes and improving the detoxification process of rice plants (Wang et al., 2016). Wang et al. (2020b) explored the use of ground-based HSI to assess the toxicity of the herbicide quinclorac and alleviating effects of salicylic acid on rice plants. This study examines the influence of rice varieties on detection performance, establishing detection models and visualizing leaves with different treatments. Rice herbicide toxicity can be observed by changes in the reflectance spectrum and physiological measurements, and visualizations of herbicide toxicity in rice can also provide an insight into the process.

Bloem et al. (2020) applied HSI technology to identify glyphosate-specific spectrum signatures for control and drought-stressed plants. In this paper, eight spectral vegetation indices were selected based on spectral analysis, and their effectiveness for sensing glyphosate application on pots with rolled grass sods was explored. Also, photosynthetic pigments, polyphenols, and dry matter content of the leaves were evaluated, as these are indicators of plant health and stress. An early detection of glyphosate application can be made using the normalized difference lignin index (NDLI).

Monitoring the impact of herbicide applications on invasive conifers at large scales is essential for evaluating their effectiveness and selecting the proper doses. Scholten et al. (2019) used hyperspectral data to explore methodologies for quantifying herbicide stress in *Pinus contorta* (Douglas), a widely distributed exotic conifer. To detect the effects of herbicide application before visible changes occurred, the effects of herbicide treatment on needle discoloration, spectra, and four important physiological characteristics were investigated. Results demonstrated that remote monitoring of indicators, such as the photochemical reflectance index (PRI), could distinguish between the two herbicide applications and the control within two days after herbicide treatments. It is useful for determining the extent of damage resulting from herbicide applications to determine whether additional treatment is necessary.

A growing number of herbicide-resistant weeds pose a challenge to the economic viability of crop production systems by decreasing crop yields. It was applied ground-based hyperspectral imagery to classify herbicide-resistant and herbicide-susceptible kochia biotypes, which have shown resistance to both glyphosate and dicamba (Nugent et al., 2018). Up to 80 % classification accuracy can be achieved by using support vector machines (SVM). During another study undertaken by this group (Scherrer et al., 2019), data were collected on a broader set of crops and weed species as well as a variety of resistance rates and types. The process involves imaging kochia biotypes at various stages of growth and analyzing the accuracy of the classification over time. Further, the results were derived from neural networks, which led to improvements of up to 99 % in classification accuracy.

2.6. High and low temperatures

Global warming has led to an increase in the frequency and intensity of adverse weather conditions, which in turn have caused a rise in the damage caused by natural disasters. Climate change has the potential to pose a threat to food safety as adverse changes in temperature may negatively impact crop yields. The effects of these alterations on plants can result in their death. However, based on their severity, plants may be able to survive and may even thrive despite stresses (Feng et al., 2018). It is important to note, however, that recovery from such stresses is often complicated by a decline in the level of productivity. It is recommended that reflectance data be used to track the effects of temperature changes, as these fluctuations affect leaf water characteristics, pigmentation, growth, and chemical composition (Kumagai et al., 2022). In addition, quantifying damage can be effective in alleviating the adverse effects of temperature injury. Table 6 presents studies that used proximal hyperspectral technologies to detect temperature-induced stress in plants.

2.6.1. Leaf scale

Wheat yields can be affected significantly by frost damage as the plants grow. In spite of limited options for frost protection, the ability to quickly determine frost-induced damage would provide timely remedial measures. In a controlled environment room, Murphy et al. (2020) investigated the effects of frost stress on the spectral characteristics of wheat plant parts

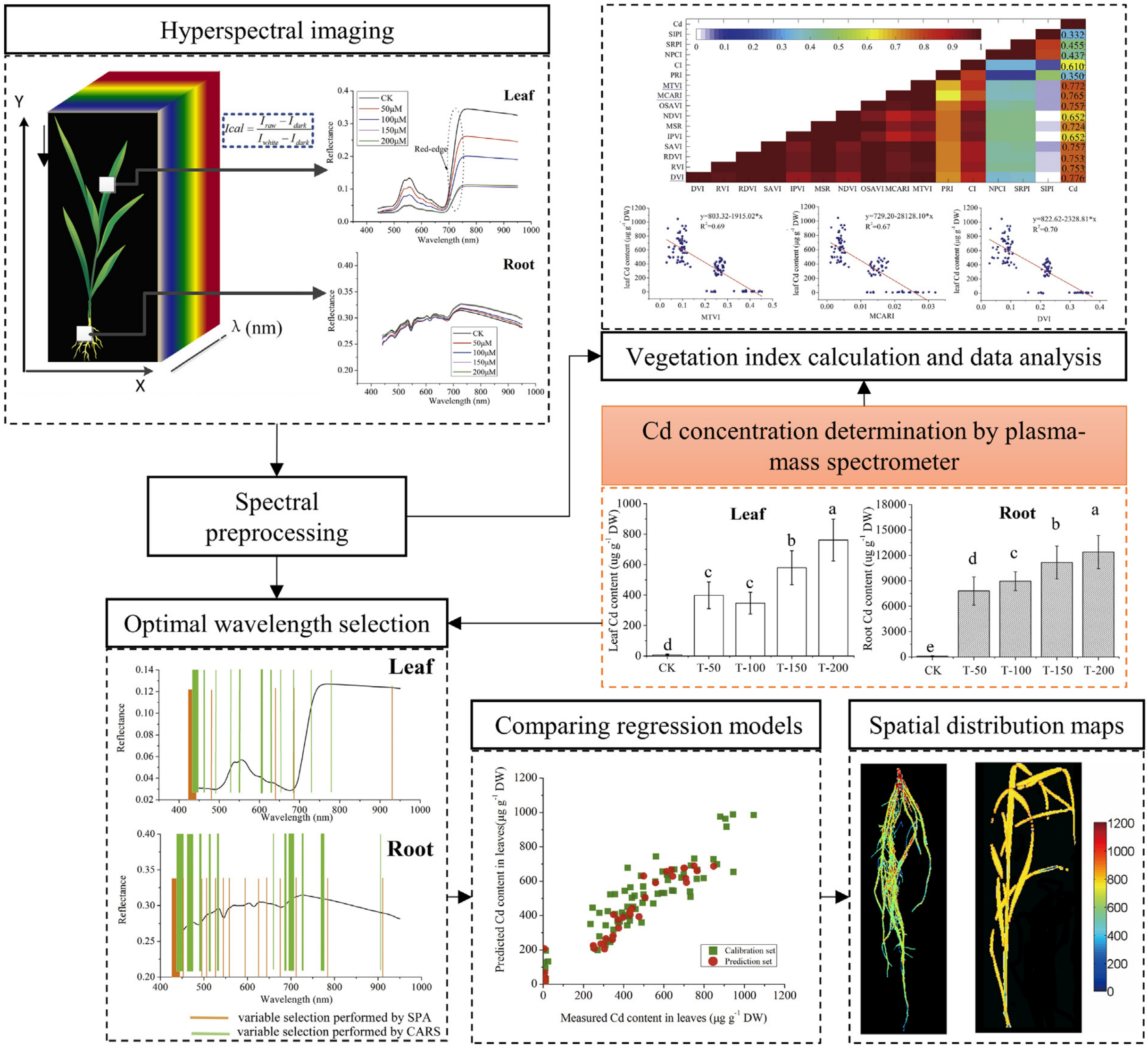

Fig. 6. Illustration of the process of image processing and data analysis for quantifying Cd concentrations in *M. sacchariflorus*. Redrawn with permission from Ref. (Feng et al., 2019).

(heads and flag leaves) using HSI. Spectral reflectance changes caused by frost stresses can be identified in the samples from one to five days after frosting. In both wheat heads and leaves, significant differences were detected over time between treatments across several wavelength bands, including blue, red, and NIR. Furthermore, the relationship between time and treatment resulted in significant changes in the spectra, especially in the green and NIR spectra for leaves and in the green and red spectra for heads. Results were then compared to those of existing multispectral techniques to determine whether frost damage could be identified in the field.

Cold temperatures in winter and early spring can be problematic for blueberry producers since this can severely damage the buds. By using HSI, Gao et al. (2019b) studied the possibility of detecting damaged blueberry buds when early spring frost occurs. Lab-simulated freezing treatments were conducted at two phenological stages (bud swell and early pink) as a preliminary development test. As a result of PCA and SPA techniques, 615, 673, 690, 756, 979, and 1467 nm were identified as the key bands to be used to distinguish healthy buds from injured ones. Using the PLS-DA model, an accuracy of >0.75 was obtained. In another study, this research team examined the status of buds throughout the entire growth cycle in winter and early spring (Gao et al., 2021).

Drought and heat are often concurrent events during the growing season that result in reduced crop growth and yields. Identifying phenotypic features associated with the physiology of resistance to drought and heat stress would be imperative to produce crops adapted to climate change. Leaf metabolomes reflect changes that occur due to stress in the plant's physiology, and these changes are referred to as an intermediate phenotype. Melandri et al. (2021) studied the effects of leaf metabolites on leaf reflection under water and heat stress in 22 cotton genotypes over two years. It was found that lipid changes were the most important factor in adapting leaves to drought. Adaptations made by plants to drought and how they affected fiber characteristics were linked to the level of stress. In this study, hyperspectral reflection measurements were employed to predict leaf metabolites that were successful in differentiating stressed from non-stressed samples and showing which spectrum regions have the greatest significance.

2.6.2. Canopy scale

Loblolly pine seedling growth is affected by the yearly average minimum winter temperature (MWT) in the area where the seeds are produced and it guides the distribution of more suitable seeds. According to the MWTs of seed sources, plants are allocated to climatic regions where they are cold hardy. However, this method may become ineffective over time and as the number of ancestors grows. An innovative technique based on hyperspectral imaging was developed by Lu et al. (2021b) for evaluating freeze damage and predicting MWT based on the seed source origin of

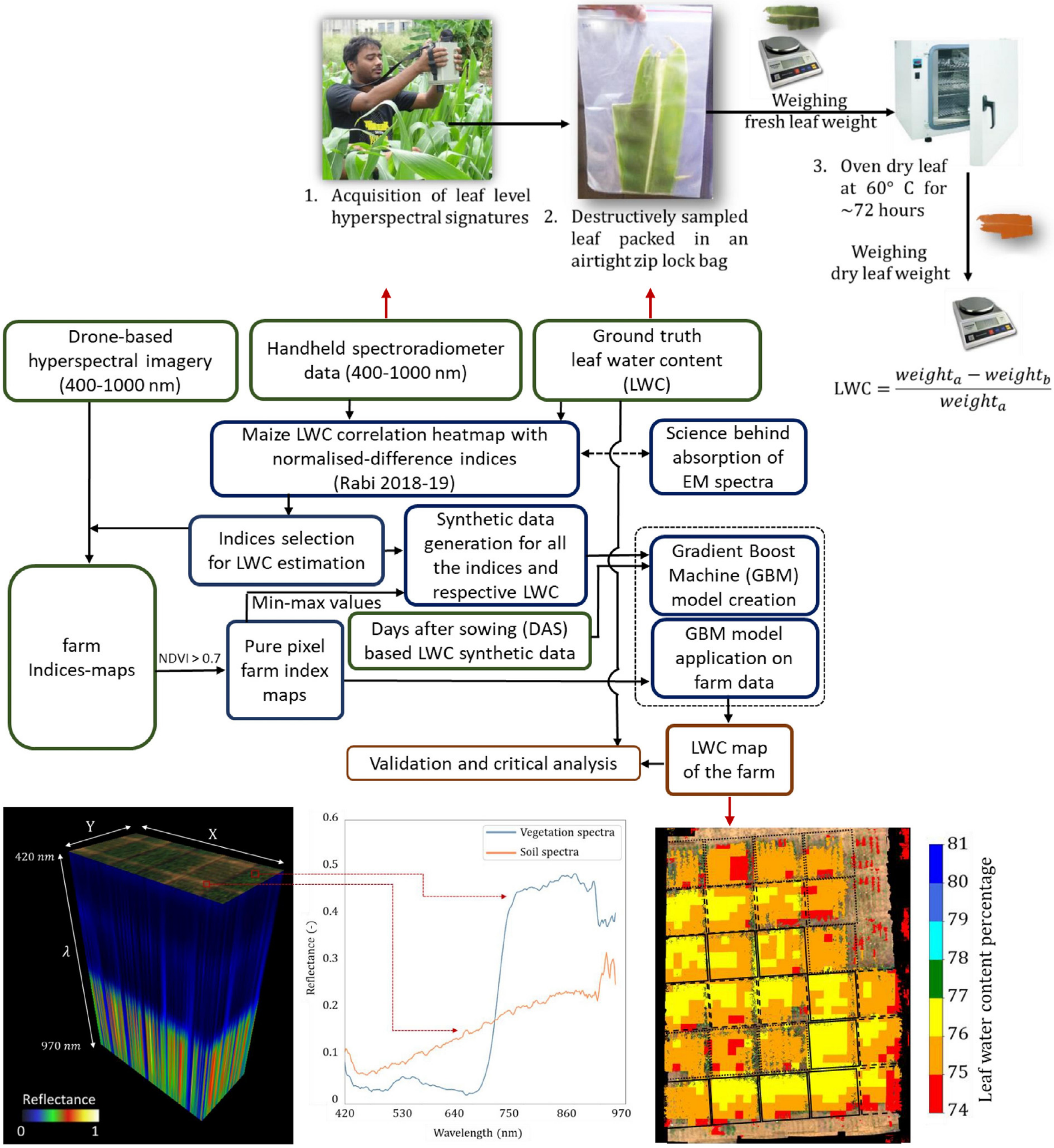

Fig. 7. Framework for the development of leaf water content maps on a maize farm. Redrawn with permission from Ref. (Raj et al., 2021).

the seedlings. The work evaluated the effects of an artificial freeze event on seedlings from different geographical areas, which represent various levels of MWT at seed origin. Seedling images were taken at different time intervals before and after freezing. There was a significant correlation between the MWT and freeze damage, and models built on the top portion were the most accurate predictors of both. According to the study, HSI may be a useful method for assessing the cold hardiness of coniferous species without destroying them. Additionally, this group developed classification models using SVM and variable selection to identify healthy and stressed seedlings prior to and following freezing (Lu et al., 2021a).

As a method of evaluating the optimal period for yield estimation, hyperspectral measurements can be applied in-situ for winter wheat under freeze stress and to perform a yield estimation model. Xie et al. (2020b) investigated the canopy reflectance response of winter wheat under freeze stress by inducing low temperatures during early growth, as well as quantifying the relationship between canopy reflectance and yield. Based on the reflectance data, it was shown that the red edge region under freeze stress was associated with crop yield, with around 38 % of the extracted bands located in this region (680-780 nm). Three calibration methods and field validation results were compared to determine the most appropriate monitoring time period and the best model to predict winter wheat yield during the early growth phase under freezing conditions. Using hyperspectral technology, a monitoring and yield prediction study can be conducted under cold weather conditions for winter wheat.

Heat stress remains a serious environmental issue affecting the growth and long-term viability of ginseng plants despite advances in agronomy for cultivating elite ginseng. To develop a model to assess the sensitivity and resistance of ginseng plants to heat stress, visible and near-infrared hyperspectral images were captured in the laboratory (Park et al., 2021). In order to analyze the acquired hyperspectral images, the PLS-DA technique combining variable selection algorithms was applied. Based on validation data, models developed provided 79.2 % accuracy along 12 bands in the Visible/NIR spectrum and over 98.9 % accuracy along 18 bands in the SWIR spectrum. In this study, it has been shown that heat stress negatively impacts ginseng's photosynthetic process by affecting its internal proteins. Additionally, the spectral image proved to be more effective than a color image in classifying heat-stressed plants. The results demonstrate that the HSI is able to distinguish between heat-susceptible plants and heat-resistant plants accurately.

2.7. Other environmental stresses

There are many environmental issues around the world that can cause plant stress, such as waterlogging, oil pollution, gas leaks, mining, hailstorms, acid rain, etc. Most crops are adversely affected by short- or long-term soil waterlogging, which is usually caused by severe weather conditions, such as flooding, heavy rain, and storms. As a result of waterlogging, plant growth, nutrient uptake, chlorophyll concentration, as well as metabolic activity can be reduced, which can be destructive to plants (Kaur et al., 2020). Also, waterlogging can cause plants to suffer from water deficiency by blocking their stomata due to the lack of oxygen.

Carbon dioxide, methane, ethane, and ozone may also cause plant stress, which are found in soils and the atmosphere. Plants are affected either directly by gaseous emissions from their leaf surfaces or indirectly by adverse environmental situations (Grulke and Heath, 2020). This is accompanied by the appearance of yellow, red, and black lesions on leaves. In Table 7, we present studies using proximal hyperspectral technologies to detect other environmental stresses than those previously considered.

2.7.1. Leaf scale

Rare earth mining disrupts the physicochemical characteristics of the reclaimed land and creates multiple stresses which interfere with the physiological functioning of the reclaimed vegetation. A variety of spectral processing methods were employed to analyze the spectra of three vegetation types found in rare earth mining regions (Li et al., 2022a). It was found that reclaimed vegetation differed significantly from typically vegetated areas. This study investigated the spectral characteristics of vegetation and found correlations between the chlorophyll concentration and the spectral indices. Also, there were specific adaptations to each kind of environment. The sparse autoencoder network proved to be the most effective model in order to quantify the amount of chlorophyll in reclaimed vegetation. The results of this study provide useful information for understanding and controlling the growth of vegetation in mining regions, as well as offering a direction for rehabilitation efforts. In another study by this research team (Zhou et al., 2022a), vegetation types were accurately distinguished from each other by identifying the most appropriate feature bands, which helped to categorize the various species present in the mining area, thereby reducing the workload for future modeling of plant characteristics for the kind of areas.

A waterlogged oilseed rape plant may experience leaf lodging during flowering and a reduction in pollen production and plant growth as well. Furthermore, this can cause physiological damage since waterlogging can affect fertilizer absorption. Xia et al. (2019) investigated the potential use of HSI for detecting varying levels of oilseed rape waterlogging stress over a period of three to six days. Different classification models were used to identify waterlogging stress among two oilseed cultivars. The SPA algorithm was used to reduce modeling complexity, and the QDA model achieved high classification accuracy.

Monitoring ozone stress in plants can lead to the development of ozone-tolerant varieties with better yields. The negative impact of ozone on plant growth is measured through visual scores. A study performed by Gosselin et al. (2020) evaluated the effects of chlorosis and necrosis visual scores on assessing soybean ozone damage, as well as selecting spectral bands for the normalized difference spectral index (NDSI) which had a favorable relationship to foliar visual scores. In addition to confirming that NDSI was very closely related to visual scores in all species, ozone concentrations were evaluated to predict likely damage timing based on ozone-sensitive bands observed in soybean leaves and physiochemical characteristics.

2.7.2. Canopy scale

As a result of natural gas leakage into the soil, it may negatively impact plant health, leading to observable signs and changes in canopy spectral properties. HSI measurements can be used to examine the spectral properties of plants located close to leakage points, enabling leakage rates of underground pipelines to be calculated. An experiment designed by Pan et al. (2022) to simulate an underground gas pipeline leak and the effects of gas exposure on different plant cultivars provided an index model for monitoring plant health. This paper presented the variational mode decomposition index (VMDI), which employs two bands at 616 and 829 nm, that have a high correlation with gas stress. In comparison to other indices, the proposed index was able to detect stressed wheat and grass faster and more efficiently for identifying stressed vegetation during the growing season. In previous research of this research group (Jiang et al., 2020; Ran et al., 2020), it has been found that the combination of spectral and spatial information can enhance detection performance in comparison to the use of spectral features alone.

Plant morphology and physiological characteristics are negatively affected by elevated CO_2 (eCO_2) concentrations. Liu et al. (2021a) investigated the effects of different eCO_2 concentrations on winter wheat and key spectral characteristics to develop prediction models based on leaf area index (LAI) and soil and plant analysis development (SPAD), which are significant contributors to plant growth. In situ experiments were conducted using chambers to determine the phonological properties of winter wheat and their hyperspectral characteristics. LAI and SPAD were found to increase and then decrease during the winter wheat growth cycle. Moreover, the canopy reflectance was similar under different treatments. However, the level of reflectance varied. The treatment increased the reflectance of the plants during the heading and milk ripening phases of the growth cycle while decreasing it during the jointing and flowering phases.

Accurately estimating yield reduction due to hailstorm is crucial to determine insurance compensation as well as what farmers should do as a result of the damage. According to a study made by Wang et al. (2021), simulation of six hail damage treatments at four levels as well as natural tracking experiments were conducted to investigate field-scale yield predictions based on spectral characteristics. Different machine learning algorithms, based on spectral characteristic bands and vegetation indices, were evaluated to predict cotton yield. The model that used spectral reflectance to predict yields performed much more accurately than the model that used vegetation indices. Among the models, the PLS one provided the best performance.

3. Combination of proximal hyperspectral sensing with airborne or spaceborne imaging

There are different measurement scales depending on the plants and the stress factors. For example, to determine the status of a large area of vegetation, the use of imaging spectrometers mounted on UAV/drone platforms, airborne vehicles, and satellite platforms should be considered (Lassalle et al., 2021). Furthermore, proximal measurements of stress have been used in some studies to calibrate methods for detecting stress in airborne or satellite-based platforms (Murphy et al., 2020). Platforms based on satellites can provide measurements of vast areas at once, but data resolution is a big problem, along with cloud coverage, which greatly affects the information gathered. Although proximal sensing provided flexibility in terms of time, satellite-based sensors can be re-visited on a daily to weekly basis, which implies that the revisit time for these sensors could impair their effectiveness as they might fail to detect the earliest signs of stress (Li et al., 2019a). Moreover, some environmental conditions, such as the aftermath of frost events, are not always suitable for gathering spectral data, resulting in another limitation of satellite sensors. It is also unclear whether some stress signals can be detected by satellites with spatial resolutions of

1-30 m (Murphy et al., 2020). In recent years, UAVs equipped with compact cameras have become an affordable alternative for imaging landscapes, providing an opportunity to increase precision agriculture and monitoring of the environment. In addition to acquiring spectral images of discrete portions of the spectrum, drones can also be equipped with custom sensors as this knowledge base grows, potentially enabling the detection of abiotic stresses in their early stages through multispectral imagery. They provide canopy-scale data with high spatial resolutions (<1 m), but have some limitations regarding payload and flight time. In ground-based measurements, data can be acquired at fine spatial resolutions and without consideration of sensor size or weight, but sampling is slower and may be affected by environmental drift, as occurs in large-scale studies (Liu et al., 2020b). Obtaining comprehensive information about plant stress over a wide area with a high level of spatial and spectral resolution is possible through a multiscale imaging technique that combined proximal hyperspectral sensing with airborne or satellite imagery, from leaf to satellite scale. Additionally, advanced satellite spectrometers, which provide spatially and spectrally detailed information, are under development and will play an increasing role in providing accurate information about crops and the environment (Lassalle, 2021).

In terms of assessing metal uptake by plants, it would be useful to evaluate the environmental risks associated with industrial brownfields and monitor plants on a large scale. This would be done using proximal reflectance measurements in the field that could be adapted to aerial or satellite optical imaging. A study of Lassalle et al. (2021) provided an estimate of the concentration of heavy metals in plant leaves based on hyperspectral measurements in the field to aerial images. The proposed method involves constructing leaf-level vegetation indices for different metals, followed by an evaluation of their relevance to the application at canopy scale and analysis based on high-resolution aerial imagery. The method can be easily applied to drones with embedded sensors for accurate mapping of heavy metals on the ground. In other studies, advances were also made in building models derived from multi-source remote sensing data, which was based on proximal hyperspectral and satellite data to monitor heavy metal stress on rice (Li et al., 2019a) and *Quercus spinosa* (He et al., 2020) plants.

Using both ground-based and airborne reflectance measurements, a number of spectral and temperature-based indicators were assessed for the simultaneous determination of nitrogen and water content in winter wheat, to minimize potential confounding effects (Pancorbo et al., 2021). Based on this approach, it may be possible to optimize N fertilization and irrigation by integrating spectral and thermal information. It is necessary to monitor leaf water content to detect plants under water stress at an early stage in crop growth. Since optical data have a limited resolution and satellite data are impacted by atmospheric conditions, its exact estimation remains difficult. Furthermore, canopy density is low at the beginning of the growth cycle, which increases the effect of bare soil overshadowing. To determine leaf water stress early in the growth cycle, Raj et al. (2021) developed a new method using high resolution hyperspectral drone imagery to assess leaf water stress based on water sensitive indices (Fig. 7). As well as using handheld and drone hyperspectral technologies for leaf-level hyperspectral data analysis, leaf samples were taken and oven dried to determine the water content of the leaves. With portable hyperspectral leaf level measurements, seven indices were proposed according to their responses to the different vibrational absorption bands of water. Through a gradient boost machine (GBM) model, a farm-scale leaf water map was derived from drone hyperspectral data, based on the minimum/maximum values set by the indices and days after planting.

The idea of coupling proximal and aerial hyperspectral measurements with high or very-high spatial resolution has also proven successful in assessing plant stress from problems such as oil (Lassalle et al., 2019a), waterlogging (Yang et al., 2022), warming and elevated CO_2 levels (McPartland et al., 2019), natural gas leakage (Du et al., 2022), herbicide exposure (Mink et al., 2020; Scherrer et al., 2019), and frost (Choudhury et al., 2019). Currently, there are a limited number of studies combining proximal and airborne hyperspectral data, but this approach is a step in the right direction and can open up opportunities for future applications in quantitative monitoring of abiotic stresses, particularly with advances in airborne or spaceborne sensors.

4. Conclusion

The overview provided by this review of recent advances made toward monitoring abiotic stressors using proximal hyperspectral remote sensing. This field has evidenced a significant increase in publications in the last few years, which has resulted in a number of scientific and technological advances in agricultural and environmental research. In spite of that, there is much work done on the development of hyperspectral techniques for long-range remote sensing using satellites or aircraft for canopy parameters than proximal sensing techniques. However, remote sensing models for large areas are not applicable to proximal HSI due to atmospheric conditions affecting long-range imaging, while proximal crop imagery should incorporate plant morphology, illumination, and leaf characteristics.

The extensive range of emerging applications of the proximal hyperspectral technologies on the leaf and canopy scales for identification of abiotic stress, emphasize the critical role that this approach can play for rapid and nondestructive evaluation of plant characteristics. In terms of processing techniques, there are numerous models that can be adapted to proximal hyperspectral data, which can have a substantial impact on its performance. Furthermore, it would be worthwhile to investigate the potential transferability of proximal sensing outside of its original context since the majority of the methods employed are focused on a single scale and are intended to be used on a single plant.

On the other hand, the concept of precision agriculture is based on monitoring stress across a specific crop field, but a large-scale approach over multiple canopy areas is needed for comprehensive monitoring of the environment. Toward this achievement, further plant ecology research aims to develop methods applicable to complex plant ecosystems containing many species, by using a spatial analysis with high resolution to investigate their spectral responses to various stressors within and across species. So, an ideal approach in the detection and characterization of plant stress might be to combine proximal and airborne hyperspectral measurements with high spatial and temporal resolution in order to maximize the overall efficiency of the measurement process. There are promising prospects of practical implementation of these methods in the near future. Given the rapid development of sensors and satellite-based imaging technologies, hyperspectral sensing will likely play a greater role in agricultural and environmental monitoring in the near future.

CRediT authorship contribution statement

Alireza Sanaeifar: Writing – original draft, Investigation, Conceptualization, Visualization. **Ce Yang:** Writing – review & editing, Validation. **Miguel de la Guardia:** Writing – review & editing. **Wenkai Zhang:** Visualization. **Xiaoli Li:** Conceptualization, Writing – review & editing, Supervision, Funding acquisition. **Yong He:** Writing – review & editing, Funding acquisition.

Data availability

Data will be made available on request.

Declaration of competing interest

The authors declare that they have no known competing financial interests or personal relationships that could have appeared to influence the work reported in this paper.

Acknowledgements

The research was funded by the Key R&D Projects in Zhejiang Province (Project No: 2022C02044) and National Natural Science Foundation of China (Project No: 32171889 and 32071895). The authors wish to express their sincere gratitude to Dr. Hamed Tavakoli for his invaluable assistance and advice in structuring the manuscript.

References

Abenina, M.I.A., Maja, J.M., Cutulle, M., Melgar, J.C., Liu, H., 2022. Prediction of potassium in peach leaves using hyperspectral imaging and multivariate analysis. AgriEngineering 4, 400–413. https://doi.org/10.3390/agriengineering4020027.

Amirruddin, A.D., Muharam, F.M., Ismail, M.H., Tan, N.P., Ismail, M.F., 2020. Hyperspectral spectroscopy and imbalance data approaches for classification of oil palm's macronutrients observed from frond 9 and 17. Comput. Electron. Agric. 178, 105768. https://doi.org/10.1016/j.compag.2020.105768.

Asaari, M.S.M., Mertens, S., Dhondt, S., Inzé, D., Wuyts, N., Scheunders, P., 2019. Analysis of hyperspectral images for detection of drought stress and recovery in maize plants in a high-throughput phenotyping platform. Comput. Electron. Agric. 162, 749–758. https://doi.org/10.1016/j.compag.2019.05.018.

Asante, E.A., Du, Z., Lu, Y., Hu, Y., 2021. Detection and assessment of nitrogen effect on cold tolerance for tea by hyperspectral reflectance with PLSR, PCR, and LM models. Inf. Process. Agric. 8, 96–104. https://doi.org/10.1016/j.inpa.2020.03.001.

Atun, R., Uçar, E., Gürsoy, Ö., 2020. Investigation of salt stress in rosemary (Rosmarinus officinalis L.) with the remote sensing technique. Turk. Tarim. Arast. Derg. 7, 120–127. https://doi.org/10.19159/tutad.585170.

Badzmierowski, M.J., McCall, D.S., Evanylo, G., 2019. Using hyperspectral and multispectral indices to detect water stress for an urban turfgrass system. Agronomy 9, 439. https://doi.org/10.3390/agronomy9080439.

Ball, K.R., Liu, H., Brien, C., Berger, B., Power, S.A., Pendall, E., 2022. Hyperspectral imaging predicts yield and nitrogen content in grass–legume polycultures. Precis. Agric. 23, 2270–2288. https://doi.org/10.1007/s11119-022-09920-4.

Bloem, E., Gerighausen, H., Chen, X., Schnug, E., 2020. The potential of spectral measurements for identifying glyphosate application to agricultural fields. Agronomy 10, 1409. https://doi.org/10.3390/agronomy10091409.

Boshkovski, B., Doupis, G., Zapolska, A., Kalaitzidis, C., Koubouris, G., 2022. Hyperspectral imagery detects water deficit and salinity effects on photosynthesis and antioxidant enzyme activity of three greek olive varieties. Sustainability (Switzerland) 14, 1432. https://doi.org/10.3390/su14031432.

Brugger, A., Behmann, J., Paulus, S., Luigs, H.G., Kuska, M.T., Schramowski, P., Kersting, K., Steiner, U., Mahlein, A.K., 2019. Extending hyperspectral imaging for plant phenotyping to the UV-range. Remote Sens. 11, 1401. https://doi.org/10.3390/rs11121401.

Burnett, A.C., Serbin, S.P., Davidson, K.J., Ely, K.S., Rogers, A., 2021. Detection of the metabolic response to drought stress using hyperspectral reflectance. J. Exp. Bot. 72, 6474–6489. https://doi.org/10.1093/JXB/ERAB255.

Calzone, A., Cotrozzi, L., Lorenzini, G., Nali, C., Pellegrini, E., 2021. Hyperspectral detection and monitoring of salt stress in pomegranate cultivars. Agronomy 11, 1038. https://doi.org/10.3390/agronomy11061038.

Cao, Y., Sun, J., Yao, K., Xu, M., Tang, N., Zhou, X., 2021. Nondestructive detection of lead content in oilseed rape leaves based on MRF-HHO-SVR and hyperspectral technology. J. Food Process Eng. 44, e13793. https://doi.org/10.1111/jfpe.13793.

Chen, T., Wang, L., Qi, H., Wang, X., Zeng, R., Zhu, B., Lan, Y., Zhang, L., 2020. Monitoring of water stress in peanut using multispectral indices derived from canopy hyperspectral. Int. J. Precis. Agric. Aviat. 3.

Chen, S., Gao, Y., Fan, K., Shi, Y., Luo, D., Shen, J., Ding, Z., Wang, Y., 2021. Prediction of drought-induced components and evaluation of drought damage of tea plants based on hyperspectral imaging. Front. Plant Sci. 12, 1699. https://doi.org/10.3389/fpls.2021.695102.

Cheshkova, A.F., 2022. A review of hyperspectral image analysis techniques for plant disease detection and identification. Vavilovskii Zh. Genet. Selektsii. https://doi.org/10.18699/VJGB-22-25.

Choudhary, M., Jetley, U.K., Abash Khan, M., Zutshi, S., Fatma, T., 2007. Effect of heavy metal stress on proline, malondialdehyde, and superoxide dismutase activity in the cyanobacterium Spirulina platensis-S5. Ecotoxicol. Environ. Saf. 66, 204–209. https://doi.org/10.1016/j.ecoenv.2006.02.002.

Choudhury, B.U., Webster, R., Sharma, V., Goswami, J., Meetei, T.T., Krishnappa, R., Raju, P.L.N., 2019. Frost damage to maize in Northeast India: assessment and estimated loss of yield by hyperspectral proximal remote sensing. J. Appl. Remote. Sens. 13, 1. https://doi.org/10.1117/1.jrs.13.044527.

Chu, H., Zhang, C., Wang, M., Gouda, M., Wei, X., He, Y., Liu, Y., 2022a. Hyperspectral imaging with shallow convolutional neural networks (SCNN) predicts the early herbicide stress in wheat cultivars. J. Hazard. Mater. 421, 126706. https://doi.org/10.1016/j.jhazmat.2021.126706.

Chu, H., Zhang, C., Wang, M., Gouda, M., Wei, X., He, Y., Liu, Y., 2022b. Hyperspectral imaging with shallow convolutional neural networks (SCNN) predicts the early herbicide stress in wheat cultivars. J. Hazard. Mater. 421, 126706. https://doi.org/10.1016/j.jhazmat.2021.126706.

Cotrozzi, L., Couture, J.J., 2020. Hyperspectral assessment of plant responses to multi-stress environments: prospects for managing protected agrosystems. Plants People Planet 2, 244–258. https://doi.org/10.1002/ppp3.10080.

Crusiol, L.G.T., Nanni, M.R., Furlanetto, R.H., Sibaldelli, R.N.R., Cezar, E., Sun, L., Foloni, J.S.S., Mertz-Henning, L.M., Nepomuceno, A.L., Neumaier, N., Farias, J.R.B., 2021. Classification of soybean genotypes assessed under different water availability and at different phenological stages using leaf-based hyperspectral reflectance. Remote Sens. 13, 1–24. https://doi.org/10.3390/rs13020172.

Cui, S., Ding, R., Zhou, K., 2019. A new hyperspectral index for estimating copper content in an indicative Plant for the Exploration of copper deposit. J. Plant Growth Regul. 38, 956–965. https://doi.org/10.1007/s00344-018-9905-9.

Dao, P.D., He, Y., Proctor, C., 2021. Plant drought impact detection using ultra-high spatial resolution hyperspectral images and machine learning. Int. J. Appl. Earth Obs. Geoinf. 102, 102364. https://doi.org/10.1016/J.JAG.2021.102364.

Das, B., Manohara, K.K., Mahajan, G.R., Sahoo, R.N., 2020. Spectroscopy based novel spectral indices, PCA- and PLSR-coupled machine learning models for salinity stress phenotyping of rice. Spectrochim. Acta A Mol. Biomol. Spectrosc. 229, 117983. https://doi.org/10.1016/j.saa.2019.117983.

Debnath, S., Paul, M., Motiur Rahaman, D.M., Debnath, T., Zheng, L., Baby, T., Schmidtke, L.M., Rogiers, S.Y., 2021. Identifying individual nutrient deficiencies of grapevine leaves using hyperspectral imaging. Remote Sens. 13, 3317. https://doi.org/10.3390/rs13163317.

Du, Y., Jiang, J., Liu, Z., Pan, Y., 2022. Combining a crop growth model with CNN for underground natural gas leakage detection using hyperspectral imagery. IEEE J. Sel. Top. Appl. Earth Obs. Remote Sens. 15, 1846–1856. https://doi.org/10.1109/JSTARS.2022.3150089.

Duarte-Carvajalino, J.M., Silva-Arero, E.A., Góez-Vinasco, G.A., Torres-Delgado, L.M., Ocampo-Paez, O.D., Castaño-Marín, A.M., 2021. Estimation of water stress in potato plants using hyperspectral imagery and machine learning algorithms. Horticulturae 7, 176. https://doi.org/10.3390/horticulturae7070176.

El-Hendawy, S., Al-Suhaibani, N., Alotaibi, M., Hassan, W., Elsayed, S., Tahir, M.U., Mohamed, A.I., Schmidhalter, U., 2019a. Estimating growth and photosynthetic properties of wheat grown in simulated saline field conditions using hyperspectral reflectance sensing and multivariate analysis. Sci. Rep. 9, 1–15. https://doi.org/10.1038/s41598-019-52802-5.

El-Hendawy, S., Al-Suhaibani, N., Dewir, Y.H., Elsayed, S., Alotaibi, M., Hassan, W., Refay, Y., Tahir, M.U., 2019b. Ability of modified spectral reflectance indices for estimating growth and photosynthetic efficiency of wheat under saline field conditions. Agronomy 9, 35. https://doi.org/10.3390/agronomy9010035.

El-Hendawy, S., Al-Suhaibani, N., Elsayed, S., Alotaibi, M., Hassan, W., Schmidhalter, U., 2019c. Performance of optimized hyperspectral reflectance indices and partial least squares regression for estimating the chlorophyll fluorescence and grain yield of wheat grown in simulated saline field conditions. Plant Physiol. Biochem. 144, 300–311. https://doi.org/10.1016/j.plaphy.2019.10.006.

El-Hendawy, S.E., Al-Suhaibani, N.A., Hassan, W.M., Dewir, Y.H., Elsayed, S., Al-Ashkar, I., Abdella, K.A., Schmidhalter, U., 2019d. Evaluation of wavelengths and spectral reflectance indices for high-throughput assessment of growth, water relations and ion contents of wheat irrigated with saline water. Agric. Water Manag. 212, 358–377. https://doi.org/10.1016/j.agwat.2018.09.009.

El-Hendawy, S., Al-Suhaibani, N., Mubushar, M., Tahir, M.U., Refay, Y., Tola, E., 2021a. Potential use of hyperspectral reflectance as a high-throughput nondestructive phenotyping tool for assessing salt tolerance in advanced spring wheat lines under field conditions. Plants 10, 2512. https://doi.org/10.3390/plants10112512.

El-Hendawy, S., Elsayed, S., Al-Suhaibani, N., Alotaibi, M., Tahir, M.U., Mubushar, M., Attia, A., Hassan, W.M., 2021b. Use of hyperspectral reflectance sensing for assessing growth and chlorophyll content of spring wheat grown under simulated saline field conditions. Plants 10, 1–26. https://doi.org/10.3390/plants10010101.

Eshkabilov, S., Lee, A., Sun, X., Lee, C.W., Simsek, H., 2021. Hyperspectral imaging techniques for rapid detection of nutrient content of hydroponically grown lettuce cultivars. Comput. Electron. Agric. 181, 105968. https://doi.org/10.1016/j.compag.2020.105968.

Fallon, B., Yang, A., Lapadat, C., Armour, I., Juzwik, J., Montgomery, R.A., Cavender-Bares, J., 2020. Spectral differentiation of oak wilt from foliar fungal disease and drought is correlated with physiological changes. Tree Physiol. 40, 377–390. https://doi.org/10.1093/treephys/tpaa005.

Feng, M., Guo, X., Wang, C., Yang, W., Shi, C., Ding, G., Zhang, X., Xiao, L., Zhang, M., Song, X., 2018. Monitoring and evaluation in freeze stress of winter wheat (Triticum aestivum L.) through canopy hyperspectrum reflectance and multiple statistical analysis. Ecol. Indic. 84, 290–297. https://doi.org/10.1016/j.ecolind.2017.08.059.

Feng, X., Chen, H., Chen, Y., Zhang, C., Liu, X., Weng, H., Xiao, S., Nie, P., He, Y., 2019. Rapid detection of cadmium and its distribution in Miscanthus sacchariflorus based on visible and near-infrared hyperspectral imaging. Sci. Total Environ. 659, 1021–1031. https://doi.org/10.1016/j.scitotenv.2018.12.458.

Feng, X., Zhan, Y., Wang, Q., Yang, X., Yu, C., Wang, H., Tang, Z.Y., Jiang, D., Peng, C., He, Y., 2020. Hyperspectral imaging combined with machine learning as a tool to obtain high-throughput plant salt-stress phenotyping. Plant J. 101, 1448–1461. https://doi.org/10.1111/tpj.14597.

Fitzgerald, G.J., Perry, E.M., Flower, K.C., Nikolaus Callow, J., Boruff, B., Delahunty, A., Wallace, A., Nuttall, J., 2019. Frost damage assessment in wheat using spectral mixture analysis. Remote Sens. 11, 2476. https://doi.org/10.3390/rs11212476.

Franke, J., Menz, G., 2007. Multi-temporal wheat disease detection by multi-spectral remote sensing. Precis. Agric. 8, 161–172. https://doi.org/10.1007/S11119-007-9036-Y/TABLES/1.

Fu, P., Zhang, W., Yang, K., Meng, F., 2020. A novel spectral analysis method for distinguishing heavy metal stress of maize due to copper and lead: RDA and EMD-PSD. Ecotoxicol. Environ. Saf. 206, 111211. https://doi.org/10.1016/j.ecoenv.2020.111211.

Fu, L., Sun, J., Wang, S., Xu, M., Yao, K., Zhou, X., 2022. Nondestructive evaluation of zn content in rape leaves using MSSAE and hyperspectral imaging. Spectrochim. Acta A Mol. Biomol. Spectrosc. 281, 121641. https://doi.org/10.1016/j.saa.2022.121641.

Galieni, A., D'Ascenzo, N., Stagnari, F., Pagnani, G., Xie, Q., Pisante, M., 2021. Past and future of plant stress detection: an overview from remote sensing to positron emission tomography. Front. Plant Sci. https://doi.org/10.3389/fpls.2020.609155.

Gao, Y., Qiu, J., Miao, Y., Qiu, R., Li, H., Zhang, M., 2019a. Prediction of leaf water content in maize seedlings based on hyperspectral information. IFAC-PapersOnLine. Elsevier, pp. 263–269 https://doi.org/10.1016/j.ifacol.2019.12.532.

Gao, Z., Zhao, Y., Khot, L.R., Hoheisel, G.A., Zhang, Q., 2019b. Optical sensing for early spring freeze related blueberry bud damage detection: hyperspectral imaging for salient spectral wavelengths identification. Comput. Electron. Agric. 167, 105025. https://doi.org/10.1016/j.compag.2019.105025.

Gao, Z., Zhao, Y., Hoheisel, G.A., Khot, L.R., Zhang, Q., 2021. Blueberry bud freeze damage detection using optical sensors: identification of spectral features through hyperspectral imagery. J. Berry Res. 11, 631–646. https://doi.org/10.3233/JBR-211506.

García-Martín, J.F., Badaró, A.T., Barbin, D.F., Álvarez-Mateos, P., 2020. Identification of copper in stems and roots of Jatropha curcas L. By hyperspectral imaging. Processes 8, 823. https://doi.org/10.3390/pr8070823.

Ge, Y., Atefi, A., Zhang, H., Miao, C., Ramamurthy, R.K., Sigmon, B., Yang, J., Schnable, J.C., 2019. High-throughput analysis of leaf physiological and chemical traits with VIS-NIR-SWIR spectroscopy: a case study with a maize diversity panel. Plant Methods 15, 1–12. https://doi.org/10.1186/s13007-019-0450-8.

Gerhards, M., Schlerf, M., Mallick, K., Udelhoven, T., 2019. Challenges and future perspectives of multi-/Hyperspectral thermal infrared remote sensing for crop water-stress detection: a review. Remote Sens. https://doi.org/10.3390/rs11101240.

Goldsmith, S.B., Eon, R.S., Lapszynski, C.S., Badura, G.P., Osgood, D.T., Bachmann, C.M., Tyler, A.C., 2020. Assessing salt marsh vulnerability using high-resolution hyperspectral imagery. Remote Sens. 12, 2938. https://doi.org/10.3390/RS12182938.

Gosselin, N., Sagan, V., Maimaitiyiming, M., Fishman, J., Belina, K., Podleski, A., Maimaitijiang, M., Bashir, A., Balakrishna, J., Dixon, A., 2020. Using visual ozone damage scores and spectroscopy to quantify soybean responses to background ozone. Remote Sens. 12, 93. https://doi.org/10.3390/RS12010093.

Grieco, M., Schmidt, M., Warnemünde, S., Backhaus, A., Klück, H.C., Garibay, A., Tandrón Moya, Y.A., Jozefowicz, A.M., Mock, H.P., Seiffert, U., Maurer, A., Pillen, K., 2022a. Dynamics and genetic regulation of leaf nutrient concentration in barley based on hyperspectral imaging and machine learning. Plant Sci. 315, 111123. https://doi.org/10.1016/j.plantsci.2021.111123.

Grieco, M., Schmidt, M., Warnemünde, S., Backhaus, A., Klück, H.C., Garibay, A., Tandrón Moya, Y.A., Jozefowicz, A.M., Mock, H.P., Seiffert, U., Maurer, A., Pillen, K., 2022b. Dynamics and genetic regulation of leaf nutrient concentration in barley based on hyperspectral imaging and machine learning. Plant Sci. 315, 111123. https://doi.org/10.1016/j.plantsci.2021.111123.

Grulke, N.E., Heath, R.L., 2020. Ozone effects on plants in natural ecosystems. Plant Biol. https://doi.org/10.1111/plb.12971.

Guilherme Teixeira Crusiol, L., Braga, P., Rafael Nanni, M., Furlanetto, R.H., Sibaldelli, R.N.R., Cezar, E., Sun, L., Foloni, J.S.S., Mertz-Henning, L.M., Lima Nepomuceno, A., Neumaier, N., Bouças Farias, J.R., 2021. Using leaf-based hyperspectral reflectance for genotype classification within a soybean germplasm collection assessed under different levels of water availability. Int. J. Remote Sens. 42, 8165–8184. https://doi.org/10.1080/01431161.2021.1975841.

Hariharan, J., Fuller, J., Ampatzidis, Y., Abdulridha, J., Lerwill, A., 2019. Finite difference analysis and bivariate correlation of hyperspectral data for detecting Laurel wilt disease and nutritional deficiency in avocado. Remote Sens. 11, 1748. https://doi.org/10.3390/rs11151748.

He, L., Li, A., Nan, X., 2020. Study of vegetation spectral anomaly behaviour in a porphyry copper mine area based on hyperspectral indices. Int. J. Remote Sens. 41, 911–928. https://doi.org/10.1080/01431161.2019.1651949.

Huang, Y., Zhao, X., Pan, Z., Reddy, K.N., Zhang, J., 2022. Hyperspectral plant sensing for differentiating glyphosate-resistant and glyphosate-susceptible johnsongrass through machine learning algorithms. Pest Manag. Sci. 78, 2370–2377. https://doi.org/10.1002/ps.6864.

Jiang, J., Ran, W., Xiong, K., Pan, Y., 2020. A spectral-spatial approach for detection of single-point natural gas leakage using hyperspectral imaging. Int. J. Greenhouse Gas Control 103, 103181. https://doi.org/10.1016/j.ijggc.2020.103181.

Jiao, W., Wang, L., McCabe, M.F., 2021. Multi-sensor remote sensing for drought characterization: current status, opportunities and a roadmap for the future. Remote Sens. Environ. 256, 112313. https://doi.org/10.1016/j.rse.2021.112313.

Jin, J., Wang, Q., Wang, J., 2019. Combing both simulated and field-measured data to develop robust hyperspectral indices for tracing canopy transpiration in drought-tolerant plant. Environ. Monit. Assess. 191, 1–13. https://doi.org/10.1007/s10661-018-7140-2.

Jun, S., Xin, Z., Xiaohong, W., Bing, L., Chunxia, D., Jifeng, S., 2019. Research and analysis of cadmium residue in tomato leaves based on WT-LSSVR and Vis-NIR hyperspectral imaging. Spectrochim. Acta A Mol. Biomol. Spectrosc. 212, 215–221. https://doi.org/10.1016/j.saa.2018.12.051.

Kaur, G., Singh, G., Motavalli, P.P., Nelson, K.A., Orlowski, J.M., Golden, B.R., 2020. Impacts and management strategies for crop production in waterlogged or flooded soils: a review. Agron. J. https://doi.org/10.1002/agj2.20093.

Kovar, M., Brestic, M., Sytar, O., Barek, V., Hauptvogel, P., Zivcak, M., 2019. Evaluation of hyperspectral reflectance parameters to assess the leafwater content in soybean. Water (Switzerland) 11, 443. https://doi.org/10.3390/w11030443.

Krishna, G., Sahoo, R.N., Singh, P., Bajpai, V., Patra, H., Kumar, S., Dandapani, R., Gupta, V.K., Viswanathan, C., Ahmad, T., Sahoo, P.M., 2019. Comparison of various modelling approaches for water deficit stress monitoring in rice crop through hyperspectral remote sensing. Agric. Water Manag. 213, 231–244. https://doi.org/10.1016/j.agwat.2018.08.029.

Krishna, G., Sahoo, R.N., Singh, P., Patra, H., Bajpai, V., Das, B., Kumar, S., Dhandapani, R., Vishwakarma, C., Pal, M., Chinnusamy, V., 2021. Application of thermal imaging and hyperspectral remote sensing for crop water deficit stress monitoring. Geocarto Int 36, 481–498. https://doi.org/10.1080/10106049.2019.1618922.

Kumagai, E., Burroughs, C.H., Pederson, T.L., Montes, C.M., Peng, B., Kimm, H., Guan, K., Ainsworth, E.A., Bernacchi, C.J., 2022. Predicting biochemical acclimation of leaf photosynthesis in soybean under in-field canopy warming using hyperspectral reflectance. Plant Cell Environ. 45, 80–94. https://doi.org/10.1111/pce.14204.

Küpper, H., Andresen, E., 2016. Mechanisms of metal toxicity in plants. Metallomics https://doi.org/10.1039/c5mt00244c.

Laroche-Pinel, E., Albughdadi, M., Duthoit, S., Chéret, V., Rousseau, J., Clenet, H., 2021. Understanding vine hyperspectral signature through different irrigation plans: a first step to monitor vineyard water status. Remote Sens. 13, 536. https://doi.org/10.3390/rs13030536.

Lassalle, G., 2021. Monitoring natural and anthropogenic plant stressors by hyperspectral remote sensing: recommendations and guidelines based on a meta-review. Sci. Total Environ. https://doi.org/10.1016/j.scitotenv.2021.147758.

Lassalle, G., Elger, A., Credoz, A., H'dacq, R., Bertoni, G., Dubucq, D., Fabre, S., 2019a. Toward quantifying oil contamination in vegetated areas using very high spatial and spectral resolution imagery. Remote Sens. 11, 2241. https://doi.org/10.3390/rs11192241.

Lassalle, G., Fabre, S., Credoz, A., Hédacq, R., Bertoni, G., Dubucq, D., Elger, A., 2019b. Application of PROSPECT for estimating total petroleum hydrocarbons in contaminated soils from leaf optical properties. J. Hazard. Mater. 377, 409–417. https://doi.org/10.1016/j.jhazmat.2019.05.093.

Lassalle, G., Fabre, S., Credoz, A., Hédacq, R., Borderies, P., Bertoni, G., Erudel, T., Buffan-Dubau, E., Dubucq, D., Elger, A., 2019c. Detection and discrimination of various oil-contaminated soils using vegetation reflectance. Sci. Total Environ. 655, 1113–1124. https://doi.org/10.1016/j.scitotenv.2018.11.314.

Lassalle, G., Fabre, S., Credoz, A., Hédacq, R., Dubucq, D., Elger, A., 2021. Mapping leaf metal content over industrial brownfields using airborne hyperspectral imaging and optimized vegetation indices. Sci. Rep. 11, 1–13. https://doi.org/10.1038/s41598-020-79439-z.

Li, X., Li, L., Liu, X., 2019a. Collaborative inversion heavy metal stress in rice by using two-dimensional spectral feature space based on HJ-1 a HSI and radarsat-2 SAR remote sensing data. Int. J. Appl. Earth Obs. Geoinf. 78, 39–52. https://doi.org/10.1016/j.jag.2018.12.011.

Li, Z., Li, Zhenhong, Fairbairn, D., Li, N., Xu, B., Feng, H., Yang, G., 2019b. Multi-LUTs method for canopy nitrogen density estimation in winter wheat by field and UAV hyperspectral. Comput. Electron. Agric. 162, 174–182. https://doi.org/10.1016/J.COMPAG.2019.04.005.

Li, D., Li, C., Yao, Y., Li, M., Liu, L., 2020. Modern imaging techniques in plant nutrition analysis: a review. Comput. Electron. Agric. https://doi.org/10.1016/j.compag.2020.105459.

Li, Y., Yang, K., Gao, W., Han, Q., Zhang, J., 2021a. A spectral characteristic analysis method for distinguishing heavy metal pollution in crops: VMD-PCA-SVM. Spectrochim. Acta A Mol. Biomol. Spectrosc. 255, 119649. https://doi.org/10.1016/j.saa.2021.119649.

Li, Y., Yang, K., Han, Q., Gao, W., Zhang, J., Wu, B., 2021b. A new method that combines spectral indexes and Naive Bayes to distinguish heavy metal pollution in crops. Remote Sens. Lett. 12, 666–673. https://doi.org/10.1080/2150704X.2021.1910364.

Li, Z., Zhou, J., Dong, T., Xu, Y., Shang, Y., 2021c. Application of electrochemical methods for the detection of abiotic stress biomarkers in plants. Biosens. Bioelectron. https://doi.org/10.1016/j.bios.2021.113105.

Li, M., Chu, R., Sha, X., Ni, F., Xie, P., Shen, S., Islam, A.R.M.T., 2021d. Hyperspectral characteristics and scale effects of leaf and canopy of summer maize under continuous water stresses. Agriculture (Switzerland) 11, 1180. https://doi.org/10.3390/agriculture11121180.

Li, H., Zhou, B., Xu, F., Wei, Z., 2022a. Hyperspectral characterization and chlorophyll content inversion of reclaimed vegetation in rare earth mines. Environ. Sci. Pollut. Res. 1–15. https://doi.org/10.1007/s11356-021-16772-4.

Li, Q., Gao, M., Li, Z.L., 2022b. Ground hyper-spectral remote-sensing monitoring of wheat water stress during different growing stages. Agronomy 12, 2267. https://doi.org/10.3390/agronomy12102267.

Lin, D., Li, G., Zhu, Y., Liu, H., Li, L., Fahad, S., Zhang, X., Wei, C., Jiao, Q., 2021. Predicting copper content in chicory leaves using hyperspectral data with continuous wavelet transforms and partial least squares. Comput. Electron. Agric. 187, 106293. https://doi.org/10.1016/j.compag.2021.106293.

Liu, H., Bruning, B., Garnett, T., Berger, B., 2020a. Hyperspectral imaging and 3D technologies for plant phenotyping: from satellite to close-range sensing. Comput. Electron. Agric. https://doi.org/10.1016/j.compag.2020.105621.

Liu, H., Bruning, B., Garnett, T., Berger, B., 2020b. Hyperspectral imaging and 3D technologies for plant phenotyping: from satellite to close-range sensing. Comput. Electron. Agric. https://doi.org/10.1016/j.compag.2020.105621.

Liu, H., Bruning, B., Garnett, T., Berger, B., 2020c. The performances of hyperspectral sensors for proximal sensing of nitrogen levels in wheat. Sensors (Switzerland) 20, 1–21. https://doi.org/10.3390/s20164550.

Liu, S., Yang, X., Guan, Q., Lu, Z., Lu, J., 2020d. An ensemble modeling framework for distinguishing nitrogen, phosphorous and potassium deficiencies in winter oilseed rape (Brassica napus l.) using hyperspectral data. Remote Sens. 12, 1–17. https://doi.org/10.3390/rs12244060.

Liu, C., Hu, Z., Islam, A.R.M.T., Kong, R., Yu, L., Wang, Y., Chen, S., Zhang, X., 2021a. Hyperspectral characteristics and inversion model estimation of winter wheat under different elevated CO2 concentrations. Int. J. Remote Sens. 42, 1035–1053. https://doi.org/10.1080/01431161.2020.1823038.

Liu, W., Yu, Q., Niu, T., Yang, L., Liu, H., 2021b. Inversion of soil heavy metal content based on spectral characteristics of peach trees. Forests 12, 1208. https://doi.org/10.3390/f12091208.

Lowe, A., Harrison, N., French, A.P., 2017. Hyperspectral image analysis techniques for the detection and classification of the early onset of plant disease and stress. Plant Methods 13, 80. https://doi.org/10.1186/s13007-017-0233-z.

Lu, J., Yang, T., Su, X., Qi, H., Yao, X., Cheng, T., Zhu, Y., Cao, W., Tian, Y., 2020. Monitoring leaf potassium content using hyperspectral vegetation indices in rice leaves. Precis. Agric. 21, 324–348. https://doi.org/10.1007/s11119-019-09670-w.

Lu, Y., Payn, K.G., Pandey, P., Acosta, J.J., Heine, A.J., Walker, T.D., Young, S., 2021a. Hyperspectral imaging with cost-sensitive learning for high-throughput screening of Loblolly Pine (Pinus taeda L.) seedlings for freeze tolerance. Trans. ASABE 64, 2045–2059. https://doi.org/10.13031/trans.14708.

Lu, Y., Walker, T.D., Acosta, J.J., Young, S., Pandey, P., Heine, A.J., Payn, K.G., 2021b. Prediction of freeze damage and minimum winter temperature of the seed source of loblolly pine seedlings using hyperspectral imaging. For. Sci. 67, 321–334. https://doi.org/10.1093/forsci/fxab003.

Ma, D., Wang, L., Zhang, L., Song, Z., Rehman, T.U., Jin, J., 2020. Stress distribution analysis on hyperspectral corn leaf images for improved phenotyping quality. Sensors 20, 1–13. https://doi.org/10.3390/s20133659.

Ma, D., Rehman, T.U., Zhang, L., Maki, H., Tuinstra, M.R., Jin, J., 2021a. Modeling of environmental impacts on aerial hyperspectral images for corn plant phenotyping. Remote Sens. 13, 2520. https://doi.org/10.3390/RS13132520 2021, Vol. 13, Page 2520.

Ma, D., Rehman, T.U., Zhang, L., Maki, H., Tuinstra, M.R., Jin, J., 2021b. Modeling of diurnal changing patterns in airborne crop remote sensing images. Remote Sens. 13, 1719. https://doi.org/10.3390/rs13091719.

Manley, P.V., Sagan, V., Fritschi, F.B., Burken, J.G., 2019. Remote sensing of explosives-induced stress in plants: hyperspectral imaging analysis for remote detection of unexploded threats. Remote Sens. 11, 1827. https://doi.org/10.3390/rs11151827.

Mazis, A., Choudhury, S.Das, Morgan, P.B., Stoerger, V., Hiller, J., Ge, Y., Awada, T., 2020. Application of high-throughput plant phenotyping for assessing biophysical traits and drought response in two oak species under controlled environment. For. Ecol. Manag. 465, 118101. https://doi.org/10.1016/j.foreco.2020.118101.

McPartland, M.Y., Falkowski, M.J., Reinhardt, J.R., Kane, E.S., Kolka, R., Turetsky, M.R., Douglas, T.A., Anderson, J., Edwards, J.D., Palik, B., Montgomery, R.A., 2019. Characterizing boreal peatland plant composition and species diversity with hyperspectral remote sensing. Remote Sens. 11, 1685. https://doi.org/10.3390/rs11141685.

Melandri, G., Thorp, K.R., Broeckling, C., Thompson, A.L., Hinze, L., Pauli, D., 2021. Assessing drought and heat stress-induced changes in the cotton leaf metabolome and their relationship with hyperspectral reflectance. Front. Plant Sci. 12, 2393. https://doi.org/10.3389/fpls.2021.751868.

Mertens, S., Verbraeken, L., Sprenger, H., Demuynck, K., Maleux, K., Cannoot, B., De Block, J., Maere, S., Nelissen, H., Bonaventure, G., Crafts-Brandner, S.J., Vogel, J.T., Bruce, W., Inzé, D., Wuyts, N., 2021. Proximal hyperspectral imaging detects diurnal and drought-induced changes in maize physiology. Front. Plant Sci. 12, 240. https://doi.org/10.3389/fpls.2021.640914.

Mevy, J.P., Biryol, C., Boiteau-Barral, M., Miglietta, F., 2022. The optical response of a Mediterranean shrubland to climate change: hyperspectral reflectance measurements during spring. Plants 11, 505. https://doi.org/10.3390/plants11040505.

Mink, R., Linn, A.I., Santel, H.J., Gerhards, R., 2020. Sensor-based evaluation of maize (Zea mays) and weed response to post-emergence herbicide applications of isoxaflutole and cyprosulfamide applied as crop seed treatment or herbicide mixing partner. Pest Manag. Sci. 76, 1856–1865. https://doi.org/10.1002/ps.5715.

Mirzaei, M., Verrelst, J., Marofi, S., Abbasi, M., Azadi, H., 2019. Eco-friendly estimation of heavy metal contents in grapevine foliage using in-field hyperspectral data and multivariate analysis. Remote Sens. 11, 2731. https://doi.org/10.3390/rs11232731.

Mishra, P., Asaari, M.S.M., Herrero-Langreo, A., Lohumi, S., Diezma, B., Scheunders, P., 2017. Close range hyperspectral imaging of plants: a review. Biosyst. Eng. https://doi.org/10.1016/j.biosystemseng.2017.09.009.

Mishra, P., Lohumi, S., Ahmad Khan, H., Nordon, A., 2020. Close-range hyperspectral imaging of whole plants for digital phenotyping: recent applications and illumination correction approaches. Comput. Electron. Agric. https://doi.org/10.1016/j.compag.2020.105780.

Mishra, P., Sadeh, R., Ryckewaert, M., Bino, E., Polder, G., Boer, M.P., Rutledge, D.N., Herrmann, I., 2021. A generic workflow combining deep learning and chemometrics for processing close-range spectral images to detect drought stress in Arabidopsis thaliana to support digital phenotyping. Chemom. Intell. Lab. Syst. 216, 104373. https://doi.org/10.1016/j.chemolab.2021.104373.

Mohd Asaari, M.S., Mishra, P., Mertens, S., Dhondt, S., Inzé, D., Wuyts, N., Scheunders, P., 2018. Close-range hyperspectral image analysis for the early detection of stress responses in individual plants in a high-throughput phenotyping platform. ISPRS J. Photogramm. Remote Sens. 138, 121–138. https://doi.org/10.1016/j.isprsjprs.2018.02.003.

Mohd Asaari, M.S., Mertens, S., Verbraeken, L., Dhondt, S., Inzé, D., Bikram, K., Scheunders, P., 2022. Non-destructive analysis of plant physiological traits using hyperspectral imaging: a case study on drought stress. Comput. Electron. Agric. 195, 106806. https://doi.org/10.1016/j.compag.2022.106806.

Mohseni-Moghadam, M., Wolfe, S., Dami, I., Doohan, D., 2016. Response of wine grape cultivars to simulated drift rates of 2,4-D, dicamba, and glyphosate, and 2,4-D or dicamba plus glyphosate. Weed Technol. 30, 807–814. https://doi.org/10.1614/wt-d-15-00106.1.

Moroni, M., Porti, M., Piro, P., 2019. Design of a remote-controlled platform for green roof plants monitoring via hyperspectral sensors. Water (Switzerland) 11, 1368. https://doi.org/10.3390/w11071368.

Morton, M.J.L., Awlia, M., Al-Tamimi, N., Saade, S., Pailles, Y., Negrão, S., Tester, M., 2019. Salt stress under the scalpel – dissecting the genetics of salt tolerance. Plant J. 97, 148–163. https://doi.org/10.1111/tpj.14189.

Murphy, M.E., Boruff, B., Callow, J.N., Flower, K.C., 2020. Detecting frost stress in wheat: a controlled environment hyperspectral study on wheat plant components and implications for multispectral field sensing. Remote Sens. 12, 477. https://doi.org/10.3390/rs12030477.

Navarro, A., Nicastro, N., Costa, C., Pentangelo, A., Cardarelli, M., Ortenzi, L., Pallottino, F., Cardi, T., Pane, C., 2022. Sorting biotic and abiotic stresses on wild rocket by leaf-image hyperspectral data mining with an artificial intelligence model. Plant Methods 18, 1–14. https://doi.org/10.1186/s13007-022-00880-4.

Nguyen, H.D.D., Pan, V., Pham, C., Valdez, R., Doan, K., Nansen, C., 2020a. Night-based hyperspectral imaging to study association of horticultural crop leaf reflectance and nutrient status. Comput. Electron. Agric. 173, 105458. https://doi.org/10.1016/j.compag.2020.105458.

Nguyen, H.D.D., Pan, V., Pham, C., Valdez, R., Doan, K., Nansen, C., 2020b. Night-based hyperspectral imaging to study association of horticultural crop leaf reflectance and nutrient status. Comput. Electron. Agric. 173, 105458. https://doi.org/10.1016/j.compag.2020.105458.

Nugent, P.W., Shaw, J.A., Jha, P., Scherrer, B., Donelick, A., Kumar, V., 2018. Discrimination of herbicide-resistant kochia with hyperspectral imaging. J. Appl. Remote. Sens. 12, 1. https://doi.org/10.1117/1.jrs.12.016037.

de Oliveira, K.M., Furlanetto, R.H., Rodrigues, M., dos Santos, G.L.A.A., Reis, A.S., Teixeira Crusiol, L.G., Rafael Nanni, M., Cezar, E., de Oliveira, R.B., 2022. Assessing phosphorus nutritional status in maize plants using leaf-based hyperspectral measurements and multivariate analysis. Int. J. Remote Sens. 43, 2581–2601. https://doi.org/10.1080/01431161.2022.2064198.

Osco, L.P., Ramos, A.P.M., Moriya, É.A.S., Bavaresco, L.G., de Lima, B.C., Estrabis, N., Pereira, D.R., Creste, J.E., Júnior, J.M., Gonçalves, W.N., Imai, N.N., Li, J., Liesenberg, V., de Araújo, F.F., 2019. Modeling hyperspectral response of water-stress induced lettuce plants using artificial neural networks. Remote Sens. 11, 2797. https://doi.org/10.3390/rs11232797.

Osco, L.P., Ramos, A.P.M., Pinheiro, M.M.F., Moriya, É.A.S., Imai, N.N., Estrabis, N., Ianczyk, F., de Araújo, F.F., Liesenberg, V., de Castro Jorge, L.A., Li, J., Ma, L., Gonçalves, W.N., Marcato, J., Creste, J.E., 2020. A machine learning framework to predict nutrient content in Valencia-orange leaf hyperspectral measurements. Remote Sens. 12, 906. https://doi.org/10.3390/rs12060906.

Pan, X., Jiang, J., Xiao, Y., 2022. Identifying plants under natural gas micro-leakage stress using hyperspectral remote sensing. Ecol. Inform. 68, 101542. https://doi.org/10.1016/j.ecoinf.2021.101542.

Pancorbo, J.L., Camino, C., Alonso-Ayuso, M., Raya-Sereno, M.D., Gonzalez-Fernandez, I., Gabriel, J.L., Zarco-Tejada, P.J., Quemada, M., 2021. Simultaneous assessment of nitrogen and water status in winter wheat using hyperspectral and thermal sensors. Eur. J. Agron. 127, 126287. https://doi.org/10.1016/j.eja.2021.126287.

Park, E., Kim, Y.S., Omari, M.K., Suh, H.K., Faqeerzada, M.A., Kim, M.S., Baek, I., Cho, B.K., 2021. High-throughput phenotyping approach for the evaluation of heat stress in korean ginseng (Panax ginseng meyer) using a hyperspectral reflectance image. Sensors 21, 5634. https://doi.org/10.3390/s21165634.

Paulus, S., Mahlein, A.K., 2020. Technical workflows for hyperspectral plant image assessment and processing on the greenhouse and laboratory scale. Gigascience 9, 1–10. https://doi.org/10.1093/gigascience/giaa090.

Payne, W.Z., Kurouski, D., 2021. Raman-based diagnostics of biotic and abiotic stresses in plants. A review. Front. Plant Sci. https://doi.org/10.3389/fpls.2020.616672.

Peng, Y., Zhang, M., Xu, Z., Yang, T., Su, Y., Zhou, T., Wang, H., Wang, Y., Lin, Y., 2020. Estimation of leaf nutrition status in degraded vegetation based on field survey and hyperspectral data. Sci. Rep. 10, 1–12. https://doi.org/10.1038/s41598-020-61294-7.

Pérez-Bueno, L., Egea, G., Guan, Q., Song, K., Feng, S., Yu, F., Xu, T., 2022. Detection of peanut leaf spot disease based on leaf-, plant-, and field-scale hyperspectral reflectance. Remote Sens. 14, 4988. https://doi.org/10.3390/RS14194988 2022, Vol. 14, Page 4988.

Pôças, I., Tosin, R., Gonçalves, I., Cunha, M., 2020. Toward a generalized predictive model of grapevine water status in Douro region from hyperspectral data. Agric. For. Meteorol. 280, 107793. https://doi.org/10.1016/j.agrformet.2019.107793.

Poobalasubramanian, M., Park, E.-S., Faqeerzada, M.A., Kim, T., Kim, M.S., Baek, I., Cho, B.-K., 2022. Identification of early heat and water stress in strawberry plants using chlorophyll-fluorescence indices extracted via hyperspectral images. Sensors 22, 8706. https://doi.org/10.3390/s22228706.

Pourdarbani, R., Sabzi, S., Rohban, M.H., Hernández-hernández, J.L., Gallardo-bernal, I., Herrera-miranda, I., García-mateos, G., 2021. One-dimensional convolutional neural networks for hyperspectral analysis of nitrogen in plant leaves. Appl. Sci. 11, 11853. https://doi.org/10.3390/app112411853.

Proctor, C., Dao, P.D., He, Y., 2021. Close-range, heavy-duty hyperspectral imaging for tracking drought impacts using the PROCOSINE model. J. Quant. Spectrosc. Radiat. Transf. 263, 107528. https://doi.org/10.1016/J.JQSRT.2021.107528.

Raj, R., Walker, J.P., Vinod, V., Pingale, R., Naik, B., Jagarlapudi, A., 2021. Leaf water content estimation using top-of-canopy airborne hyperspectral data. Int. J. Appl. Earth Obs. Geoinf. 102, 102393. https://doi.org/10.1016/j.jag.2021.102393.

Ran, W., Jiang, J., Pan, Y., Yuan, D., 2020. Spectral responses and identification of surface vegetation stressed by natural gas leakage. Int. J. Remote Sens. 41, 132–151. https://doi.org/10.1080/01431161.2019.1637960.

Ran, W., Jiang, J., Wang, X., Liu, Z., 2022. A multi-temporal method for detection of underground natural gas leakage using hyperspectral imaging. Int. J. Greenhouse Gas Control 117, 103659. https://doi.org/10.1016/j.ijggc.2022.103659.

Rehman, T.U., Ma, D., Wang, L., Zhang, L., Jin, J., 2020. Predictive spectral analysis using an end-to-end deep model from hyperspectral images for high-throughput plant phenotyping. Comput. Electron. Agric. 177, 105713. https://doi.org/10.1016/j.compag.2020.105713.

Rubio-Delgado, J., Pérez, C.J., Vega-Rodríguez, M.A., 2021. Predicting leaf nitrogen content in olive trees using hyperspectral data for precision agriculture. Precis. Agric. 22, 1–21. https://doi.org/10.1007/s11119-020-09727-1.

Rubo, S., Zinkernagel, J., 2022. Exploring hyperspectral reflectance indices for the estimation of water and nitrogen status of spinach. Biosyst. Eng. 214, 58–71. https://doi.org/10.1016/j.biosystemseng.2021.12.008.

Ruffing, A.M., Anthony, S.M., Strickland, L.M., Lubkin, I., Dietz, C.R., 2021. Identification of metal stresses in Arabidopsis thaliana using hyperspectral reflectance imaging. Front. Plant Sci. 12, 203. https://doi.org/10.3389/fpls.2021.624656.

Ryckewaert, M., Héran, D., Simonneau, T., Abdelghafour, F., Boulord, R., Saurin, N., Moura, D., Mas-Garcia, S., Bendoula, R., 2022. Physiological variable predictions using VIS–NIR spectroscopy for water stress detection on grapevine: interest in combining climate data using multiblock method. Comput. Electron. Agric. 197, 106973. https://doi.org/10.1016/j.compag.2022.106973.

Sabzi, S., Pourdarbani, R., Rohban, M.H., García-Mateos, G., Arribas, J.I., 2021a. Estimation of nitrogen content in cucumber plant (Cucumis sativus L.) leaves using hyperspectral imaging data with neural network and partial least squares regressions. Chemom. Intell. Lab. Syst. 217, 104404. https://doi.org/10.1016/j.chemolab.2021.104404.

Sabzi, S., Pourdarbani, R., Rohban, M.H., García-Mateos, G., Paliwal, J., Molina-Martínez, J.M., 2021b. Early detection of excess nitrogen consumption in cucumber plants using hyperspectral imaging based on hybrid neural networks and the imperialist competitive algorithm. Agronomy 11, 575. https://doi.org/10.3390/agronomy11030575.

Sanaeifar, A., Zhang, W., Chen, H., Zhang, D., Li, X., He, Y., 2022a. Study on effects of airborne pb pollution on quality indicators and accumulation in tea plants using Vis-NIR spectroscopy coupled with radial basis function neural network. Ecotoxicol. Environ. Saf. 229, 113056. https://doi.org/10.1016/j.ecoenv.2021.113056.

Sanaeifar, A., Zhu, F., Sha, J., Li, X., He, Y., Zhan, Z., 2022b. Rapid quantitative characterization of tea seedlings under lead-containing aerosol particles stress using Vis-NIR spectra. Sci. Total Environ. 802, 149824. https://doi.org/10.1016/j.scitotenv.2021.149824.

Sawinski, K., Mersmann, S., Robatzek, S., Böhmer, M., 2013. Guarding the green: pathways to stomatal immunity. Mol. Plant-Microbe Interact. https://doi.org/10.1094/MPMI-12-12-0288-CR.

Scherrer, B., Sheppard, J., Jha, P., Shaw, J.A., 2019. Hyperspectral imaging and neural networks to classify herbicide-resistant weeds. J. Appl. Remote. Sens. 13, 1. https://doi.org/10.1117/1.jrs.13.044516.

Scholten, R.C., Hill, J., Werner, W., Buddenbaum, H., Dash, J.P., Gomez Gallego, M., Rolando, C.A., Pearse, G.D., Hartley, R., Estarija, H.J., Watt, M.S., 2019. Hyperspectral VNIR-spectroscopy and imagery as a tool for monitoring herbicide damage in wilding conifers. Biol. Invasions 21, 3395–3413. https://doi.org/10.1007/s10530-019-02055-0.

Sellami, M.H., Albrizio, R., Čolović, M., Hamze, M., Cantore, V., Todorovic, M., Piscitelli, L., Stellacci, A.M., 2022. Selection of hyperspectral vegetation indices for monitoring yield and physiological response in sweet maize under different water and nitrogen availability. Agronomy 12, 489. https://doi.org/10.3390/agronomy12020489.

Shen, T., Zhang, C., Liu, F., Wang, W., Lu, Y., Chen, R., He, Y., 2020. High-throughput screening of free proline content in rice leaf under cadmium stress using hyperspectral imaging with chemometrics. Sensors (Switzerland) 20, 1–15. https://doi.org/10.3390/s20113229.

Shi, J., Li, W., Zhai, X., Guo, Z., Holmes, M., Elrasheid Tahir, H., Zou, X., 2019. Nondestructive diagnostics of magnesium deficiency based on distribution features of chlorophyll concentrations map on cucumber leaf. J. Plant Nutr. 42, 2773–2783. https://doi.org/10.1080/01904167.2019.1659332.

Shi, J., Wang, Y., Li, Z., Huang, X., Shen, T., Zou, X., 2021. Simultaneous and nondestructive diagnostics of nitrogen/magnesium/potassium-deficient cucumber leaf based on chlorophyll density distribution features. Biosyst. Eng. 212, 458–467. https://doi.org/10.1016/j.biosystemseng.2021.11.001.

Shi, J., Wang, Y., Li, Z., Huang, X., Shen, T., Zou, X., 2022. Characterization of invisible symptoms caused by early phosphorus deficiency in cucumber plants using near-infrared hyperspectral imaging technology. Spectrochim. Acta A Mol. Biomol. Spectrosc. 267, 120540. https://doi.org/10.1016/j.saa.2021.120540.

Siedliska, A., Baranowski, P., Pastuszka-Woźniak, J., Zubik, M., Krzyszczak, J., 2021. Identification of plant leaf phosphorus content at different growth stages based on hyperspectral reflectance. BMC Plant Biol. 21, 1–17. https://doi.org/10.1186/s12870-020-02807-4.

Singh, S., Prasad, N., Verma, R., Semwal, M., Khan, M.S., 2020. A portable Hyperspectral imaging system to assess the effect of different nutrient management practices on Chamomile (Chamomila recutita). Proceedings of the 2020 International Conference on Smart Innovations in Design, Environment, Management, Planning and Computing, ICSIDEMPC 2020. Institute of Electrical and Electronics Engineers Inc, pp. 13–19 https://doi.org/10.1109/ICSIDEMPC49020.2020.9299599.

Singh, H., Roy, A., Setia, R.K., Pateriya, B., 2022a. Estimation of nitrogen content in wheat from proximal hyperspectral data using machine learning and explainable artificial intelligence (XAI) approach. Model Earth Syst. Environ. 8, 2505–2511. https://doi.org/10.1007/S40808-021-01243-Z/TABLES/3.

Singh, H., Roy, A., Setia, R., Pateriya, B., 2022b. Estimation of chlorophyll, macronutrients and water content in maize from hyperspectral data using machine learning and explainable artificial intelligence techniques. Remote Sens. Lett. 13, 969–979. https://doi.org/10.1080/2150704X.2022.2114108.

Sobejano-Paz, V., Mikkelsen, T.N., Baum, A., Mo, X., Liu, S., Köppl, C.J., Johnson, M.S., Gulyas, L., García, M., 2020. Hyperspectral and thermal sensing of stomatal conductance, transpiration, and photosynthesis for soybean and maize under drought. Remote Sens. 12, 1–32. https://doi.org/10.3390/rs12193182.

Song, X., Xu, D., Huang, C., Zhang, K., Huang, S., Guo, D., Zhang, S., Yue, K., Guo, T., Wang, S., Zang, H., 2021. Monitoring of nitrogen accumulation in wheat plants based on hyperspectral data. Remote Sens. Appl. 23, 100598. https://doi.org/10.1016/j.rsase.2021.100598.

Suarez, L.A., Apan, A., Werth, J., 2017. Detection of phenoxy herbicide dosage in cotton crops through the analysis of hyperspectral data. Int. J. Remote Sens. 38, 6528–6553. https://doi.org/10.1080/01431161.2017.1362128.

Sun, J., Wu, M., Hang, Y., Lu, B., Wu, X., Chen, Q., 2019. Estimating cadmium content in lettuce leaves based on deep brief network and hyperspectral imaging technology. J. Food Process Eng. 42. https://doi.org/10.1111/jfpe.13293.

Sun, J., Cao, Y., Zhou, X., Wu, M., Sun, Y., Hu, Y., 2021. Detection for lead pollution level of lettuce leaves based on deep belief network combined with hyperspectral image technology. J. Food Saf. 41, e12866. https://doi.org/10.1111/jfs.12866.

Sytar, O., Brestic, M., Zivcak, M., Olsovska, K., Kovar, M., Shao, H., He, X., 2017. Applying hyperspectral imaging to explore natural plant diversity towards improving salt stress tolerance. Sci. Total Environ. 578, 90–99. https://doi.org/10.1016/j.scitotenv.2016.08.014.

Takehisa, H., Ando, F., Takara, Y., Ikehata, A., Sato, Y., 2022. Transcriptome and hyperspectral profiling allows assessment of phosphorus nutrient status in rice under field conditions. Plant Cell Environ. 45, 1507–1519. https://doi.org/10.1111/pce.14280.

Thapa, S., Kang, C., Diverres, G., Karkee, M., Zhang, Q., Keller, M., 2022. Assessment of water stress in vineyards using on-the-go hyperspectral imaging and machine learning algorithms. J. ASABE 65, 949–962. https://doi.org/10.13031/ja.14663.

Thomson, A.L., Vassiliadis, S., Copland, A., Stayches, D., Jacobs, J., Morse-McNabb, E., 2022. Comparing how accurately four different proximal spectrometers can estimate pasture nutritive characteristics: effects of spectral range and data type. Precis. Agric. 23, 2186–2214. https://doi.org/10.1007/s11119-022-09916-0.

Tirado, S.B., Dennis, S.S., Enders, T.A., Springer, N.M., 2021. Utilizing spatial variability from hyperspectral imaging to assess variation in maize seedlings. Plant Phenome J. 4, e20013. https://doi.org/10.1002/ppj2.20013.

Traversari, S., Cacini, S., Galieni, A., Nesi, B., Nicastro, N., Pane, C., 2021. Precision agriculture digital technologies for sustainable fungal disease management of ornamental plants. Sustainability (Switzerland) 13, 3707. https://doi.org/10.3390/su13073707.

Wang, J., Lv, M., Islam, F., Gill, R.A., Yang, C., Ali, B., Yan, G., Zhou, W., 2016. Salicylic acid mediates antioxidant defense system and ABA pathway related gene expression in Oryza sativa against quinclorac toxicity. Ecotoxicol. Environ. Saf. 133, 146–156. https://doi.org/10.1016/j.ecoenv.2016.07.002.

Wang, F., Gao, J., Zha, Y., 2018. Hyperspectral sensing of heavy metals in soil and vegetation: feasibility and challenges. ISPRS J. Photogramm. Remote Sens. https://doi.org/10.1016/j.isprsjprs.2017.12.003.

Wang, G., Wang, Q., Su, Z., Zhang, J., 2020a. Predicting copper contamination in wheat canopy during the full growth period using hyperspectral data. Environ. Sci. Pollut. Res. 27, 39029–39040. https://doi.org/10.1007/s11356-020-09973-w.

Wang, J., Zhang, C., Shi, Y., Long, M., Islam, F., Yang, C., Yang, S., He, Y., Zhou, W., 2020b. Evaluation of quinclorac toxicity and alleviation by salicylic acid in rice seedlings using ground-based visible/near-infrared hyperspectral imaging. Plant Methods 16, 1–16. https://doi.org/10.1186/s13007-020-00576-7.

Wang, L., Jin, J., Song, Z., Wang, J., Zhang, L., Rehman, T.U., Ma, D., Carpenter, N.R., Tuinstra, M.R., 2020c. LeafSpec: an accurate and portable hyperspectral corn leaf imager. Comput. Electron. Agric. 169, 105209. https://doi.org/10.1016/j.compag.2019.105209.

Wang, M., Yang, K.M., Zhang, W., 2020d. Hyperspectral monitoring of maize leaves under copper stress at different growth stages. Remote Sens. Lett. 11, 343–352. https://doi.org/10.1080/2150704X.2020.1716408.

Wang, L., Liu, Y., Wen, M., Li, M., Dong, Z., He, Z., Cui, J., Ma, F., 2021. Using field hyperspectral data to predict cotton yield reduction after hail damage. Comput. Electron. Agric. 190, 106400. https://doi.org/10.1016/j.compag.2021.106400.

Watt, M.S., Buddenbaum, H., Leonardo, E.M.C., Estarija, H.J., Bown, H.E., Gomez-Gallego, M., Hartley, R.J.L., Pearse, G.D., Massam, P., Wright, L., Zarco-Tejada, P.J., 2020a. Monitoring biochemical limitations to photosynthesis in N and P-limited radiata pine using plant functional traits quantified from hyperspectral imagery. Remote Sens. Environ. 248, 112003. https://doi.org/10.1016/j.rse.2020.112003.

Watt, M.S., Buddenbaum, H., Leonardo, E.M.C., Estarija, H.J.C., Bown, H.E., Gomez-Gallego, M., Hartley, R., Massam, P., Wright, L., Zarco-Tejada, P.J., 2020b. Using hyperspectral plant traits linked to photosynthetic efficiency to assess N and P partition. ISPRS J. Photogramm. Remote Sens. 169, 406–420. https://doi.org/10.1016/j.isprsjprs.2020.09.006.

Watt, M.S., Leonardo, E.M.C., Estarija, H.J.C., Massam, P., de Silva, D., O'Neill, R., Lane, D., McDougal, R., Buddenbaum, H., Zarco-Tejada, P.J., 2021. Long-term effects of water stress on hyperspectral remote sensing indicators in young radiata pine. For. Ecol. Manag. 502, 119707. https://doi.org/10.1016/j.foreco.2021.119707.

Weksler, S., Rozenstein, O., Haish, N., Moshelion, M., Walach, R., Ben-Dor, E., 2020. A hyperspectral-physiological phenomics system: measuring diurnal transpiration rates and diurnal reflectance. Remote Sens. 12, 1493. https://doi.org/10.3390/RS12091493.

Weksler, S., Rozenstein, O., Haish, N., Moshelion, M., Wallach, R., Ben-Dor, E., 2021. Detection of potassium deficiency and momentary transpiration rate estimation at early growth stages using proximal hyperspectral imaging and extreme gradient boosting. Sensors (Switzerland) 21, 1–19. https://doi.org/10.3390/s21030958.

Wu, L., Jiang, Q., Zhang, Y., Du, M., Ma, L., Ma, Y., 2022. Peroxidase activity in tomato leaf cells under salt stress based on micro-hyperspectral imaging technique. Horticulturae 8, 813. https://doi.org/10.3390/horticulturae8090813.

Xia, J.A., Cao, H.X., Yang, Y.W., Zhang, W.X., Wan, Q., Xu, L., Ge, D.K., Zhang, W.Y., Ke, Y.Q., Huang, B., 2019. Detection of waterlogging stress based on hyperspectral images of oilseed rape leaves (Brassica napus L.). Comput. Electron. Agric. 159, 59–68. https://doi.org/10.1016/j.compag.2019.02.022.

Xie, X.J., Zhang, Y.H., Li, R.Y., Shen, S.H., Bao, Y.X., 2019. Prediction model of rice crude protein content, amylose content and actual yield under high temperature stress based on hyper-spectral remote sensing. Qual. Assur. Saf. Crops Food 11, 517–527. https://doi.org/10.3920/QAS2018.1295.

Xie, Y., Feng, M., Wang, C., Yang, W., Sun, H., Yang, C., Jing, B., Qiao, X., Saleem Kubar, M., Song, J., 2020a. Hyperspectral monitor on chlorophyll density in winter wheat under water stress. Agron. J. 112, 3667–3676. https://doi.org/10.1002/agj2.20306.

Xie, Y., Wang, C., Yang, W., Feng, M., Qiao, X., Song, J., 2020b. Canopy hyperspectral characteristics and yield estimation of winter wheat (Triticum aestivum) under low temperature injury. Sci. Rep. 10, 1–10. https://doi.org/10.1038/s41598-019-57100-8.

Xin, Z., Jun, S., Yan, T., Quansheng, C., Xiaohong, W., Yingying, H., 2020. A deep learning based regression method on hyperspectral data for rapid prediction of cadmium residue in lettuce leaves. Chemom. Intell. Lab. Syst. 200, 103996. https://doi.org/10.1016/j.chemolab.2020.103996.

Yamashita, H., Sonobe, R., Hirono, Y., Morita, A., Ikka, T., 2020. Dissection of hyperspectral reflectance to estimate nitrogen and chlorophyll contents in tea leaves based on machine learning algorithms. Sci. Rep. 10, 1–11. https://doi.org/10.1038/s41598-020-73745-2.

Yang, M., 2022. Physiological disorder diagnosis of plant leaves based on full-Spectrum hyperspectral images with convolutional neural network. Horticulturae 8, 854. https://doi.org/10.3390/horticulturae8090854.

Yang, W., Yang, C., Hao, Z., Xie, C., Li, M., 2019. Diagnosis of plant cold damage based on hyperspectral imaging and convolutional neural network. IEEE Access 7, 118239–118248. https://doi.org/10.1109/ACCESS.2019.2936892.

Yang, F., Liu, S., Wang, Q., Liu, T., Li, S., 2022. Assessing waterlogging stress level of winter wheat from hyperspectral imagery based on harmonic analysis. Remote Sens. 14, 122. https://doi.org/10.3390/rs14010122.

Yu, F., Feng, S., Du, W., Wang, D., Guo, Z., Xing, S., Jin, Z., Cao, Y., Xu, T., 2020. A study of nitrogen deficiency inversion in Rice leaves based on the hyperspectral reflectance differential. Front. Plant Sci. 11, 1758. https://doi.org/10.3389/fpls.2020.573272.

Yu, K., Fang, S., Zhao, Y., 2021. Heavy metal hg stress detection in tobacco plant using hyperspectral sensing and data-driven machine learning methods. Spectrochim. Acta A Mol. Biomol. Spectrosc. 245, 118917. https://doi.org/10.1016/j.saa.2020.118917.

Zea, M., Souza, A., Yang, Y., Lee, L., Nemali, K., Hoagland, L., 2022. Leveraging high-throughput hyperspectral imaging technology to detect cadmium stress in two leafy green crops and accelerate soil remediation efforts. Environ. Pollut. 292, 118405. https://doi.org/10.1016/j.envpol.2021.118405.

Żelazny, W.R., Lukáš, J., 2020. Drought stress detection in juvenile oilseed rape using hyperspectral imaging with a focus on spectra variability. Remote Sens. 12, 1–27. https://doi.org/10.3390/rs12203462.

Zhang, F., Zhou, G., 2019. Estimation of vegetation water content using hyperspectral vegetation indices: a comparison of crop water indicators in response to water stress treatments for summer maize. BMC Ecol. 19, 1–12. https://doi.org/10.1186/s12898-019-0233-0.

Zhang, J., Huang, Y., Reddy, K.N., Wang, B., 2019a. Assessing crop damage from dicamba on non-dicamba-tolerant soybean by hyperspectral imaging through machine learning. Pest Manag. Sci. 75, 3260–3272. https://doi.org/10.1002/ps.5448.

Zhang, L., Maki, H., Ma, D., Sánchez-Gallego, J.A., Mickelbart, M.V., Wang, L., Rehman, T.U., Jin, J., 2019b. Optimized angles of the swing hyperspectral imaging system for single corn plant. Comput. Electron. Agric. 156, 349–359. https://doi.org/10.1016/j.compag.2018.11.030.

Zhang, S., Zhu, Y., Wang, M., Fei, T., 2019c. Selection of the optimal spectral resolution for the cadmium-lead cross contamination diagnosing based on the hyperspectral reflectance of rice canopy. Sensors (Switzerland) 19, 3889. https://doi.org/10.3390/s19183889.

Zhang, N., Yang, G., Pan, Y., Yang, X., Chen, L., Zhao, C., 2020a. A review of advanced technologies and development for hyperspectral-based plant disease detection in the past three decades. Remote Sens. https://doi.org/10.3390/rs12193188.

Zhang, S., Li, J., Wang, S., Huang, Y., Li, Y., Chen, Y., Fei, T., 2020b. Rapid identification and prediction of cadmium-Lead cross-stress of different stress levels in Rice canopy based on visible and near-infrared spectroscopy. Remote Sens. 12, 469. https://doi.org/10.3390/rs12030469.

Zhang, S., Fei, T., You, X., Wan, Y., Wang, Y., Bian, M., 2021a. Two hyperspectral indices for detecting cadmium and lead contamination from arice canopy spectrum. Land Degrad. Dev. 32, 66–78. https://doi.org/10.1002/ldr.3721.

Zhang, T., Huang, Y., Reddy, K.N., Yang, P., Zhao, X., Zhang, J., 2021b. Using machine learning and hyperspectral images to assess damages to corn plant caused by glyphosate and to evaluate recoverability. Agronomy 11, 583. https://doi.org/10.3390/agronomy11030583.

Zhao, H., Cui, B., Jia, G., Gan, F., 2020. The influence analysis of reflectance anisotropy of canopy on the prediction accuracy of Cu stress based on laboratory multi-directional measurement. In: Osten, W., Situ, G., Cao, X. (Eds.), International Conference on Optical Instruments and Technology: Optoelectronic Imaging/Spectroscopy and Signal Processing Technology. SPIE, p. 49 https://doi.org/10.1117/12.2547342.

Zhou, W., Zhang, J., Zou, M., Liu, X., Du, X., Wang, Q., Liu, Yangyang, Liu, Ying, Li, J., 2019a. Prediction of cadmium concentration in brown rice before harvest by hyperspectral remote sensing. Environ. Sci. Pollut. Res. 26, 1848–1856. https://doi.org/10.1007/s11356-018-3745-9.

Zhou, W., Zhang, J., Zou, M., Liu, X., Du, X., Wang, Q., Liu, Yangyang, Liu, Ying, Li, J., 2019b. Feasibility of using Rice leaves hyperspectral data to estimate CaCl2-extractable concentrations of heavy metals in agricultural soil. Sci. Rep. 9, 1–9. https://doi.org/10.1038/s41598-019-52503-z.

Zhou, X., Sun, J., Tian, Y., Wu, X., Dai, C., Li, B., 2019c. Spectral classification of lettuce cadmium stress based on information fusion and VISSA-GOA-SVM algorithm. J. Food Process Eng. 42, e13085. https://doi.org/10.1111/jfpe.13085.

Zhou, X., Sun, J., Tian, Y., Lu, B., Hang, Y., Chen, Q., 2020a. Hyperspectral technique combined with deep learning algorithm for detection of compound heavy metals in lettuce. Food Chem. 321, 126503. https://doi.org/10.1016/j.foodchem.2020.126503.

Zhou, X., Sun, J., Tian, Y., Lu, B., Hang, Y., Chen, Q., 2020b. Development of deep learning method for lead content prediction of lettuce leaf using hyperspectral images. Int. J. Remote Sens. 41, 2263–2276. https://doi.org/10.1080/01431161.2019.1685721.

Zhou, X., Sun, J., Zhang, Y., Tian, Y., Yao, K., Xu, M., 2021a. Visualization of heavy metal cadmium in lettuce leaves based on wavelet support vector machine regression model and visible-near infrared hyperspectral imaging. J. Food Process Eng. 44, e13897. https://doi.org/10.1111/jfpe.13897.

Zhou, X., Zhao, C., Sun, J., Cao, Y., Fu, L., 2021b. Classification of heavy metal cd stress in lettuce leaves based on WPCA algorithm and fluorescence hyperspectral technology. Infrared Phys. Technol. 119, 103936. https://doi.org/10.1016/j.infrared.2021.103936.

Zhou, J.J., Zhang, Y.H., Han, Z.M., Liu, X.Y., Jian, Y.F., Hu, C.G., Dian, Y.Y., 2021c. Evaluating the performance of hyperspectral leaf reflectance to detect water stress and estimation of photosynthetic capacities. Remote Sens. 13, 2160. https://doi.org/10.3390/rs13112160.

Zhou, B., Li, H., Xu, F., 2022a. Analysis and discrimination of hyperspectral characteristics of typical vegetation leaves in a rare earth reclamation mining area. Ecol. Eng. 174, 106465. https://doi.org/10.1016/j.ecoleng.2021.106465.

Zhou, B., Li, H., Xu, F., 2022b. Analysis and discrimination of hyperspectral characteristics of typical vegetation leaves in a rare earth reclamation mining area. Ecol. Eng. 174, 106465. https://doi.org/10.1016/j.ecoleng.2021.106465.

Zhou, X., Sun, J., Tian, Y., Yao, K., Xu, M., 2022c. Detection of heavy metal lead in lettuce leaves based on fluorescence hyperspectral technology combined with deep learning algorithm. Spectrochim. Acta A Mol. Biomol. Spectrosc. 266, 120460. https://doi.org/10.1016/j.saa.2021.120460.

Zhu, K., Sun, Z., Zhao, F., Yang, T., Tian, Z., Lai, J., Zhu, W., Long, B., 2021. Relating hyperspectral vegetation indices with soil salinity at different depths for the diagnosis ofwinter wheat salt stress. Remote Sens. 13, 1–21. https://doi.org/10.3390/rs13020250.

Zhu, Y., Abdalla, A., Tang, Z., Cen, H., 2022. Improving rice nitrogen stress diagnosis by denoising strips in hyperspectral images via deep learning. Biosyst. Eng. 219, 165–176. https://doi.org/10.1016/j.biosystemseng.2022.05.001.

Žibrat, U., Susič, N., Knapič, M., Širca, S., Strajnar, P., Razinger, J., Vončina, A., Urek, G., Gerič Stare, B., 2019. Pipeline for imaging, extraction, pre-processing, and processing of time-series hyperspectral data for discriminating drought stress origin in tomatoes. MethodsX 6, 399–408. https://doi.org/10.1016/j.mex.2019.02.022.

Zovko, M., Žibrat, U., Knapič, M., Kovačić, M.B., Romić, D., 2019. Hyperspectral remote sensing of grapevine drought stress. Precis. Agric. 20, 335–347. https://doi.org/10.1007/s11119-019-09640-2.

Zubler, A.V., Yoon, J.Y., 2020. Proximal methods for plant stress detection using optical sensors and machine learning. Biosensors (Basel) https://doi.org/10.3390/bios10120193.